

Haul Truck Tire Reliability and Condition Monitoring

by

Roya Vaghar Anzabi

A thesis submitted in partial fulfillment of the requirements for the degree of

Master of Science

Department of Mechanical Engineering  
University of Alberta

© Roya Vaghar Anzabi, 2015

## **Abstract**

Pneumatic tires are costly components of large off-road haul trucks used in surface mining operations. Tires are prone to premature damage during operation which can lead to hazard events and injury of personnel, loss of equipment and reduced productivity. Currently, monitoring of tire condition is performed by physical inspection which is not efficient. Options for new condition monitoring methods include off-board optical methods for detecting abnormal deformation and surface features. Physics-based modeling of the tire can provide a good understanding of tire behavior for further improved monitoring systems.

This research is mainly focused on development of a dynamic model to simulate the response of haul truck tire in presence of a fault. A finite element model is applied to explore the effect of damage on tire original properties such as stiffness. To obtain the material properties, the kinematic field of rubber specimen with a defined fault is measured in laboratory scale using optical technique.

The dynamic simulation presented in this research has shown that the differences between tire displacements can be an indicator to determine the presence of damage in the tire, for tire fault detection purposes.

## Preface

This thesis is an original work by Roya Vaghar Anzabi.

Part of Chapter 1 and 2 of this thesis has been published as Lipsett, M., Vaghar- Anzabi, R., Kotchon, A., and Nobes, D., "Condition monitoring for mining haul truck tires," Proceedings of the Eighth International Conference on Condition Monitoring and Machinery Failure Prevention Technologies (CM 2011 and MFPT 2011), Cardiff, UK, 2011, 12 pp.

A version of Chapter3, Section 3.3 of this thesis has been published as Lipsett, M., and Vaghar Anzabi, R., 2013, "Seasonal Effects on Haul Truck Tire Life," International journal of Strategic Asset Management, 2013, 13 pp.

A version of Chapter 5 of this thesis has been published as Vaghar- Anzabi, R., Nobes, D.S. and Lipsett, M.G., "Haul truck tire dynamics due to tire condition," Journal of Physics: Conference Series, 2012, 364(1).

A version of Chapter 4 of this thesis has been published as Vaghar Anzabi, R., and Lipsett, M.G., "Reliability analysis and condition monitoring methods for off-road haul truck tires," Proc 24th COMADEM Stavanger Norway, 2011, 10 pp.

<b>Table of Contents</b>	<b>page</b>
<b>Chapter 1. Introduction</b> .....	<b>1</b>
1.1. Background and motivation .....	1
1.2. Haul truck tire characteristics .....	4
1.2.1. Tire structure .....	4
1.2.2. Tire manufacturing .....	6
1.3. Project objectives .....	8
1.4. Thesis organization .....	9
<b>Chapter 2. Literature Review</b> .....	<b>10</b>
2.1. Tire failure studies .....	10
2.1.1. Reliability modeling of tires .....	10
2.1.2. Tire failure dynamic modeling .....	11
2.1.3. Tire failure modeling .....	11
2.1.4. Experimental studies of tire failure .....	12
2.2. Tire monitoring methods .....	14
2.2.1. Current condition monitoring methods .....	14
2.2.2. Optical methods for tire condition monitoring .....	15
2.3. Rubber failure studies .....	18
<b>Chapter 3. Haul Truck Tire Failure</b> .....	<b>19</b>
3.1. Haul truck tire failure modes .....	19
3.2. Common causes of haul truck tire failures .....	23
3.3. Seasonal effect on haul truck tire failure .....	26
3.3.1. Seasonal effects on tire life .....	26
3.3.2. Tire life for different damage modes .....	27
3.4. Road quality estimation .....	29
3.5. Concluding remarks on tire failure studies .....	31
<b>Chapter 4. Reliability Model of Haul Truck Tires</b> .....	<b>32</b>
4.1. Reliability modeling .....	32
4.1.1. Collecting data .....	33
4.1.2. Estimating failure probability function .....	33
4.1.3. Fitting the distribution .....	34
4.1.4. Estimating parameters .....	35
4.1.5. Goodness-of-fit test .....	37
4.1.6. Reliability function .....	38
4.2. Concluding remarks on reliability model .....	39

<b>Chapter 5. Dynamic Model of Tire with Failure .....</b>	<b>40</b>
5.1. Tire dynamics simulation .....	40
5.2. Governing equations of model .....	41
5.3. Definition of parameters .....	43
5.4. Road profile excitation.....	43
5.5. Effect of tire damage .....	45
5.5.1. Finite element model of tire.....	46
5.5.2. Tire stiffness estimation .....	51
5.6. Solving the governing equations .....	53
5.7. Tire dynamic model results.....	53
5.8. Concluding remarks on tire dynamic modeling.....	55
<b>Chapter 6. Rubber Damage Study .....</b>	<b>56</b>
6.1. Rubber strain measurement using Digital Image Correlation method .....	56
6.1.1. Digital image correlation principle .....	56
6.1.2. Digital image correlation apparatus .....	58
6.1.3. DIC experiment setup.....	59
6.1.4. Rubber deformation data collection .....	66
6.1.5. Processing of recorded images.....	67
6.1.6. DIC experimental results .....	68
6.2. Finite element model of rubber with crack .....	72
6.2.1. Rubber specimen finite element model.....	72
6.2.2. FE model results of rubber with crack.....	75
6.3. Heat generation of rubber with crack .....	78
6.3.1. Basic Theory of rubber heat generation.....	78
6.3.2. Basics of thermomechanical modeling.....	80
6.3.3. Thermomechanical model summary.....	81
6.4. Concluding remarks on rubber damage study .....	82
<b>Chapter 7. Conclusions and Future Work .....</b>	<b>85</b>
7.1. Conclusions .....	85
7.2. Future work.....	87
7.2.1. Recommendation for future studies .....	87
7.2.2. Industrial application.....	88
<b>References.....</b>	<b>89</b>
<b>Appendices.....</b>	<b>95</b>

---

Table 1-1: Haul truck tire and long haul trailer tire comparison .....	1
Table 1-2: Properties of various rubbers .....	7
Table 1-3: Percentage of rubbers component in different tires.....	8
Table 3-1: Tire removal reasons.....	19
Table 5-1: Parameters of quarter vehicle model .....	43
Table 5-2: Convergence study for tire FE model .....	48
Table 6-1: Specifications of AVT GX3300 camera and its components .....	60
Table 6-2: Mean speckle size for the three subset sizes .....	62
Table 6-3: Convergence study for rubber FE model .....	74

Figure 1-1: Photograph of inspection of a haul-truck tire in a shop.....	2
Figure 1-2: Schematic of tire structure .....	4
Figure 1-3: Structural diagram of typical off-the road radial tire .....	5
Figure 3-2: Proportion of different failure modes of haul truck tires .....	21
Figure 3-3: Frequency of modes of damages in haul truck tires .....	22
Figure 3-4: Model of tire as spring-dampener and its stored energy .....	24
Figure 3-5: Tire heat transfer and heat generation .....	24
Figure 3-6: Tire heat generation diagram.....	25
Figure 3-7: Overall seasonal variation in tire end of life.....	26
Figure 3-8: Frequency of major modes of tire damage by month .....	27
Figure 3-9: Frequency of tread cuts in August and December .....	28
Figure 3-10: Strut pressure monthly mean and variance .....	30
Figure 4-1: Finding reliability model algorithm .....	32
Figure 4-2: Estimated probability function .....	34
Figure 4-3: Fitted cumulative distribution function (CDF).....	35
Figure 4-4: Estimated reliability function of haul truck tire .....	38
Figure 5-1: Quarter-vehicle model.....	41
Figure 5-2: Assumed road roughness profile.....	44
Figure 5-3: Schematic of tire deformation under load .....	45
Figure 5-4: The finite element model of tire and road .....	47
Figure 5-5: Convergence of maximum von-Mises stresses for tire FE model .....	48
Figure 5-6: Results of tire deflection at different rotation angles.....	49
Figure 5-7: Tire deformation with respect to rotation angle (results of tire FEM) .....	50
Figure 5-8: Tire stiffness with respect to rotation angle (results of tire FEM) .....	51
Figure 5-9: Estimated tire stiffness function with respect to rotation angle .....	52
Figure 5-10: Plots of vertical displacement and velocity of tire exited by step disturbance .....	53
Figure 5-11: Plots of vertical displacement and velocity of tire exited by road roughness .....	54
Figure 6-1 :Illustration of digital image correlation principle.....	57

Figure 6-2 : Schematic of 3-D DIC experimental setup to measure rubber deformation .....	58
Figure 6-3 : Photo of 3-D DIC experimental setup.....	59
Figure 6-4 : Using air brush technique to seed the rubber sample surface .....	63
Figure 6-5: The random speckle pattern using air brush.....	63
Figure 6-6 : Schematic of a typical 2D calibration plate .....	64
Figure 6-7 : Camera configuration as the result of calibration procedure .....	65
Figure 6-9 : Crack opening sequence in rubber sample .....	67
Figure 6-10: Rubber samples geometry in tension test .....	68
Figure 6-11: Stress and stiffness values in tensile test of rubber samples.....	69
Figure 6-12: Improvement of deformation measurement using different seeding methods .....	70
Figure 6-13: Deformation and strain field of crack rubber sample in tension .....	71
Figure 6-14: Finite element model of rubber with crack.....	73
Figure 6-15: Mesh generation around crack for FE model of rubber.....	74
Figure 6-16: Convergence of maximum von-Mises stresses of rubber FE model .....	75
Figure 6-17 : Crack opening sequence in rubber FE model .....	75
Figure 6-18: Deformation vector field of rubber in tension using FE model.....	76
Figure 6-19: Deformation and strain field of rubber FE model around the crack.....	77
Figure 6-20: Fully coupled thermomechanical model .....	80
Figure 6-21: Maximum principal strain field around crack.....	83
Figure 6-22: Maximum principal strain along y direction.....	83
Figure 6-23: Relative error of FEM and DIC methods (maximum principal strain) .....	84
Figure 6-24: Experiment design to observe the effect of crack angle.....	84

# Chapter 1. Introduction

---

## 1.1. Background and motivation

Surface mining operations of metals, coal, and soils (such as oilsands) often rely on a truck and shovel mining method. For economy of scale and reduced personnel costs, large operations use ultra-class haul trucks that can haul up to 400 tonnes of material. These trucks ride on six wheels, using front steering and dual wheels at the rear. Haul truck tires are made as large as possible to fit within a highway transportation envelope, and so they are about 4m in diameter, with a mass of up to 5,300 kg and cost on the order of USD\$ 60,000 each (depending on the tire type). A single tire can account for 20-25% of a haul trucks operating costs [Dhillon, 2008].

In contrast with tires for highway vehicles (which are designed for controlled road conditions), tires in off-road service experience highly variable operating conditions such as road condition, severe loading and temperature [Bolster and Joseph, 2005].

The heavy hauling capacity makes haul truck special in terms of their characteristics in comparison with normal trucks. Table 1-1 shows the basic specifications and differences between a tire for a haul truck in oilsand service and a typical tire used for an on-road trailer.

**Table 1-1: Haul truck tire and long haul trailer tire comparison**

	Ultra-class haul truck tire	Haul trailer tire
Tire	55/80R63	10.00R15
Application	Haul truck mining	long haul truck load
Tire type	Radial	Radial
Max load (kg)	93,000	2,900
Tire pressure (kPa)	Up to 600	250
Tire diameter (m)	4.0	0.9
Max speed (km/hr)	50	90
Tire price (USD\$)	60,000	500

Haul truck tires are prone to premature damage during operation and damage to these tires can cause loss of production and pose a great potential risk to personnel. On a mining site, where the number of trucks limits production, the loss of a single tire can result in hundreds of thousands of dollars in lost production. In addition, unreliable haul truck tires can cause loss of vehicle control or may suffer an explosive loss of pressure under full load and thus pose a hazard to drivers, other operators, and maintenance personnel. This is a particularly critical issue for mining operations that have poor in-pit driving conditions, which subjects tires to local overload conditions and heat generation.

Syncrude Canada Ltd operates an oilsands mine in Northern Alberta Canada employing a truck-and-shovel mining method. Oilsand haul roads can be problematic because oilsand is an unconsolidated soil, comprising bitumen, sand, clay, and water. Oilsand has an undrained shear strength that depends on temperature (which can vary between  $-40\text{ }^{\circ}\text{C}$  to  $+40\text{ }^{\circ}\text{C}$  in the region of interest). To reduce the risk of sudden failures, off-road tires are physically inspected periodically (typically once per week) to identify gross faults, such as tread cuts, sidewall cuts, and bulging caused by internal delamination or cord damage. Figure 1-1 shows a shop for inspection of a typical tire mounted on an ultra-class haul truck.



**Figure 1-1: Photograph of inspection of a haul-truck tire in a shop  
(Used with permission of Syncrude Canada Ltd.)**

If a possible fault is discovered, then the extent of the damage is assessed by tire technicians, based on their experience. If the damage is severe, then actions are taken to repair or replace the tire before returning the truck to service [Zhou et al., 2008]. This inspection process is time-consuming and reduces productivity. Unfortunately, in many operations, the interval between regular inspections is too long to ensure that damage is remedied before a failure occurs. Because some fault modes can develop between inspection intervals, new methods for condition monitoring are being developed. For these reasons, there is an interest to research haul truck tires failure types and monitoring of haul truck tires to detect anomalies.

Tire faults can be detected applying different monitoring methods rather than periodic manual inspection by technicians, which is time consuming. Using tires equipped with internal sensors to measure important parameters such as pressure, temperature, or acceleration has limitations as an instrumental contact method [Zhou et al., 2008]. However, an optical monitoring system can be employed as a non-contact method for fault detection and identification.

Optical condition monitoring methods include off-board thermal imaging or camera-based optical methods for detecting abnormal deformation and surface features to detect tire faults during vehicle operation [Donati, 2004]. Digital image correlation (DIC) is chosen for further investigation. DIC allows for remote, safe inspection of the tires, and could potentially be implemented in an automated computer system. DIC is a well-established method for obtaining strain, displacement, and velocity measurements, especially in materials which are otherwise difficult to instrument. Physics-based modeling can provide a good understanding of the tire behavior, and give insight into observability requirements for improved monitoring systems.

In this project there is a motivation to study tire failure characteristics and also determine if deformation of rubber as the main material of tread and sidewall of the tire, can be an indicator of presence of a fault in laboratory scale and also using physics-based model. Given the constraints due to the tires on the size of haul trucks and the high cost of tires, it is important to understand the construction of tires and their likely failure modes.

## 1.2. Haul truck tire characteristics

As part of the study on monitoring the condition of haul truck tires in oilsands services, it is necessary to have an overall view of haul truck tire characteristics and the nature of their failure. This section summarizes the characteristics of haul truck tires and their manufacturing.

### 1.2.1. Tire structure

A haul truck tire structure includes layers of different materials such as steel cable, nylon and rubber resulting in nonlinear deformation characteristics. Because haul truck tires are used in rough operating conditions, they should provide high strength, compared to passenger car tires, hauler tires have more layers; i.e., 200 vs 50 layers, as structural layers increase strength and wear resistance [Netscher et al., 2008]. Figure 1-2 shows the schematic of tire structure and its different areas. The main parts of tire include the tread with grooves, shoulder, sidewall, rim, bead bundle, and inner liner.

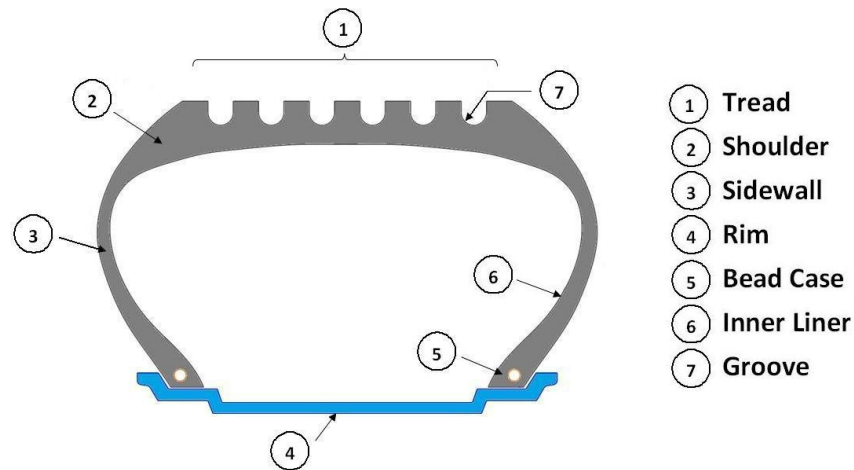


**Figure 1-2: Schematic of tire structure**

Different types of rubber material are utilized as a protective coating over the different components. The inner liner consists of layers of rubber used to seal air in the tire, replacing the inner tube that was used in the past. The bead bundle comprises of steel wire and bead filler. The bead bundle is applied to keep the tire tightly against the rim and holding the other plies and belts of the tire. Bead bundle transfer the forces from rim to the tire. Haul truck tires have 3-4 wire loops in the bead bundle and their bead filler consists of a hard rubber material.

The main parts of the body of a tire are the sidewall and tread, which are made of rubber. The sidewall of a tire prevents the tire from bending, adding lateral stability which is particularly important during cornering and hard braking. The sidewall transmits the force from the ground to the tire and also protects the body plies and maintains the air inside the tire [Li et al., 2012; McGarry, 2007].

The tread is the contact area of a tire and the ground providing traction between the road and the tire. In case of haul truck tires, the tread is made of several different types of rubber, both synthetic and natural. If the tread is too soft it will increase the chance of wear of tire; thus, tread rubber compounds used to manufacture the tread are important for tire life. Depth of grooves and their pattern depends on tire application. According to Tire and Rim Association (TRA) haul truck tires can be classified as E-2, E-3 and E-4 in the group of earthmovers. As per the tread depths is regular or deep tread design for different haulage services [OTR tire handbook, 2010]. The thicker treads have greater cut and wear resistance; however, they also generate and retain more heat. The depth and pattern of the tread are selected based on tire operating conditions. The major components of an off-road radial tire are shown in Figure 1-3.

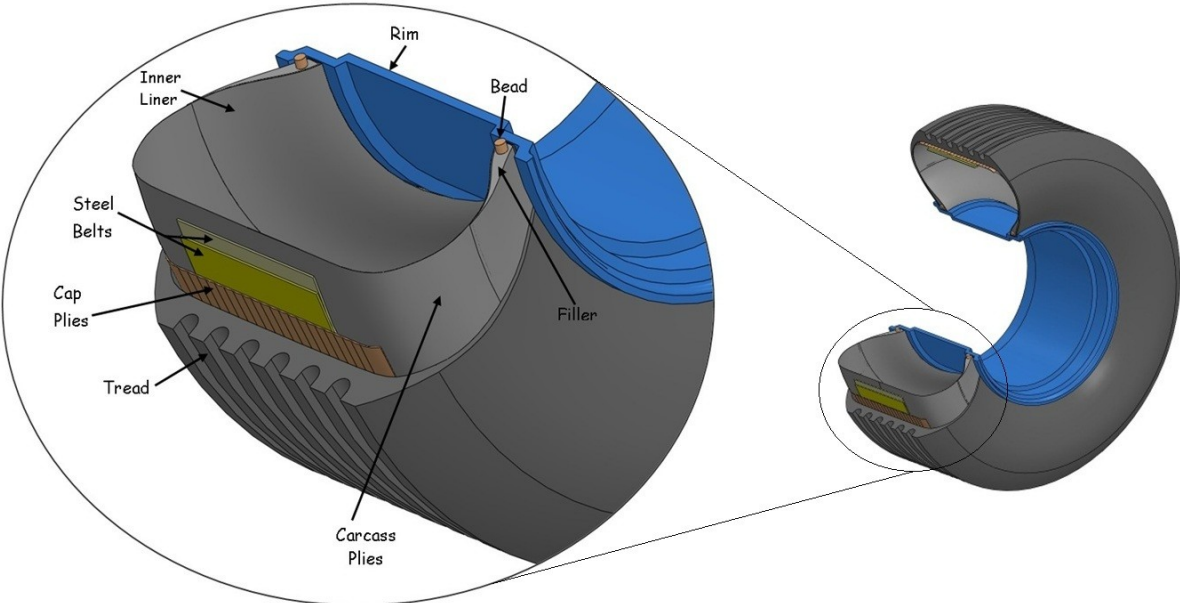


**Figure 1-3: Structural diagram of typical off-the road radial tire**

In general, according to the direction of reinforcement cord, tires are categorized into bias tire and radial tire. Bias tire is the older type of construction. Commercially trailer tires are bias but today's haul trucks mostly use radial tires. Radial tires generally use a steel carcass ply radially about the tire.

The radial tire has two main internal steel components. The first part which is steel bead, keeps carcass ply carrying the load and supporting the tread. The carcass ply runs at a 90° angle with respect to the tire bead. The carcass is fixed by wrapping around the bead wire on both sides, and the orientation is radial. The second part is the set of steel belts placed on the top of the carcass ply and under tread rubber to minimize tread distortion and improve the tire resistance to puncturing. Using steel for these belts increases the rate of heat dissipation. The carcass and belt maintain the shape of the tire when it is inflated. Compared to bias ply tires, radial tires have longer tread life, greater stability, more uniform ground pressure, and lower rolling resistance. For these reasons, radial carcass orientation is the preferred design for haul trucks [Tannant and Regensburg, 2001].

### ***1.2.2. Tire manufacturing***

There are several processes required for tire manufacturing. These processes require individual plants that are separate factories or separate parts of a larger factory. Tire manufacturing process can be summarized in four steps: preparation, assembly, curing and quality control.

The first step is preparing the different parts of tire such as rubber, textile, metal plies and beads. Then, various elements will be assembled onto an inflating drum to form the tire template. This product is "green tire" and needs to be transformed from plastic to elastic state by curing process which vulcanizes the tire using heat and pressure. The final quality verification is applied by visual inspection, x-ray, ultrasound or other methods.

There is limited published information about the details of manufacturing process of haul truck tires. However, it is clear that their fabrication is more complicated than car tires since haul truck tires must have high heat and wear resistance. Their curing time can reach to 24 hours in comparison to passenger car tire that is about 15 minutes [McGarry, 2007].

Depending on the ultimate usage of a tire, the ingredients and the amount of each ingredient vary. The ingredients for tire production are processed in batch form and the time required to process a batch of rubber compound is roughly three to four minutes. The main materials which are used for manufacturing the complex structure of a tire are rubber (both synthetic and natural), carbon black, steel cord, bead wire, nylon and other chemicals. Rubber is the main portion of tire structure.

For a radial car tire, proportion of rubber to other materials is equal but for an off-road haul truck tire, this ratio is 4 [Tannant and Regensburg, 2001]. Both synthetic and natural rubber is used in tire structure; however each of them has their own advantages. Natural rubber is used to reduce heat build-up inside the tire and also to provide higher mechanical strength. Synthetic rubber can be engineered to create particular characteristics such as cut and wear or ozone resistance. The most common synthetic rubbers being used for tires are Styrene Butadiene Rubber (SBR) and Butadiene Rubber (BR). Some of mechanical and thermal properties of various rubbers are listed in Table 1-2 [Schaefer, 2002].

**Table 1-2: Properties of various rubbers**

Rubber Properties	Natural Rubber	Synthetic Rubber	
	(NR)	SBR	BR
Main Use for Tire	General Use	Tread	Sidewall
Main characteristic	Less heat	Oxidation	wear resistance
<b>Mechanical properties</b>			
Density (kg/m <sup>3</sup> )	930	940	1000
Max Tensile strength (Mpa)	30	25	15
Max Elongation (%)	850	700	400
Young's modulus (Mpa)	5	10	10
<b>Thermal properties</b>			
Glass temperature (°C)	-73	-62	-102
min Service temperature (°C)	-50	-30	-70
max Service temperature (°C)	85	70	70
Specific heat (J/kg. °K)	1880	2000	2000
Thermal conductivity (W/m. °K)	0.14	0.25	0.25
Thermal expansion (e – 6/°K)	6.7	6.7	6.6

The percentage of synthetic and natural rubber depends on tire application which is summarized in Table 1-3 [Kogel, 2009]. Natural rubber is superior component for off-road truck tires since the resistance to heat generation, cut and tear is required for tire longer life.

**Table 1-3: Percentage of rubbers component in different tires**

Tire type	natural rubber	synthetic rubber
Off-road truck tires	80%	20%
Light-truck tires	50%	50%
Passenger car tires	45%	55%
Racing car tires	35%	65%

The complex structure of a tire and the nonlinear nature of its behavior make it challenging to determine how its properties change when a fault occurs. Studying natural rubber specimens is a simplification approach to investigate the complicated tire failure problem.

### **1.3. Project objectives**

The main purpose of this research is to develop a method to detect the existence of a failure in haul truck tire. The first step would be studying the haul truck tire response to damage, their most important failure modes and their time to failure. The second step of this project is to evaluate tire damage condition based on its dynamic characteristics. The hypothesis is that the dynamic response of the system can be related to a fault in a tire. For this reason, a model-based approach is considered for fault observability.

Literature review shows limited studies in the field of model based monitoring of tires. In this project, to investigate the effect of faults on tire behavior, different analyses are necessary to be considered. A finite-element model of specimen of rubber with a defined fault is developed for predicting strain field of rubber material. In addition, the kinematic field is measured in laboratory scale using optical techniques to validate the numerical model. This model can be used for tire stiffness calculations to simulate the dynamics of haul truck tire that can be used to detect a fault. The relationship between heat generation in rubber and its strength is studied, as it pertains to how a fault can affect rubber integrity by local temperature increase and devolcanization.

## **1.4. Thesis organization**

In this thesis, following the introduction chapter, review of relevant literature about reliability modeling of tires, tire failure and tire condition monitoring methods is presented in Chapter 2. The studies carried out on haul truck tires are discussed in Chapter 3. The topics covered in the chapter are tires failure modes, main reasons for removing tire from service, seasonal effect on their life and road quality estimation, respectively. The haulage truck tire reliability modeling based on mining open-pit database is covered in Chapter 4. Chapter 5 is devoted to the effect of presence of a failure in dynamic response of the tire. Finite element model is used to calculate the stiffness of tire. Experimental design to measure rubber deformation using digital image correlation and the results of the study are provided in Chapter 6. Finite element modeling of a rubber sample with known crack and the results comparison to the strain map obtained from experiments are also covered in this chapter. A simple relationship between tire temperature and material strength is developed for heat generation by hysteresis. Finally, Chapter 7 presents the conclusions of the project as well as introducing suggestions for the future work.

## Chapter 2. Literature Review

---

The literature of this project can be categorized in three sections which are tire failure studies, monitoring techniques for tire damages and rubber failure analysis. The first section presents the studies that investigated the tire reliability modeling and also the simulation of tire dynamical and mechanical behavior in presence of tire damage. In addition, the literature for experimental attempts to study the tire failure is covered. The second section discusses the current condition monitoring methods of tires and also reviews the optical method literature as suggested approach. Finally, a summary of rubber inspection researches is explained.

### 2.1. Tire failure studies

#### 2.1.1. *Reliability modeling of tires*

Reliability is the probability that a system will perform in a satisfactory manner for a given period of time when used under specified operating conditions. The objective of reliability modeling is to obtain a life distribution that describes the times-to-failure of the system which is based on life data analysis, using time of successful operation or time-to-failure data.

A number of researchers have modeled the reliability of tires in several applications. Dey studied field data of dumper tires and found that the failure probability model follows a Gaussian distribution, based on experimental data [Dey et al., 1994]. Other researchers examined the reliability analysis of aircraft landing-tire failure data in terms of flight time and number of landings, obtaining a model based on fitting a distribution to aircraft tire failure data [Sheikh et al., 1996]. An empirical approach was also taken in [Krivtson et al., 2002] which analyzed a certain kind of automobile tire failure. In this approach tire life data were obtained from laboratory tests, and analysis of the life test data was performed. It is illustrated that higher loads and temperature help faster aging of tire using Weibull analysis [Wu, 2002]. Artificial neural network technique is applied to conduct the reliability analysis of airplane tires. Weibull regression model of two years data are used for model validation reports the suitability of the model for future predictions [Al-Garni et al., 2011].

### **2.1.2. Tire failure dynamic modeling**

A review of the literature indicates that there are limited studies to model the tire failure and vehicle dynamic response. However, the tire dynamic characteristics have been widely studied in the laboratory and road tests. Weispfenning (1997) studied the model and signal-based methods for supervision of dynamic behavior of a vehicle. A 'quarter car' model and signal-based approach was employed to detect the tire pressure loss using the measurements of the vertical acceleration of the wheel. There is a study on effect of fault of tires on dynamic response of the vehicle, in which four degree of freedom has been used to simulate the vehicle and also experiments were developed by instrumented cleat to demonstrate the feasibility of this approach [Tiffany et al., 2009]. Sudden failure of a car tire has been identified using tire dynamic model. In this study, an indirect real-time monitoring method is presented that combines analysis of tire vibration with effective radius, to indicate that a blowout has occurred [Chen et al., 2014].

### **2.1.3. Tire failure modeling**

There are limited analytical models to describe tire failure mechanism, due to complexity of their structure and nonlinear physical properties. Challenges and developments in FEA modeling of tire mechanics are summarized by Ghoreishy (2008). There are different sources of non-linearity in structural modeling such as: geometry, material properties, and boundary conditions. All of these factors are important in tire modeling, because different materials are used in tires, and the tire experiences different boundary conditions depending on operating conditions.

Most of the initial FE analysis and models were limited to static condition of a tire. However, after development of FE programs and computer hardware, investigations show that there exist many publications in structural analysis of tires by computer simulation. In the field of tire failure analysis finite element approach is used to find the energy release rate of a failed tire in most previous works.

Ebbott (1996) first used a two-dimensional, plane-strain tire model to predict the number of cycles in a real tire, with a focus on bead separation. There are researches focused on belt edge area failure using the finite-element method and fracture mechanics concepts to calculate the energy release rate to study the initiation and growth of crack [Han et al., 2004 and Ok et al., 2007].

The durability simulation of tire by developing a three-dimensional FEM based on material force approach to define discrete crack is carried out [Kaliske et al., 2007]. The virtual crack closure technique (VCCT) is presented to compute the strain energy release rate to substitute into the law of fatigue crack growth (FCG) and consequently the endurance of the tire failure has been estimated [Wei et al., 1999, Feng, 2004 and Zhong, 2006]. There are studies about the relationship between generated heat in tire and its fracture mechanics. Fracture analysis in finite element tire model is accomplished to calculate strain energy density, and steady-state temperature distribution of tire and to solve thermo-mechanical problem of tire and its fracture behavior [Wei et al., 1999 and Yin et al. 2006].

#### ***2.1.4. Experimental studies of tire failure***

Researchers are interested in experimental approaches for tire studies because of the complex construction and geometry of tires. Bennett et al. (1975) tested pneumatic truck tires and large solid tires under controlled conditions that lead to failure. They found that truck tires failed at tread lift or blow-out which is developed by crack propagation around a tire in the outer ply area. This rate is slow at first but very rapid at the end. Fatigue tests showed that fatigue resistance at high temperatures can be significantly reduced by ageing in pneumatic truck tires.

Kainradl reported that the highest temperature of a tire under loading can be observed at tire shoulder. Because it is the thickest part of tire cross section, therefore; the largest heat generation and less heat dissipation occurs at tire shoulder [Kainradl, 1976].

In 1985, a set of laboratory wheel tests were carried out to study the frequently failure mode of bias truck tire which is believed to be shoulder separation [Prevorsek et al., 1985]. This research showed that crack initiation occurs in the rubber at the shoulder area. The other results determined the significant effect of temperature on crack propagation rate and also the high contribution of the cord to heat generation.

Castillo et al. (2006) described the design and instrumentation of laboratory-based tire testing systems, although this work focuses mainly on tire inspection, understanding tire failures and damage mechanisms.

In the past, limited studies employing IR thermography for tires were reported, mainly in the area of tire tread wear [Kerchman and Shaw, 2003]. Miller et al. (2000) used thermal image inspection system to predict truck tire faults in the field and laboratory scale. Images have been recorded by thermal camera in the lab from the tire running on the tire test machine (dynamometer). Authors indicated that by comparison of thermal images recorded in the lab and in the field, the suggested test method is effective for preventive tire fault detection.

Some of the experimental works studied the effects of operating conditions on the tire thermal behavior and showed that the vehicle load has the most effect on tire temperature in comparison to speed, inflation pressure and slip angle [Yeow et al., 1978]. Oh et al. (1995) measured the tire surface temperature by an infrared camera and the temperature of the contained air by a thermocouple.

Other studies examined the temperature distributions in the tires for various structures, materials and thermal characteristics of the tire [Netscher et al., 2008]. Allouis et al., (2012) presented an approach to measure the thermal diffusivity of tire by thermocouples and IR camera. The measurement of the thermal diffusivity is performed with a simple identification technique based on the experimental data derived from the set up test and a theoretical model.

## **2.2. Tire monitoring methods**

### **2.2.1. Current condition monitoring methods**

Since the late 1990s several companies have implemented real-time tire monitoring using pressure and temperature sensors at a number of locations within the tire with embedded wireless sensors that send signals to a receiver on the truck [Otraco, 1993, Brothen et al., 2008 and Carter, 2011]. This monitoring approach is effective for highway truck tires, but less suited for off-road tires, which are much larger, reducing the sensitivity to local faults that are not near a sensor. There is also a rim-mounted pressure sensor intended to flag general over-pressure and under-pressure conditions. Indirect approaches to tire monitoring have been attempted using acoustics [Orrell, 2008] for on-road tire monitoring; but these methods are not appropriate for equipment operating off-road with large changes in speed and road conditions.

Periodic visual inspections are made to identify off-road haul truck tire incipient failures by features such as minor tread cuts, sidewall cuts, and bulging. Inspection results are used to determine whether the tire needs replacement or repair [Zhou et al., 2008]. This process of inspection and assessment is very time consuming and depends on individual expertise.

There is also the possibility that a new tire has an internal defect, which does not become apparent until after the tire goes into service. The x-ray inspection techniques have been developed to inspect new tires for structural integrity, but it has not been evaluated on used tires [Wilson, 2010]. Also, the system requires the tire to be off its rim, and so it cannot be used as a field monitoring method. There has also been some proof-of-concept work done on using microwave-based imaging NDT for measuring the effect of tread cuts, but not yet for commercial systems. Microwave imaging can detect internal faults in composite materials that do not have significant conductivity.

Since the interval between two scheduled inspections may be too long to catch early failures, operators and maintainers would prefer to have a method of field monitoring of haul truck tire to detect early indicators of impending faults. A noncontact method that can be employed while the truck is in operation (or stopped briefly in the field) would be ideal.

### **2.2.2. Optical methods for tire condition monitoring**

Noncontact, optically based methods for assessing tire damage are being considered to decouple a complex inspection task from operation of the truck. This would provide a low-risk environment for workers and would not take the equipment out of service for its inspection [Malamasa et al., 2003]. In comparison to installing physical gauges on tire, optical method can obtain full-field measurements, removing error due to gauge separation, and eliminating the need for wiring or bulky wireless transmitters [Lipsett et al., 2011].

A typical optical system includes hardware for illumination and detection, and software for analysis the gathered data. The general approach for fault detection in this method would be to determine a change in shape of the surface of the tire, and to send status information to a tire maintenance technician when potential anomalies are identified [Ruel et al., 2005].

There are a number of optical approaches that can be considered. Line-of-sight laser distance measurement can use a triangulation, interferometric, phased-shift, or time-of-flight approach [Donati, 2004]. The first two methods offer high resolution but generally have a limited range of operation. The latter two methods are usually used for longer distances (greater than 10 m). For all cases, a single measurement at a single location is determined. To resolve a surface shape, this measurement location needs to be scanned over a region of interest, which has a minimum scanning time requirement.

Surface shape and distance measurement can also be determined using two-dimensional imaging techniques [Cloud, 1998]. Stereo-imaging with a minimum of two cameras can determine surface shape by correlating the position of a resolvable object in an overlapping field-of-view. It has been shown that increasing the number of cameras viewing the same overlap region results in a significantly more accurate system [Elsinga et al., 2006]. High, changing contrast, such as a random array of dots on the surface gives best results for determining surface position and shape. These surface marks can be tracked to a resolution on the order of the contrast shape. In low contrast situations, topical illumination (structured lighting) can be used to generate a known illumination pattern. Changes in the pattern can be

used to determine shape and position of the surface of interest. A higher resolution variant of this approach is projection Moiré interferometry [Cloud, 1998], which can be used with a standard fringe-processing method that relies on a simple analytical model to recover topographic information. Higher resolution interferometric techniques such as shearography, which measures change in shape (displacement gradient) and electronic speckle pattern interferometry (ESPI), which measures distance, can also be used to determine the 3D shape of an object. While these techniques have a higher resolution than the wavelength of the illumination source that is used, there are typically limited in range and are sensitive to environmental conditions.

Digital image correlation (DIC) techniques are relatively robust and have been developed to have measurement resolutions on the order of interferometric techniques [Chu et al., 1985; Réthoré et al., 2008]. The approach requires high, relative image contrast and, for high position resolution, a large number of pixels in the camera array. Commercial, consumer-grade cameras now commonly have high pixel counts (>10 megapixels) and good light sensitivity, making the application of this approach in an industrial setting relevant. An inspection system based on digital image correlation would consist of a number of cameras with an overlapping field of view, illumination optimized to provide high contrast, and software for control and processing of images. The narrow field of use of the inspection system would require the development of unique algorithms for interrogating processed data to locate faults in the tire and generation of useful report information to the user.

Digital image correlation and speckle was developed to determine displacements of loaded bodies. Displacement of flat and curved surfaces by using two cameras was studied in the project which approved the hypothesis that the three-dimensional deformation of a surface can be determined by combining a digital image correlation algorithm with stereoscopic photogrammetric analysis [Jetter et al., 1990]. Image processing has been used as a nondestructive testing in industrial production to inspect the flaws. As a fault detection study an aluminum casting were examined where the changes in pixels of the image occurred and the potential defects could be tracked by using CCD-camera and image processor [Mery, 2002].

Early attempts to use vision inspection techniques of tires were limited by the available hardware [Blackwell, 1989]. Optical technique which was applied to measure the deformation and strain of tires was called fringe projection. This method has been used to test aircraft tires which were subjected to different amounts of loads. There were some difficulties to select a fixed reference point to capture the images and requirement of additional devices to solve the problem [Lin et al., 1994].

Behavior of a car tire under extreme loads was studied by using stereo camera which provided deformations and strain of tire side wall. These images were recorded by the ARAMIS system during the test and computed based on three-dimensional digital imaging correlation (DIC) method [Erne, 2009]. Also agricultural tire surface strains were measured by using DIC and accuracy of method was tested by a sample of rubber under different loads [Moser et al., 2010]. Another application of image processing procedure for tires was monitoring tire-surface contact interaction and the influence of load and pressure on contact length was studied [Castillo et al., 2006 and Ivanov, 2010]. Studies show that DIC method is ideal for tire surface strain measurement because it does not require any instrumentation on the tire itself [Moser and Lightner, 2007].

A developing strategy is the use of edge-detection and other image processing algorithms on low-resolution JPEG tire images to detect external cuts, such as Wiseman (2010). As with digital image correlation, this method is sensitive to changes in tire color, surface texture, and orientation also it may be quicker than 3D surface strain measurements.

There is another optical inspection method which uses the thermal images as a non-destructive test (NDT). Rubber tire delamination was studied by using infrared thermography [Gros, 1997]. Temperature measurements were obtained by infrared cameras to determine the truck defects. Brake problem classification was done for various trucks [Green, 2009]. There may be potential to use thermography for fault detection where heat is generated within the fault. Heat generation is likely a function of tire inflation, road conditions, driving speed, load, and fault type.

### **2.3. Rubber failure studies**

An accurate tire model requires detailed constitutive relationships describing the material behavior of the belt, tread, and bead under loading. This is approached by measuring the strain of sample specimens under the desired loading conditions, such as in Sokolov (2010). In the field of failure analysis, most previous works are based on experimental measurements of rubber components. Chevalier et al. (2001), and Moser et al. (2007, 2011) use DIC to measure strain in rubber test specimens and validate predictions from FEA models. These papers suggest that it could be possible to measure strain in a rubber tire using DIC, using a specially prepared sample with a high-contrast dot pattern.

A number of studies have been done to characterize the crack growth behavior of rubbers by measuring different parameters such as temperature, using thermocouples, or crack growth rate, using fatigue testing machines. Kaang et al. (2006) used ASTM standards for specimens of reinforced rubber with length and width of 200 and 20 mm, respectively, and an initial edge cut, about 30 mm long. They tested the rubber specimen under cyclic loads to find crack growth rate as a function of the tearing energy.

The different standard test specimens that can be used for rubber fracture analysis tests edge cracked tension specimen, full cracked tension specimen and trouser test specimen. In single edge cut tension specimen, the energy release rate has an especially simple form; and cut growth results only in translation of the crack tip. The trouser specimen has been used in early studies of fatigue crack growth in rubber [Mars and Fatemi, 2002].

Mars and Fatemi (2004) reviewed the literature of factors that affect the rubber life. The failure modes of rubber which are related to heat generation mechanism has been called thermal runaway which can happen at sufficiently high strains and frequencies. They reported different studies has been proved that temperature rise cause severe degradation of the rubber and thick components exhibit a larger temperature rise than thin components. Environmental temperature can affect both the short and long term fatigue behavior of rubber.

## Chapter 3. Haul Truck Tire Failure

---

This chapter summarizes the studies carried out on haul truck tires different failure modes and most common damages reported as the reason of tire removal from oilsands service. In addition, the environmental parameters particularly seasonal effect and road condition on haul truck tire life is discussed.

### 3.1. Haul truck tire failure modes

There is currently no standardized system for classifying tire damage between different corporations or industries for large tires. In general, as summarized in Table 3-1, there are various failure modes that could happen to different parts of the tire [Zhou et al., 2008].

**Table 3-1: Tire removal reasons**

<b>Interest Area</b>	<b>Removal Reasons</b>
<b>Tread</b>	Cuts
	Separations
<b>Shoulder</b>	Cuts
	Separations
<b>Sidewall</b>	Cuts
	Separations
	Radial splits
<b>Bead</b>	Separations
	Flange erosion
	Cracking
<b>Liner</b>	Splits
	Lifting liner
	Wrinkled liner

The most common failure mode of light duty tires such as radial passenger and light truck are sidewall flex break, belt separation, tread separation and loss of air through a break in the tire [Gardner et al., 2006].

Tread and sidewall of haul truck tires are more prone to damage. Two example images of haul truck tire failures are shown in Figure 3-1. A sidewall cut, shown in Figure 3-1(a), is a break in the sidewall due to over-inflation or driving over a road hazard (material lying on the road or a curb). A tread cut, shown in Figure 3-1(b), is a localized break through the tread rubber, which can incur due to road hazards, foreign objects, over-inflation, or high-speed operation. Tread separation is a loss of a section of tread and localized wear in the tread above the separated area. This fault can be caused by excessive heat generation during driving, which is aggravated by poor road surface conditions.



**(a) Sidewall cut**



**(b) Tread cut**

**Figure 3-1: Digital images of haul truck tire failures  
(Used with permission of Syncrude Canada Ltd.)**

The failure modes of rubber which are related to heat generation mechanism has been called thermal runaway which can happen at sufficiently high strains and frequencies. Different studies has been proved that temperature rise cause severe degradation of the rubber and thick components exhibit a larger temperature rise than thin components. Environmental temperature can affect both the short and long term fatigue behavior of rubber as the main component of a tire.

Syncrude Canada Ltd. as an integrated oilsands surface-mining and heavy-oil refinery operation maintains a database of haul truck tire failures. A tire usage database is maintained by the operating company and a tire service company, which is contracted to store, install, inspect, repair, and replace the tire inventory. The database includes the tire type and serial number, its usage (in number of nominal operating hours), and a diagnosis of the mode of damage during operation at the end of tire life. The database over a five-year period is the source of information used to develop the histograms related to tire life.

Figure 3-2 illustrates the different failure modes of haul truck tires and the specific portion each mode from all possible failures that have been recorded in the database. It is shown in this figure that almost half of damages are related to tread area which can be in the form of tread cut, tread separation, impact tread and worn out tread. Tread cut and separation are reported to be the most dominant tread failure types. Sidewall failure can be in the mode of sidewall cut, separation and impact including 34% of failures as the second important damages that could happen to the tires. There are other types of failures in haul truck tires with the predominance of turn up separation (12% of all failure types) and also bead damages, heat separation, cracking in liner and some rare failures.

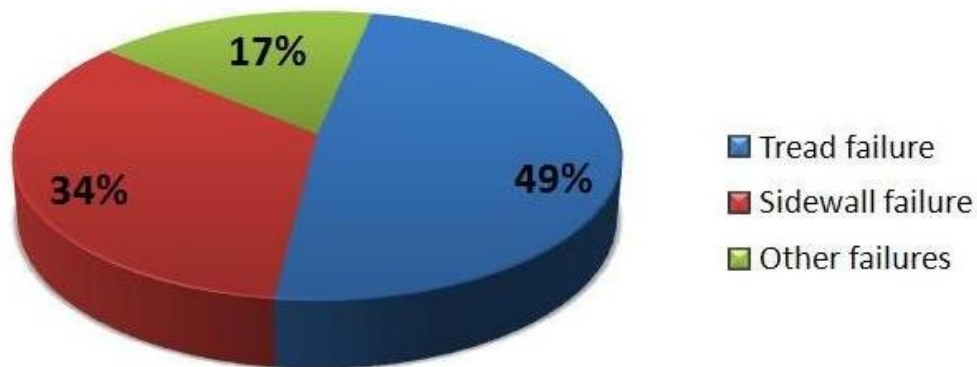


**Figure 3-2: Proportion of different failure modes of haul truck tires**

Figure 3-3 shows the frequency of different failure modes of haul truck tires based on their operation hours. The x-axis shows the time that tires are removed from service because of their damage and y-axis presents the number of failures.

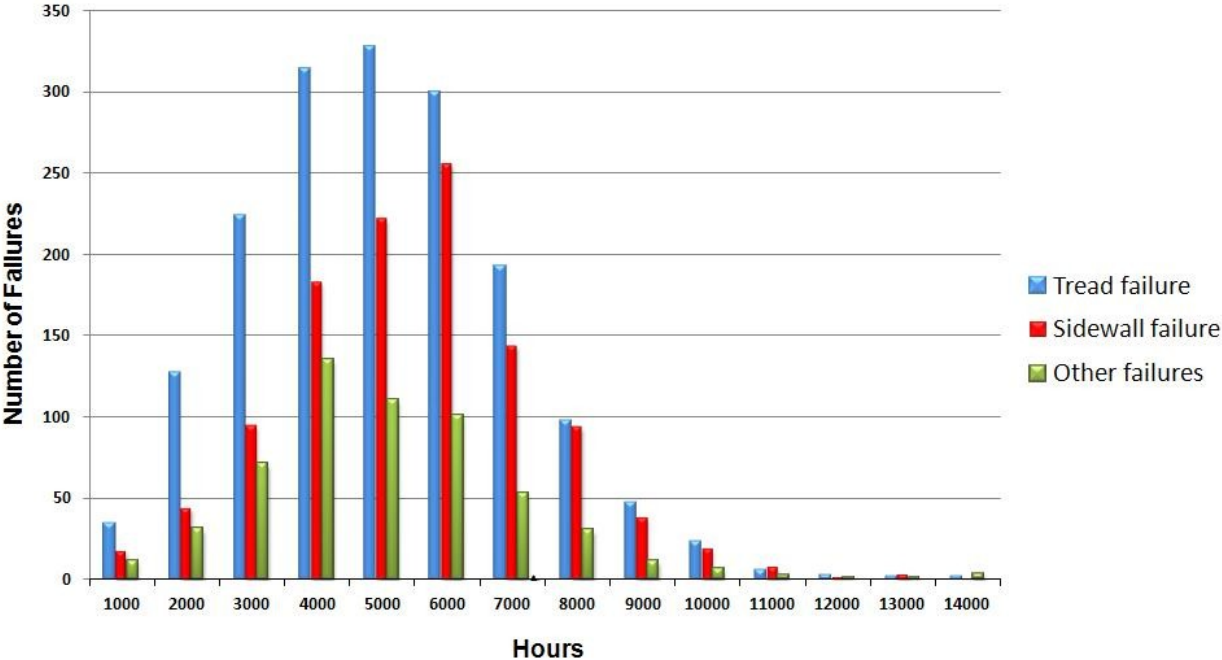


Figure 3-3: Frequency of modes of damages in haul truck tires

As is evident from this figure, the most common failures are tread failures for all operation hours while the most probability can happen at 4000-6000 hours. Sidewall damage is less dominant than tread but more frequent than other failure types. In the early hours the proportion of tread damages can be determined even to be 3 times of sidewall damages but for higher operating hours the difference is smaller. These data is used to calculate the Mean Time to Failure (MTTF) for each failure modes which are 5036, 5524 and 5019 hours for tread, sidewall and other failures. The values of MTTF show that sidewall damages are reported to happen slightly later than all other failure types.

### **3.2. Common causes of haul truck tire failures**

In comparison with tires for highway vehicles which are designed for controlled road conditions, tires in off-road service experience highly variable operating conditions [Bolster et al., 2005]. The factors affecting tire life include: road conditions (curves, grades, super-elevation, haul length, road surface quality and maintenance), operating conditions (average speed, speed in curves, haul distance), truck conditions (weight distribution, condition of suspension struts, air pressure in tires, tire matching, tread depth, and tire type), and weather (temperature and precipitation) [Tannant and Regensburg, 2001].

There is a range of possible damage mechanisms, which fall into two general categories: fatigue endurance, and damage due to some initiating event, such as driving over a rock or hitting an obstacle.

Based on Michelin data-book (2011), for small tires (smaller than 25" diameter) the failure may result from overloading or excessive speed. In the case of larger tires under/over-inflation pressure can be main factor of tire damage and also in comparison to highway vehicles, mining truck tires are operated at one of the most rugged environments, 24 hours a day, in all seasons. Poor road condition and driving style can lead to off-road truck tires damages.

Separation and related tire failures can occur due to heat generation as the tire rolls and flexes [Matthews and Nowatzki 1989]. Heat generation in a tire makes it less efficient and more susceptible to damage such as wear rate, casing fatigue rate, heat separation chance, probability of tire burst and repair failure and also less resistant to cutting.

During normal operation tire generates heat. It starts to work in the environment temperature at the beginning of rolling and finally reaches to steady temperature [Cui et al., 2011]. When a tire rotates, it deflects and stores energy. As it is shown in Figure 3-4, tire can be modeled as a spring and a dampener. The spring stores energy and releases it while the dampener absorbs some of energy in the form of heat.

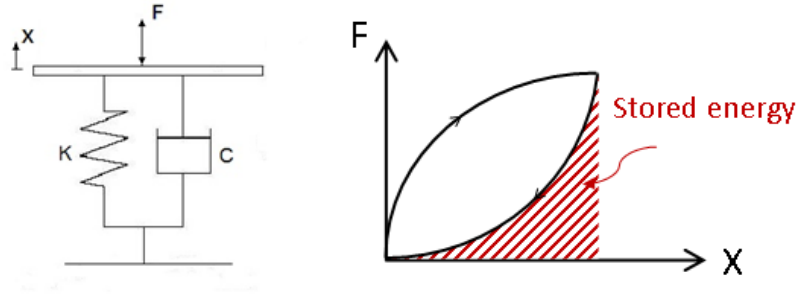
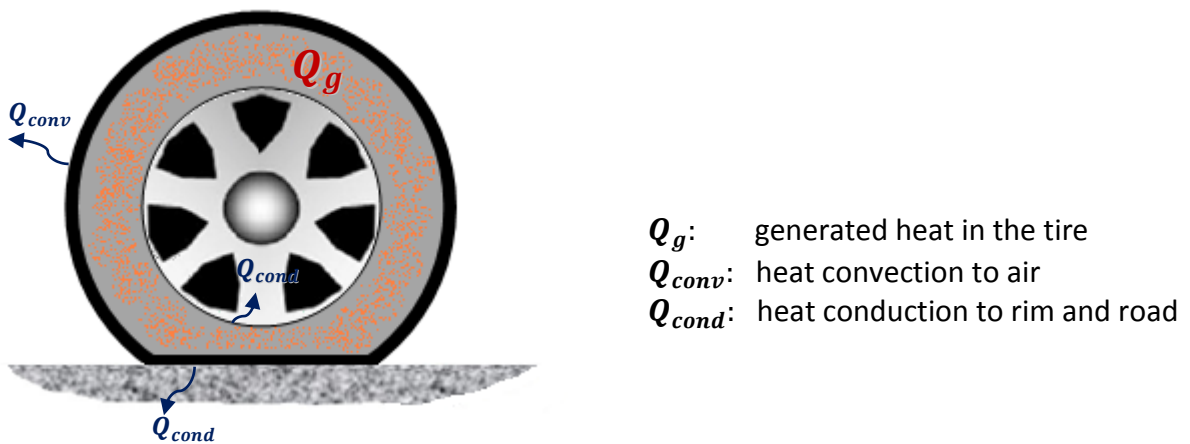


**Figure 3-4: Model of tire as spring-dampener and its stored energy**

As it is presented in Figure 3-5, the stored energy in the tire is partly transferred to the environment due to conduction and convection; whereas considerable amount of stored energy is retained in the tire in the form of heat.



$$\text{Stored energy} = \text{Generated Heat } (Q_g) - \text{Dissipated Heat } (Q_{conv} + Q_{cond})$$

**Figure 3-5: Tire heat transfer and heat generation**

The main reason of the heat generation in tires is the friction between molecules of rubber elements under a deformation by compression, tension or torsion. This phenomenon is called hysteresis effect. If the rate of energy build up in the tire is greater than the rate of dissipated energy to the environment, the temperature of the tire increases.

In addition, the friction between road and tire would be another source to increase temperature. In addition, after part of a tire is torn, separated surfaces of the crack can rub together and may build heat [Conant, 1971]. The loading, speed of vehicle, tire pressure and ambient temperature affect heat generation in a tire. If generated heat is faster than it can be radiated into the air, it gradually builds within the tire [Netscher et al., 2008].

The diagram to describe the heat generation process in tire is shown in Figure 3-6. This diagram illustrates that hysteresis effect and tire road friction are the main reasons for heat generation but crack initiation in tire affects the heat generation rate in tire.

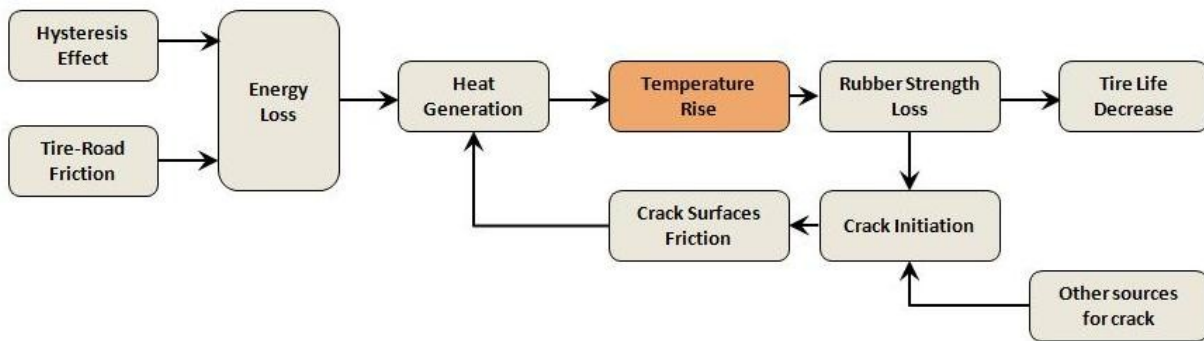


Figure 3-6: Tire heat generation diagram

### 3.3. Seasonal effect on haul truck tire failure <sup>1</sup>

The haul truck tires are operated under very severe climate conditions, with the ambient temperatures ranging from  $-40\text{ }^{\circ}\text{C}$  to  $+40\text{ }^{\circ}\text{C}$  at the Syncrude mine in Alberta, Canada. The failures may be initiated by overstressing the tire resulting from the high stress and deformation under a variety of ambient temperatures at different seasons of the year. This section observes this effect on mine tires failures.

#### 3.3.1. Seasonal effects on tire life

This section considers an analysis of tire failures for an operating oilsands mine, where tire life is affected by factors that relate to seasonal changes. An evaluation was conducted to understand the dominant modes of damages and at what times of year they are most frequent. The Syncrude tire database is the source of information used to develop the histograms related to tire life and when during the year tires are removed from service. The seasonal variability in diagnosis of what damage during operation ends the tire useful life is shown in Figure 3-7.

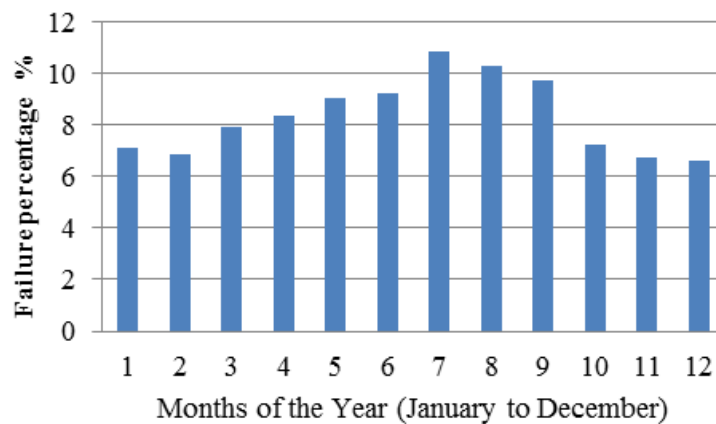


Figure 3-7: Overall seasonal variation in tire end of life

---

<sup>1</sup> A version of this section has been published as a journal paper in “International journal of Strategic Asset Management”, 2013, 13 pp.

From the figure, it is clear that tires fail more often in spring and summer than in winter. This histogram only shows when tires are taken out of service. In reality, a tire may incur damage during operation that takes some time to manifest visually in such a way that the tire is removed from service.

### 3.3.2. Tire life for different damage modes

Time distributions for the most frequently occurring modes reveal for tread cut and separation a nearly normal distribution with a mean duration of about 5000 hours. Sidewall cut and impact tread damage both show evidence of early mortality, which may be due to unsuitable operating conditions for the tire type.

When the most frequent modes are plotted with respect to time of occurrence during the year, the data yield the chart shown in Figure 3-8. As illustrated in the graph tread failures are more often damages and increases by increasing the weather temperature. It can be seen that tires fail more often in spring and summer than in winter.

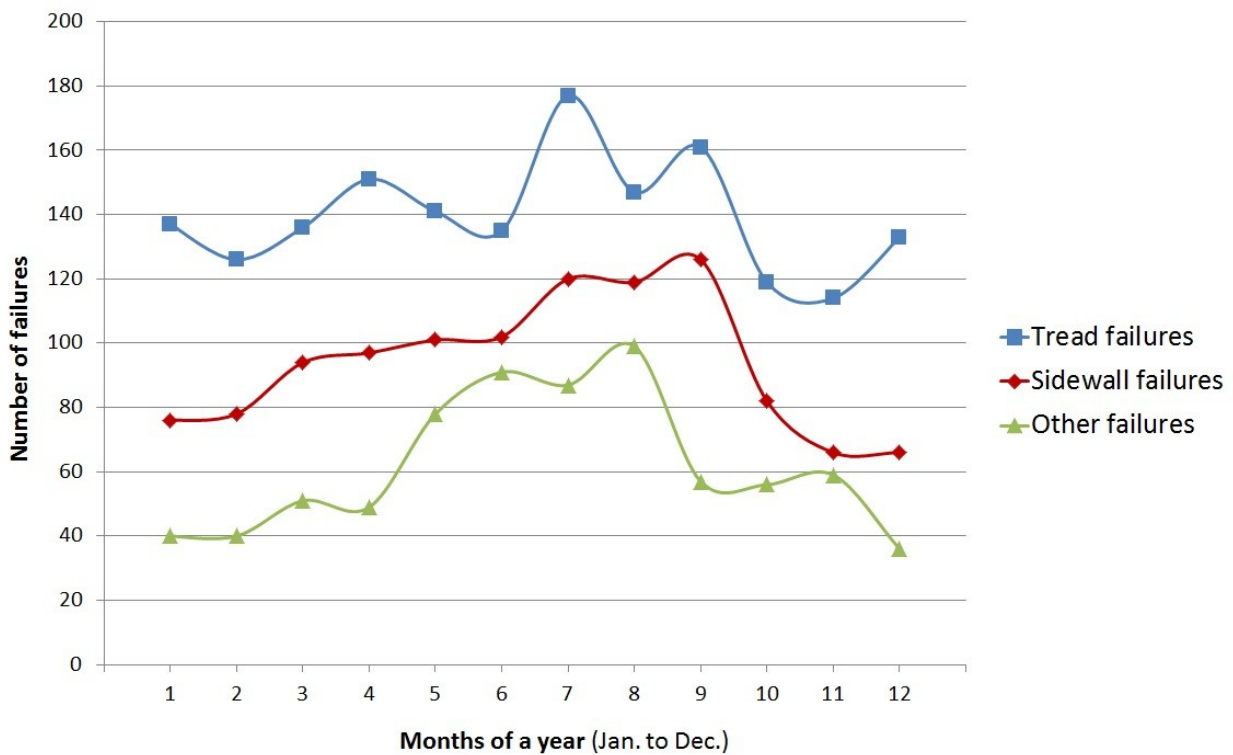
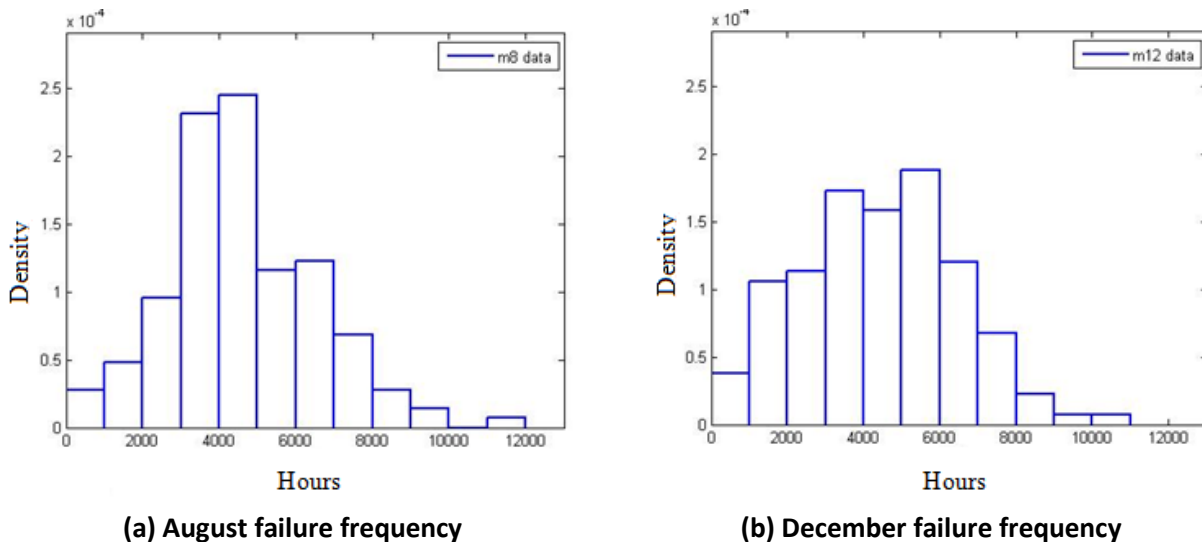


Figure 3-8: Frequency of major modes of tire damage by month

The data was then analyzed for each month when failures occurred, and the best-fit distribution and parameters were determined. Generally, the density and peak change throughout the year. This change in the distributions happens for particular modes as well.

Figure 3-9(a) shows the distribution for tread cuts during August, which is mid-summer when roads are warm (above +20 °C on average) and the shear strength is at its lowest. In contrast with the summer tread cut distribution, in December, when the average temperature is below -20 °C, the distribution is flatter and has a lower density, as shown in Figure 3-9(b). The data indicate that seasonally varying factors may affect tire life. As tires last on average only about a half year, there may be winter factors that affect summer failures; but it appears that there may be chronic endurance factors that lead to progressive failure of tires, while other injuries to tires during operation lead to end-of-life after only a short time.



**Figure 3-9: Frequency of tread cuts in August and December**

Road conditions and ambient temperature may be causal factors. In summer, rolling resistance is high in the pit (on oilsands benches). Rolling resistance causes the tires to heat up and may reduce the performance of the tire. Operators tend to drive more slowly when resistance is high. More importantly, however, any hard lumps of hard sharp material in the road bed may erupt to the surface, presenting a protuberance that can cut the tread.

In winter, the benches and roads do not require as much ongoing maintenance to keep the road surface smooth, which allows trucks to be driven faster, increasing productivity. Ironically, in winter the truck tires actually run slightly hotter (averaging  $\sim 33\text{ }^{\circ}\text{C}$  ) than in summer (averaging  $\sim 30\text{ }^{\circ}\text{C}$ ) [Syncrude staff, 2011].

### **3.4. Road quality estimation**

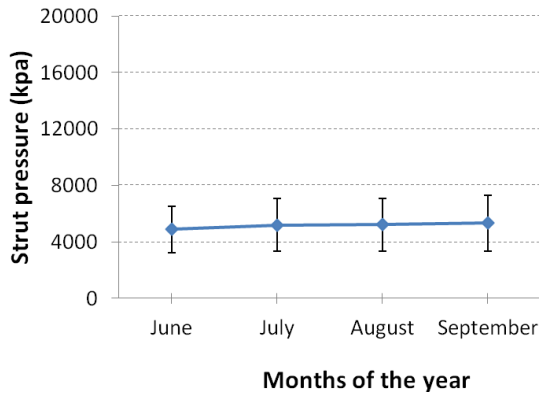
Since there appears to be a relationship between the road quality and tire life, some measure of road quality would help to predict tire damage accumulation. Road quality can be assessed as the variability in road elevation.

Uneven roads have high variability with respect to distance travelled. It is possible to use the variability in strut pressures as an indirect measure of road quality, particularly when a single type of truck is used in a fleet. Haul truck suspension struts are pressurized to act as spring-damper elements between the wheel axle and the truck body.

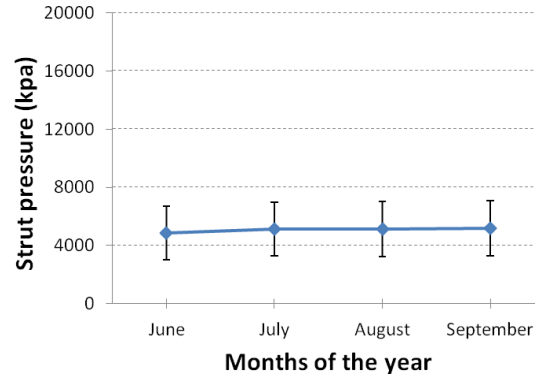
The strut pressure is the only observable feature of vehicle vertical motion; but there are four struts. Onboard machine systems, for example, can assess road conditions and quantify the severity of the haul, with sensors measuring strut pressure data. Many of these systems can then transmit real-time data to operators and maintenance personnel about problem areas to avoid and correct.

Strut pressure variability that is seen in all four struts likely indicates something that is happening to the entire vehicle due to road conditions, rather than faults in individual components (tires or struts). There are also faults signatures that can be linked to problems within the strut itself.

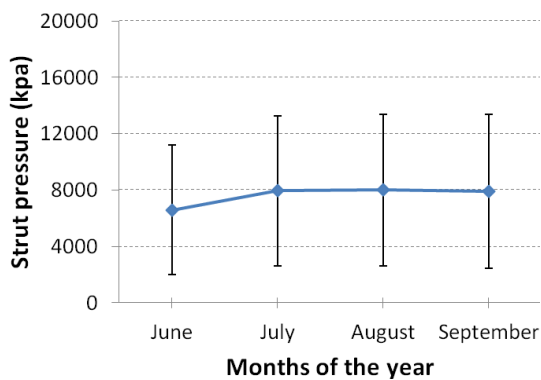
Figure 3-10 shows the mean and variance for the left/right front strut and left/right rear strut respectively during summer time. The database of other seasons has not been provided from oilsands services company.



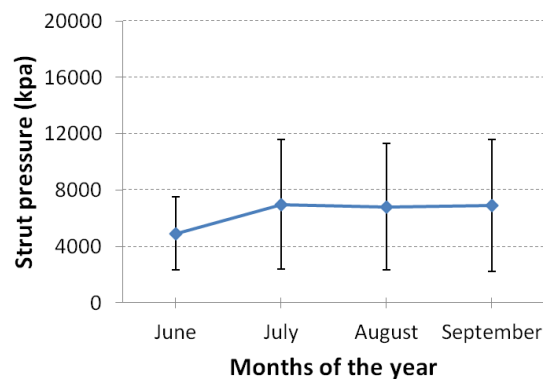
**(a) Left Front Strut Pressure**



**(b) Right Front Strut Pressure**



**(c) Left Rear Strut Pressure**



**(d) Right Rear Strut Pressure**

**Figure 3-10: Strut pressure monthly mean and variance**

Mean values of strut pressures are in the range of 4000-8000 kpa for front and rear wheels but the rear strut pressure standard deviations are about 2-3 times larger than those for front strut pressures [Syncrude staff]. It is because of loading and unloading conditions that can affect the rear part of the truck. Mean pressures are slightly lower in June for all struts. This may be due to smaller payloads in the truck during June, or longer periods of time when the truck is unloaded.

This is an example of the need for clear descriptions of operating time, and how analytics are calculated. This study shows that there is a seasonal effect on haul truck tire life in oilsands service. Possible root causes relate to haul road condition and how operators drive on rough roads.

Drivers have air-ride seats, and so they have little direct perception of changes in ride quality if the rear struts or tires are having problems. Figure 3-10(d) shows that the right rear strut was generally under-pressurized. This affects payload estimation as well as affecting structural stress on the vehicle. Right rear tires are more prone to damage, partly because the driver is located at the front left of the vehicle, and so it is more difficult to avoid obstacles while reversing and turning.

The strut pressure measurement has been suggested for road quality estimation. With an on-board global positioning system (GPS), the road conditions can be mapped. Work has been done on using vibration analysis [Thomson et al., 2003] coupled with GPS, but persistent strut pressure variability in a certain location would tell a truck dispatcher that road maintenance equipment should be deployed to fix bumps, smooth a ramp, or grade a road [Hajizadeh and Lipsett, 2013].

### **3.5. Concluding remarks on tire failure studies**

This chapter presented the studies on haul truck tire failures. There is some uncertainty about consistency of damage mode classification. This analysis assumes that all modes have been categorized correctly, when in fact there is considerable interpretation required by technicians, and there is not always agreement between the supplier and the field technicians with respect to whether a tire has a particular mode of damage. This is important when attempting to determine whether tires are being removed from service due to high-load external factors, such as hitting rocks or braking on ramps, or end-of-life from internal fatigue damage.

The analysis shows that there is a seasonal effect on haul truck tire life in oilsands service. Possible root causes relate to haul road condition and how operators drive on rough roads. Some limitations of the analysis are the classification accuracy of faults and the limited understanding of the severity of service. These are opportunities to establish clear benchmarking metrics and to assess measures beyond what are currently used, including higher data sampling rates on strut pressures to look for shock loading, measuring tire internal pressure and temperature, and linking pressure variations to road locations.

## Chapter 4. Reliability Model of Haul Truck Tires<sup>2</sup>

---

### 4.1. Reliability modeling

Reliability modeling based on lifetime distributions is a widely used reliability assessment method [Modarres et al., 2009]. This technique allows predicting the reliability of a system in several steps, as shown in Figure 4-1. After collecting data with respect to the useful lifetime of components in a system of interest, a probability distribution function can be fitted to statistical data, and related parameters of chosen distribution is calculated by mathematical methods. The goodness-of-fit for the distribution model is tested to check whether the result is acceptable; if chosen distribution is rejected by testing, then the procedure should be repeated on other distributions until an acceptable distribution model is found.

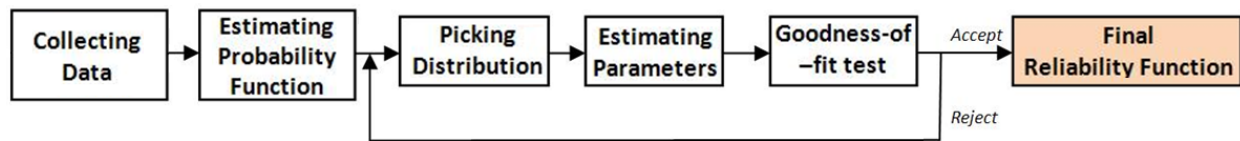


Figure 4-1: Finding reliability model algorithm

The present work examines the useful life distribution of haul truck tires in oilsands service, in order to quantify the effect of tire reliability on maintenance time and costs, risk to personnel and equipment, and mine productivity. A database of tire failures was used to generate the reliability pattern of haul truck tires. The remainder of this section describes how this distribution was found for tire failures at one mining operation, and offers insights into what types of condition monitoring should be done on these components for early detection of important fault types in a timely manner.

---

<sup>2</sup> A version of this chapter has been published as a conference paper in “Proc 24th COMADEM Stavanger Norway”, 2011, 10 pp.

#### 4.1.1. Collecting data

Tire failure data have been collected over five years (2005-2010) at Syncrude Ltd., which includes the data of about 3,500 haul truck tires with 57 – 63 in (1.4 – 1.6 m) rim diameter, of which 95.5% are Michelin brand and the rest are Bridgestone, Titan, and other brands. The tire life is presented in terms of the “Net Operating Hours” (NOH) when the tire was scrapped, based on total distance traveled by the tire over its life and estimated average speed of the trucks in the fleet. The database also identified the failure mode for each scrapped tire.

#### 4.1.2. Estimating failure probability function

To develop a distribution model, it is necessary to choose an appropriate probability distribution to fit the data. The first step is to plot a histogram of time-to-failure data to choose the corresponding distribution. This pattern can be found by using an estimation formula for the probability density function; where given time to failure can be used as known parameter:

$$\hat{f}(t_i) = \frac{1}{(n + 0.4)(t_{i+1} - t_i)} \quad \text{Equation 4-1}$$

where:

$\hat{f}(t_i)$  = estimated probability distribution function

$n$  = total number of data

$t_i$  =  $i^{\text{th}}$  time to failure

$i = 1, 2, 3, \dots, n - 1$

After estimating  $\hat{f}(t_i)$ , the pattern of probability function is shown in Figure 5.

Estimation of the cumulative distribution function (CDF) is defined as follows:

$$\hat{F}(t_i) = 1 - \left( \frac{n - i + 0.625}{n + 0.25} \right) \quad i = 1, 2, 3, \dots, n \quad \text{Equation 4-2}$$

If the result of plotted  $\hat{F}(t_i)$  versus time for the chosen distributions can be presented as a straight line in transformed form, the distribution would be acceptable.

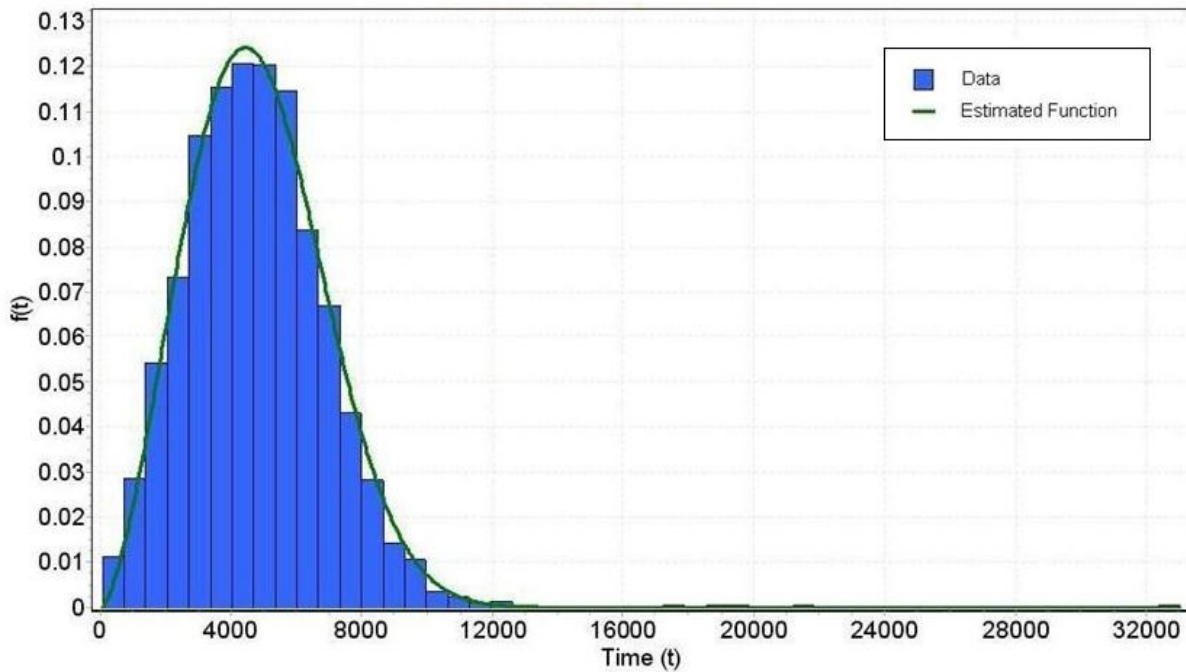
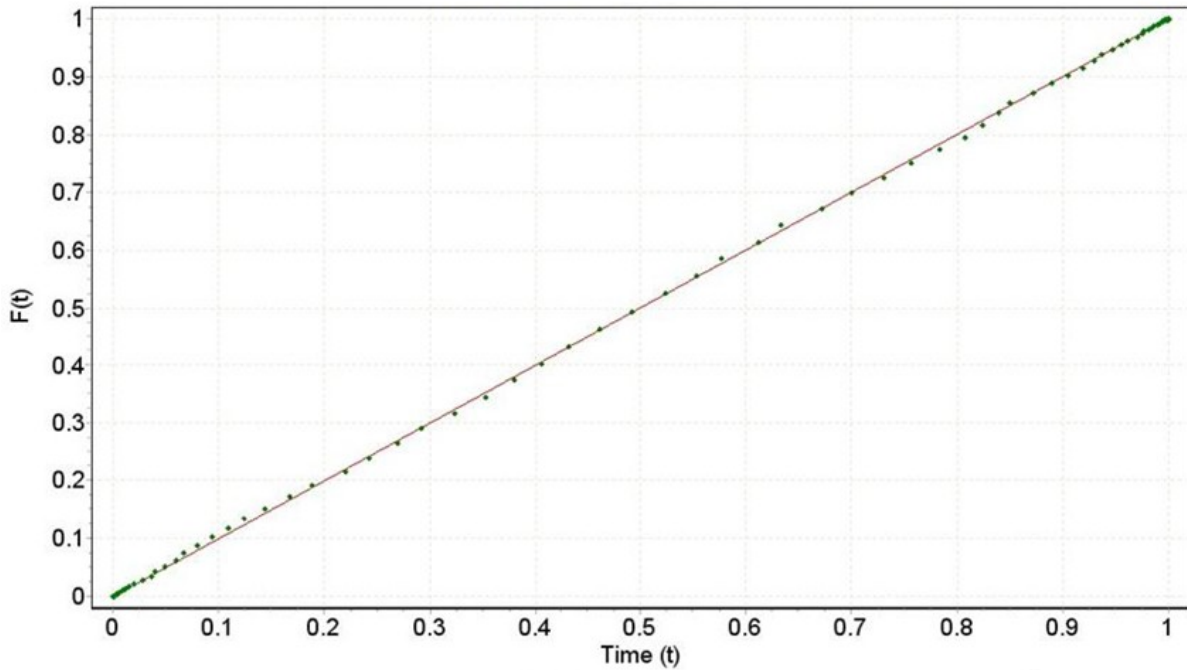


Figure 4-2: Estimated probability function

#### 4.1.3. Fitting the distribution

Based on the obtained probability function pattern, some potential distributions which are close to the pattern are checked as options to describe the data. For this purpose, the transformed cumulative distribution function (CDF),  $\hat{F}(t_i)$ , is plotted versus time. If the result of plot for the chosen distribution can be presented as a straight line, the distribution would be a candidate for final model.

The transformed  $\hat{F}(t_i)$  versus time plots have been provided for five distributions; Normal, Log-normal, Exponential, and 2 and 3-parameter Weibull distributions as it is shown in Appendix 1. From the total set of data for all failure modes, a 3-parameter Weibull distribution was found to be the best fit that can be presented as straight line to  $F(t)$ , as shown in Figure 4-3.



**Figure 4-3: Fitted cumulative distribution function (CDF)**

#### **4.1.4. Estimating parameters**

For estimating the parameters of distribution, there are several methods. Maximum likelihood estimation (MLE) is one of the most powerful methods [Tobias, 2012] used for fitting a model to data and providing estimates for the parameters of the model. The idea behind maximum likelihood parameter estimation is to determine the parameters that maximize the probability (likelihood) of the sampled data.

As already discussed, the chosen distribution for the data set is a 3-parameter Weibull distribution, which is defined by:

$$f(t) = \frac{\beta}{\alpha} \left(\frac{t-\gamma}{\alpha}\right)^{\beta-1} \exp\left(-\left(\frac{t-\gamma}{\alpha}\right)^{\beta}\right) \quad \text{Equation 4-3}$$

Where:

$f(t)$  = probability density function

$t$  = time

$\alpha$  = Scale parameter ( $\alpha > 0$ )

$\beta$  = Shape parameter ( $\beta > 0$ )

$\gamma$  = Location parameter ( $\gamma \leq t < \infty$ ) ( $\gamma = 0$  Yields the 2-parameter Weibull distribution)

The likelihood function  $L$  is defined by the following product:

$$L = \prod_{i=1}^n f(t_i) \quad \text{Equation 4-4}$$

Where:

$L$  = Likelihood function

$f(t_i)$  = estimated probability density function

$t_i$  =  $i$  th time to failure

By maximizing the function of  $L$ , the maximum likelihood estimators (MLE) of  $\alpha, \beta, \gamma$  are the simultaneous solutions of 3 equations such that:

$$\frac{\partial L}{\partial \alpha} = \frac{\partial L}{\partial \beta} = \frac{\partial L}{\partial \gamma} = 0 \quad \text{Equation 4-5}$$

Where:

$L$  = Likelihood function

$\alpha, \beta, \gamma$  = Parameters of 3-p Weibull probability density function

From the definition for a 3-parameter Weibull distribution, the following parameters are the estimated as results of the Maximum Likelihood method:

$\alpha = 5399.0033;$

$\beta = 2.5219;$

$\gamma = 34.6234$

#### 4.1.5. Goodness-of-fit test

The goodness-of-fit (GOF) tests measures the compatibility of a random sample with a theoretical probability distribution function. These tests show how well the distribution that has been selected fits the data. There are several types of tests, but the Chi-Squared Test is recommended for large samples.

The Chi-Squared test is used to determine whether a sample comes from a population with a specific distribution. The data can be categorized into intervals.

The Chi-Squared statistic is defined as:

$$W = \sum_{i=1}^{i=k} \frac{(O_i - E_i)^2}{E_i} \quad \text{Equation 4-6}$$

Where:

$O_i$  = observed frequency for interval  $i$

$E_i$  = expected frequency calculated by  $E_i = F_i - F_{i-1}$

$F$  = CDF of the probability distribution being tested

The hypothesis regarding the distributional form is rejected at the chosen significance level if:

$$W > \chi^2$$

The  $\chi^2$  is the critical parameter meaning the Chi-Squared with a significance level of  $\alpha$  and degrees of freedom which can be calculated based on the number of estimated parameters. Significant level is represented to define the tolerance of acceptance of the results.

In this case, the Chi-Squared statistic was calculated as  $W = 15.676$ . From  $\chi^2$  table, the minimum critical value is  $\chi^2 = 18.55$  for all values of significant level. Since  $W < \chi^2$ , the hypothesis was accepted that the 3-parameter Weibull distribution is well fitted to the data set.

#### 4.1.6. Reliability function

The result of goodness-of-fit analysis indicates that the chosen distribution is a suitable model for describing the data. So, reliability function for the set of haul truck tire failures in oilsands service can be presented as 3-Parameter Weibull distribution defined by:

$$R(t) = \exp\left(-\left(\frac{t - \gamma}{\alpha}\right)^\beta\right) \quad \text{Equation 4-7}$$

Where:

$\alpha = 5399.0033$ ;  $\beta = 2.5219$  and  $\gamma = 34.6234$ .

Reliability values versus time are plotted in Figure 4-4, which this curve shows the probability of survival of the tires during the time.

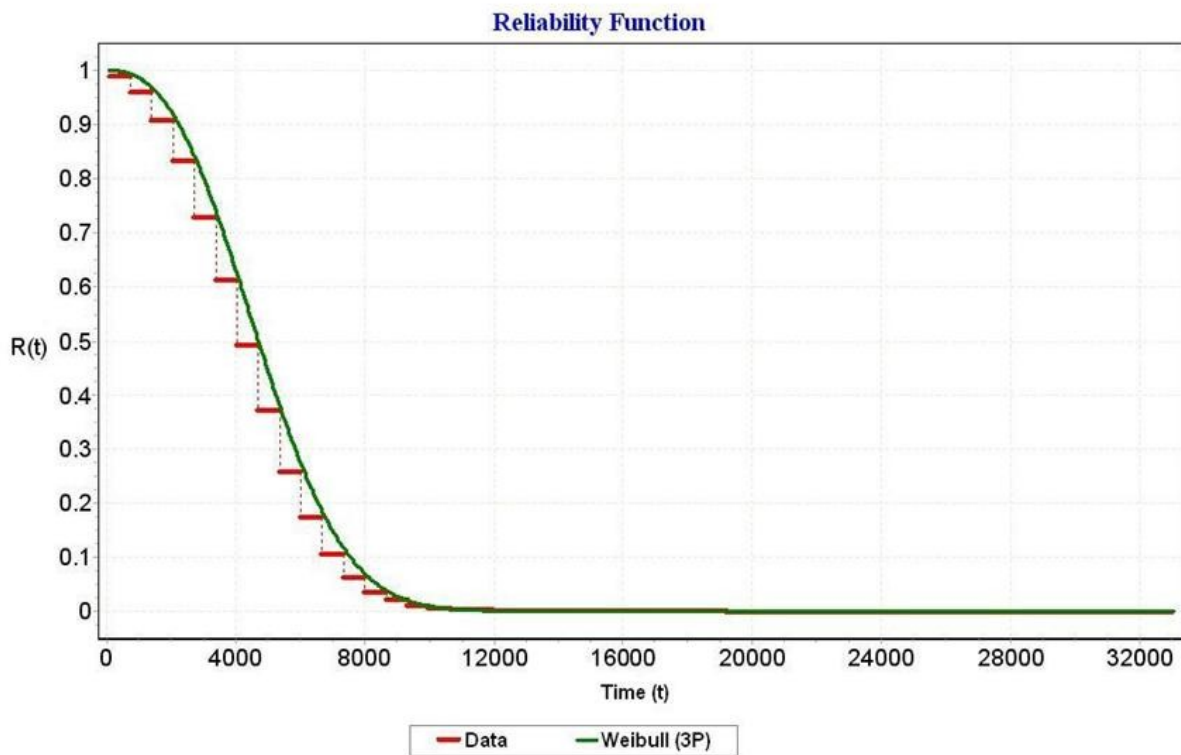


Figure 4-4: Estimated reliability function of haul truck tire

## **4.2. Concluding remarks on reliability model**

This chapter has presented the studies on life time of haul truck tires to predict the repair time, in order to minimize the serious consequences of tire failures including maintenance, loss of safety and system productivity.

In this study, an acceptable model for reliability of haul truck tires has been developed based on five- year period of field data. The results show that the 90% of their lifetime distribution is between 2000 and 8000 operating hours; and the reliability function for haul truck tires can be presented as 3-Parameter Weibull distribution. Mean Time to Failure (MTTF) parameter has been calculated to be 4,826 hours based on this reliability function and calculation is presented in Appendix 2.

The results show that tire failure rate is non constant and the reliability of the tires can be computed by using the suggested function with all values of significant level 90%. This model represents all types of failure modes of haul truck tires; other models can be developed for the distributions of the most common failure modes.

The metric for average tire life is 8000 hours or longer, which has not been met in this study. It might be due to measurement parameter (operating hours) to provide the database. It is noted that the definition of operating hours is not always consistent. Operating delays may be included, even though the vehicle is not moving, which artificially increases the tire's apparent working life. For benchmarking between different mines, the measure must be consistent.

## Chapter 5. Dynamic Model of Tire with Failure<sup>3</sup>

---

### 5.1. Tire dynamics simulation

In order to evaluate dynamics of haul truck tires, a model is required that can present the effect of changes in physical parameters. Existence of fault in a tire affects its characteristics, and therefore the fault changes the dynamic behavior of the system. Tire model suitability depends on the application of model; while detailed modeling is used to describe damage mechanism, and reduced order models the effects of damage on overall system behavior.

Model and signal-based methods for supervision of dynamic behavior of a vehicle has been used to study the effect of different faults. In addition, a signal-based approach made a detection of tire pressure loss [Weispfenning, 1997]. There is a research on effect of fault of tires on dynamic response of the vehicle, in which four degree of freedom has been used to simulate the vehicle and also experiments were developed by instrumented cleat to demonstrate the feasibility of this approach [Tiffany et al., 2009].

The selection of a suitable tire model depends on the goal of the study. In recent years researchers have developed numerous tire models such as single-point contact model (spring and damper in parallel), roller contact model (rigid wheel with one spring, one damper and a single contact point), fixed footprint model (linearly distributed stiffness and damping in the contact area), radial spring model (independent linear spring elements distributed in circumference of the tire) and flexible ring model and finite elements models [Miege, 2004].

---

<sup>3</sup> A version of this chapter has been published as a conference paper in “Journal of Physics: Conference Series”, 2012, 364(1).

To investigate the behavior of haul truck tires and the role of tire fault on the results, the present work considers a model to simulate the dynamics of haul truck tires during vehicle motion in the presence of a fault on one part of the tire.

In this chapter a lumped-parameter model is used for reduced-order dynamic modeling of the effect of a fault on vehicle dynamics. The objective of this work is a model that can show the vertical displacement of a typical haul truck tire as a response to a road profile, considering the fault effect. The response of the system may assist in detecting a fault in a tire using observable features in the dynamic response of the system.

## 5.2. Governing equations of model

There are numerous degrees of freedom associated with vehicle dynamics. One of the most simplified vehicle dynamic models is a two-degree-of-freedom 'quarter-vehicle' model which is widely used for the analysis of ride dynamics of vehicles.

The tire in this method is considered as point contact model represented by a parallel spring and damper to transmit the support force from the terrain to the vehicle and contacts the ground through a point follower. The spring constitutive relationship is chosen to simulate the effects of tire inflation pressure and carcass elasticity. The damping provides the energy dissipation caused by tire deformations as shown in Figure 5-1.

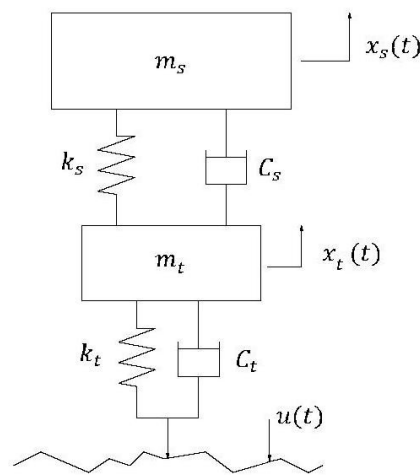


Figure 5-1: Quarter-vehicle model

The vehicle body is represented by the sprung mass  $m_s$  and the tire-wheel-axle is represented by the unsprung mass  $m_t$ . These elements are connected by springs and dampers and constrained to move in the vertical direction only. The input to the vehicle is the road profile  $u(t)$  at the tire point contact,  $k_s$  is the suspension stiffness,  $C_s$  is the suspension damping coefficients, and  $k_t$  and  $C_t$  are coefficients of tire stiffness and damping.

Applying Newton's second law to the masses based on the free body diagrams of  $m_s$  and  $m_t$  respectively gives the governing equations:

$$-k_s(x_s - x_t) - C_s(\dot{x}_s - \dot{x}_t) = m_s\ddot{x}_s$$

Equation 5-1

$$k_s(x_s - x_t) + C_s(\dot{x}_s - \dot{x}_t) - k_t(x_t - u) - C_t(\dot{x}_t - \dot{u}) = m_t\ddot{x}_t$$

The rigid-body dynamic equations of motion can be written in second-order matrix form as:

$$[M] \ddot{X} + [C] \dot{X} + [K]X = F$$

Equation 5-2

Where:

$$[M] = \begin{bmatrix} m_s & 0 \\ 0 & m_t \end{bmatrix} \quad \text{the mass matrix,}$$

$$[C] = \begin{bmatrix} C_s & -C_s \\ -C_s & C_s + C_t \end{bmatrix} \quad \text{the damping matrix,}$$

$$[K] = \begin{bmatrix} k_s & -k_s \\ -k_s & k_s + k_t \end{bmatrix} \quad \text{the stiffness matrix,}$$

$$X = \begin{pmatrix} x_s \\ x_t \end{pmatrix} \quad \text{the vector of displacements,}$$

$$F = \begin{pmatrix} 0 \\ C_t\dot{u} + k_t u \end{pmatrix} \quad \text{the vector of forces imparted by the displacement input.}$$

$$\dot{X}, \ddot{X} \quad \text{First and second derivative of } X \text{ with respect to time}$$

### 5.3. Definition of parameters

The computational model needs information about the properties of truck and tires. Based on experimental data of a sample truck tire under rated loads and inflation pressures, it is found that the value of stiffness  $k_t$  and damping coefficients  $C_t$  varies in a range for different types of tires or inflation pressure [Clark, 1981]. Tire damping coefficient can represent the heat generation characteristics of tire which is assumed to be a constant value in this study. The parameters have been chosen from a typical haul truck tire values are listed in Table 5-1.

**Table 5-1: Parameters of quarter vehicle model**

$m_s = 3600$ kg	sprung mass
$k_s = 400$ kN/m	suspension stiffness
$C_s = 10$ kNs/m	suspension damping
$m_t = 400$ kg	including mass of the wheel and tire
$k_t = 1500$ kN/m	tire stiffness (verified by FEM model)
$C_u = 1.5$ kNs/m	tire damping

### 5.4. Road profile excitation

One of the challenges in modeling the mechanics of an off-road tire is modeling the ground (that is, a time-varying displacement input to the vehicle). In the general case, soil dynamics are included in the soil-tire interface [Zhu et al., 2011], but for a simplified model of the tire, a rigid surface is commonly assumed for the driving surface. Rigid ground has been assumed in this project, which is reasonable for most mines. The road profile (that is, the vertical displacement  $u(t)$  as a function of horizontal distance traveled) is generally a random variable; but forced response due to road profile excitation has been considered for a road roughness profile excitation defined by a function that is a deterministic combination of two different oscillations. A set of periodic wave functions is reasonable for an oilsands mining bench surface in summer, or a gravel roadbed that has an undulating surface.

Forced response due to road profile excitation has been considered for two cases. In the first case, the disturbance is a step function defined by its magnitude. For mining conditions a magnitude of about 0.2 m is not unreasonable.

In the second case, the output response of the tire is studied with a road roughness profile defined by a oscillation function which happens every 4 m by maximum amplitude of 0.3 m, plus a small roughness of 0.03 m. The parameters of this profile are based on observations at an operating site.

$$u = U_1 \sin\left(\frac{2 \pi v}{L_1} t\right) + U_2 \sin\left(\frac{2 \pi v}{L_2} t\right) \quad \text{Equation 5-3}$$

Where:

- $U_1$       Magnitude of larger wave (m)
- $L_1$       Larger wave-length (m)
- $U_2$       Magnitude of smaller wave (m)
- $L_2$       Smaller wave-length (m)
- $v$         Average truck speed (m/s)
- $u$         Road roughness profile (m)
- $t$         time (s)

The assumed road roughness profile that is a combination of two different oscillations is shown in Figure 5-2. Specific road profiles are generally different from this simplified model.

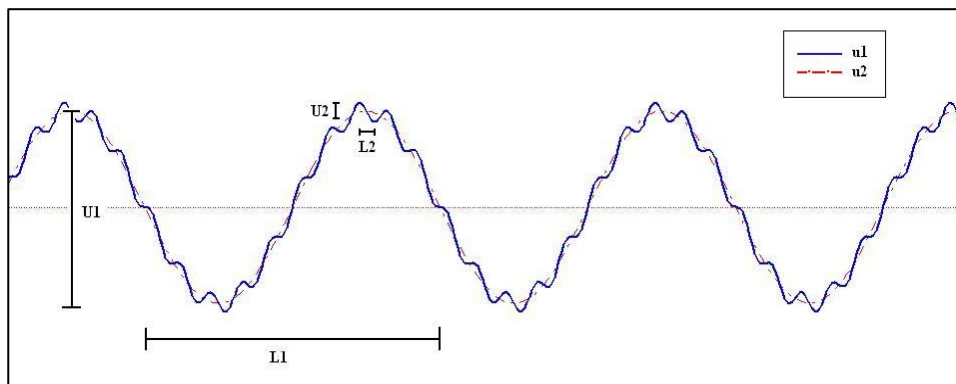


**Figure 5-2: Assumed road roughness profile**

## 5.5. Effect of tire damage

If tire has a fault, the key challenge includes modeling what the effect of the damage is on parameters such as the local stiffness of tire, that is, variability in the tire as it rotates.

Tire stiffness function can be estimated from FE model by applying vertical load to obtain tire deflection using Hook's law by treating the tire as a simple spring given as:

$$K_t = -F/\delta \quad \text{Equation 5-4}$$

where  $F$  is the vertical force applied to the tire,  $\delta$  is the tire deflection and  $K_t$  is the tire stiffness. As it is shown in Figure 5-3, tire deformation is the result of loading on tire with the major components of static inflation pressure and vertical load in conjunction with the rolling dynamic force. During the motion, new surface of tread enters continuously into the contact zone and will be deformed to a flat area

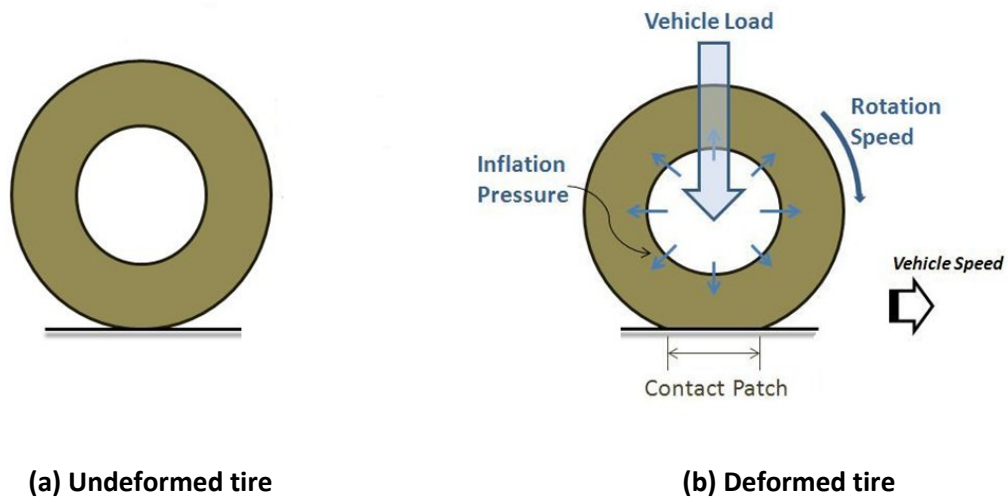


**Figure 5-3: Schematic of tire deformation under load**

The investigation of tire behavior can be performed using numerical models since the development of tire mechanics and computational technology; tire mechanical parameters could be predicted using the finite element analysis (FEA). In this project, a simplified finite element model is provided to investigate the effect of existence of a crack of tire surface on its deformation and consequently the stiffness of tire.

### **5.5.1. Finite element model of tire**

- Model Generation

A two dimensional finite element model of a tire has been developed using ABAQUS software. The model is an elastic simulation considering nonlinear hyperelastic property of rubber and analyzes the tire deformation, stress, and strain under the static vertical load conditions. The first step is to create the two dimensional tire geometry based on 59/80R63 haul truck tire to have 4m outer diameter and 2m rim diameter. The element type for tire is triangle plane-stress element and the road which is a solid wire rectangle shape has analytical rigid element type.

- Material Modeling

In this study, tire is assumed to be composed of natural rubber and Mooney-Rivlin hyperelastic model is used for rubber material [Lin and Hwang, 2004]. Chapter 6 of this work describes how Mooney-Rivlin model is capable of predicting stress-strain behavior in natural rubber material. The parameters of material constants can be obtained by standard tests.

- Boundary Conditions

To define the boundary conditions of the tire problem, the tire nodes corresponding to the rim were connected to a rigid body representing the rim. This rigid body is used to apply the rotational force of the wheel. The road surface was created as a rigid body consisting of a plane analytical surface with a reference point.

Interaction of different surfaces is defined between the outer surface of tire elements and the road surface to have hard normal and rough tangential contacts. Also, interaction between rim and tire is defined to tie the surfaces together.

Loading on the tire is defined in two steps which at the first step small displacement were applied on tire to obtain road contact. Then, vertical traction force was applied on the common surface of tire and rim to simulate real conditions of loaded tire. Known crack is applied on tire surface which is circular to eliminate the effect of crack direction on the results. Figure 5-4 illustrates the FE model of tire and road with a crack on a sidewall.

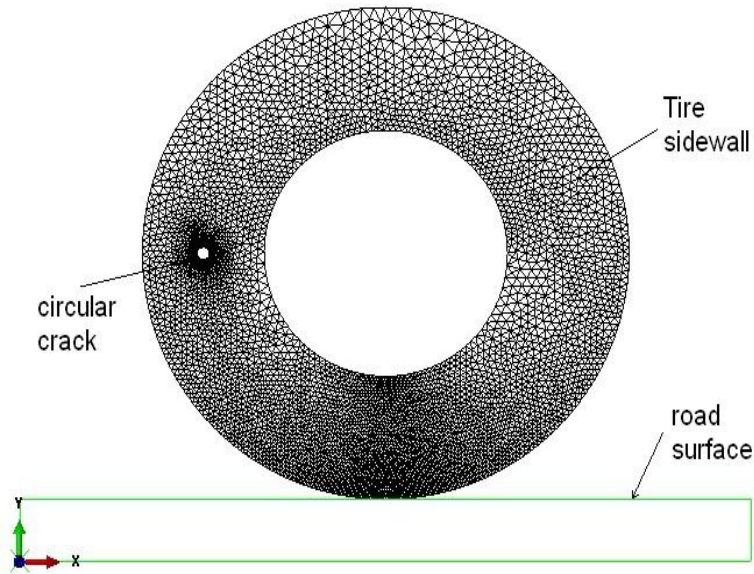


**Figure 5-4: The finite element model of tire and road**

- Mesh convergence study

In finite element modeling, a finer mesh typically provides more accurate solution. In addition, maximum number of elements for different FE software and computation time is other limitations for mesh numbers. Mesh convergence study helps to get a mesh that satisfactorily balances the accuracy and computing time. The procedure is to create a mesh, analyze the terms of interest, increase the mesh density, re-analyzing the same terms of interest and repeat the processes until the term of interest converge to fixed values.

In this study maximum von-Mises stress ( $\sigma_v$ ) is chosen as parameter of interest which is a scalar stress value that can be computed from the Cauchy stress tensor as:

$$\sigma_v = \sqrt{\frac{(\sigma_{xx} - \sigma_{yy})^2 + (\sigma_{xx} - \sigma_{xy})^2 + (\sigma_{yy} - \sigma_{xy})^2}{2}} \quad \text{Equation 5-5}$$

The convergence starts at 2,300 elements and the mesh density is increased until the maximum von-Mises value converge to its maximum value. The results of convergence study are summarized in Table 5-2; from 2,300 to 60,000 elements.

**Table 5-2: Convergence study for tire FE model**

Elements No.	2,300	6,189	8,002	18,927	24,311	27,933	32,124	40,492	50,004	60,000
max $\sigma_v$ (KN/m <sup>2</sup> )	3,304	3,482	3,467	3,482	3,507	3,501	3,501	3,501	3,501	3,501
CPU time (sec)	23	61	79	187	230	276	317	390	493	552

As it is illustrated clearly in Figure 5-5, maximum von-Mises stress changes until the number of elements is 27,900 and is remained a fixed value by increasing the elements. Therefore the value which has been chosen to mesh the model is defined by the convergence study.

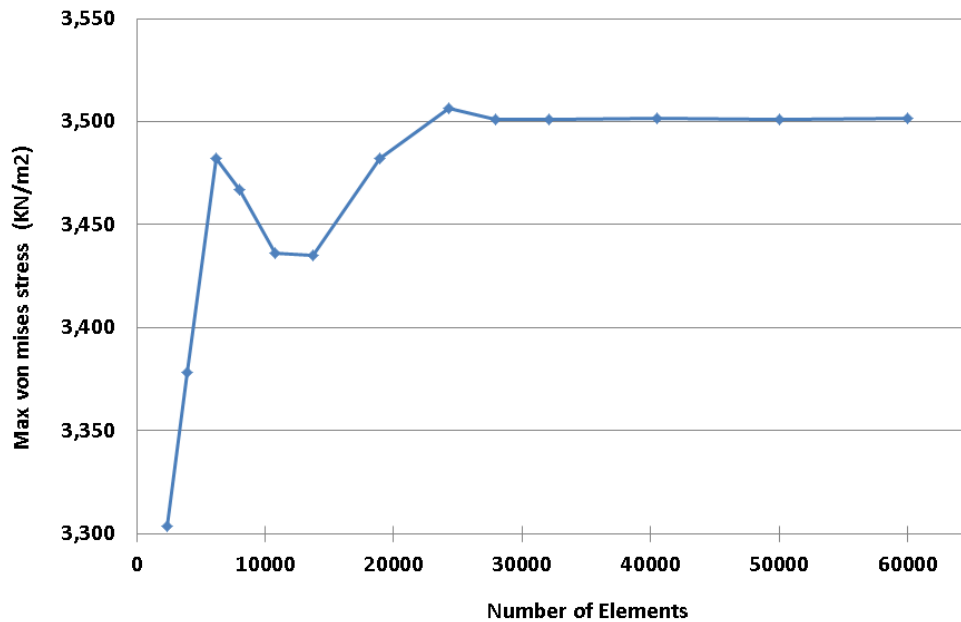
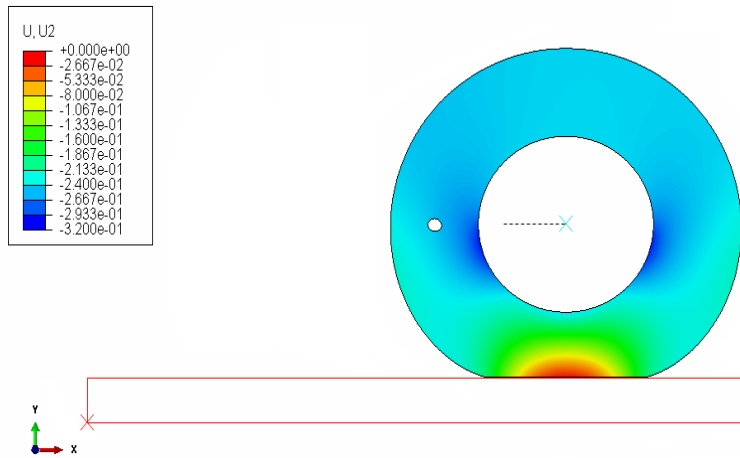


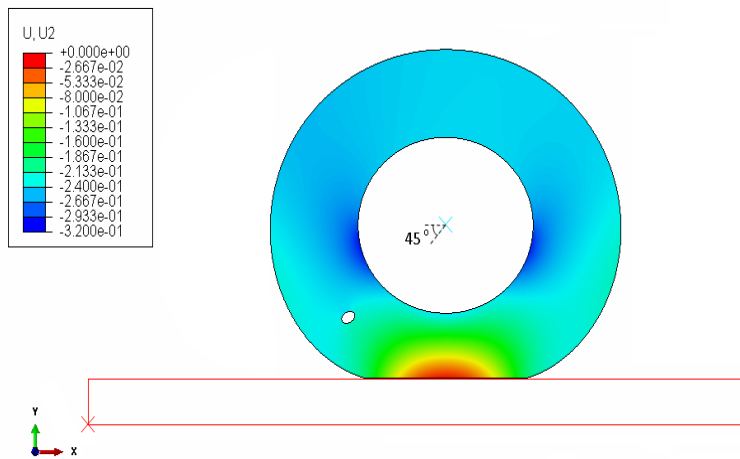
**Figure 5-5: Convergence of maximum von-Mises stresses for tire FE model**

- Stiffness vs. Rotation

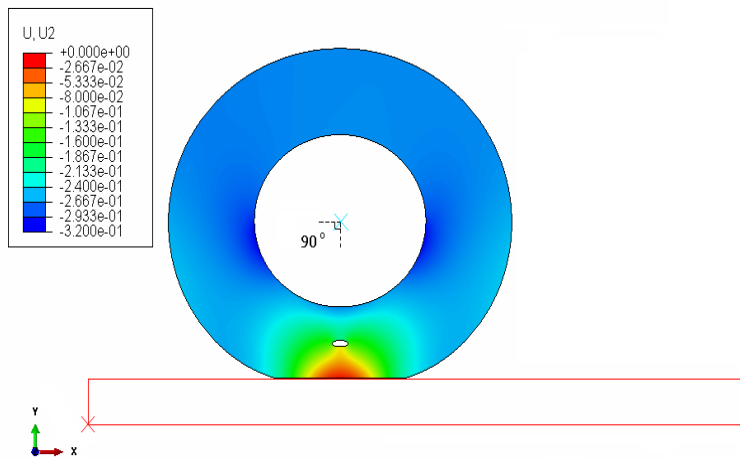
After choosing the suitable meshing for model, the static loading is applied and tire rotates with constant rotational speed. A circle shape crack is assumed to be at the middle of tire sidewall located at the points called 0° at the start of rotation. Results of deformation field are recorded for several rotation angles when crack travels around the tire during one full rotation of tire as it is shown in Figure 5-6.



(a) Tire rotation 0°



(b) Tire rotation 45°



(c) Tire rotation 90°

Figure 5-6: Results of tire deflection at different rotation angles

The displacement of the top point of tire is considered as tire deflection in each angle of rotation. The deflection value is negative number but it is shown as its absolute values in the graphs. The model result is obtained for different crack diameter of 0.15, 0.10 and 0.05 m when the sidewall height is 1 m. Figure 5-7 shows the effect of crack size on deformation of tire with respect to its rotation angle.

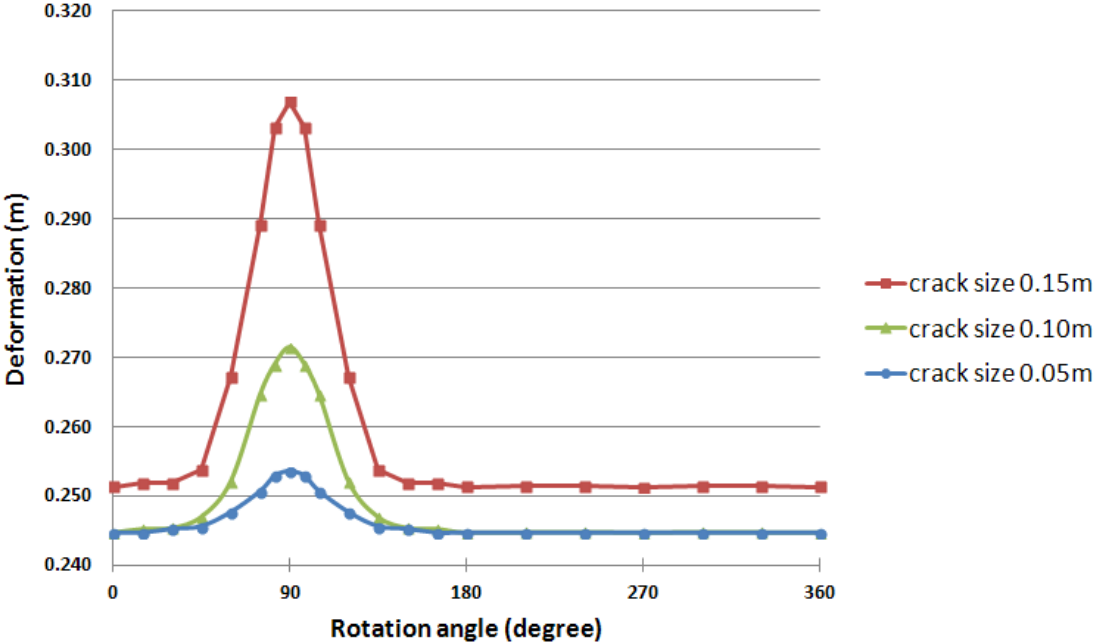


Figure 5-7: Tire deformation with respect to rotation angle (results of tire FEM)

In the last step, Hooke’s law is applied to estimate the tire stiffness as a function of rotation angle when crack is presented at sidewall area. The deflection values obtained from finite element model for each angle and known vertical load are used to calculate the stiffness of tire for different rotation angle. As it is plotted in Figure 5-8, Results show that the minimum stiffness value occurs at 90° rotation angle when the gradient of changes is mostly in the range of 30° to 150° of rotation. The minimum stiffness value strongly depends on the crack size which increases by larger crack sizes.

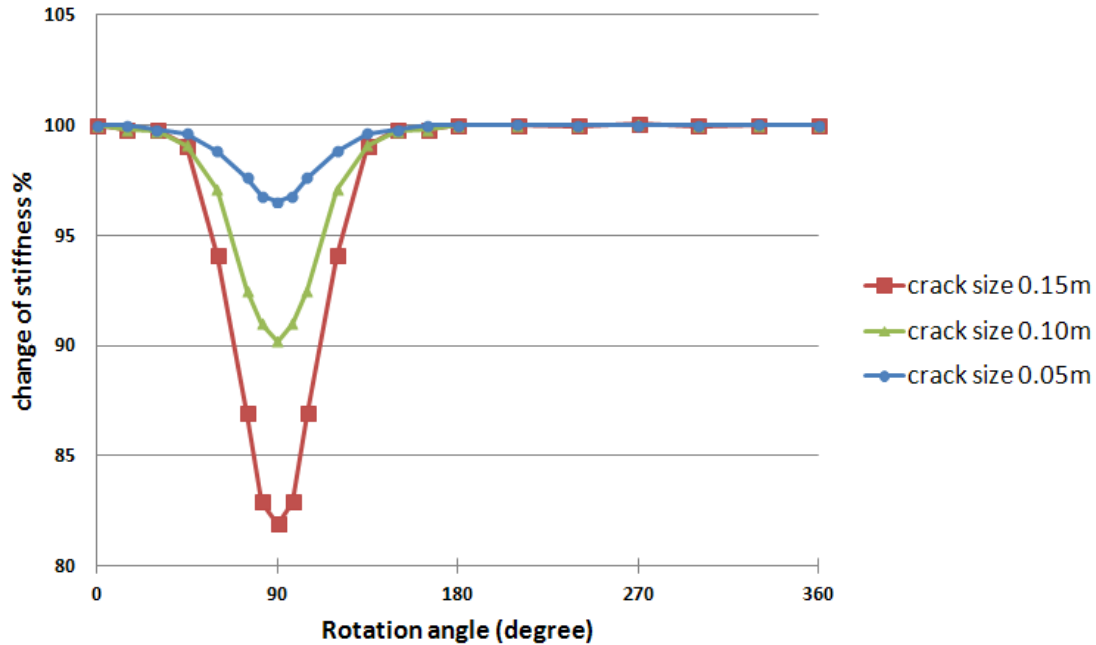


Figure 5-8: Tire stiffness with respect to rotation angle (results of tire FEM)

### 5.5.2. Tire stiffness estimation

For tire stiffness estimation, a function is fitted to FEM results data points using nonlinear least squares curve fitting in MATLAB. The method finds best-fitting curve to the data by minimizing the sum of the squares of the residuals of the data from the estimated curve. The most general definition of the nonlinear least squares statistic coefficient of determination is:

$$R^2 = 1 - \frac{\sum(y_i - f_i)^2}{\sum(y_i - \bar{y})^2} \quad \text{Equation 5-6}$$

where  $y_i$ ,  $f_i$  and  $\bar{y}$  are data set values, predicted function values and the mean of the data. The statistic  $R^2$  measures how successful the fit is in explaining the variation of the data. A value closer to 1 indicates a better fit. The result is a sigmoid function based on finite element results data points. The calculated value for  $R^2$  is calculated to be 0.96 that shows the estimated function is acceptable.

The stiffness function  $K$  with respect to rotation angle  $\theta$  is:

$$K(\theta) = \frac{1}{1 + e^{-a_2(\theta - c_2)}} - \frac{1}{1 + e^{-a_1(\theta - c_1)}} \quad \text{Equation 5-7}$$

Where:

$a_1, a_2$  : thresholds of function

$c_1$  :  $90^\circ - d\theta$

$c_2$  :  $90^\circ + d\theta$

The values of  $a_1, a_2$  are obtained to be 0.1734 and stiffness variation ranges within  $\pm 60^\circ$  of the  $90^\circ$  rotation angle resulting the value of  $c_1$  and  $c_2$  are calculated to be  $75^\circ$  and  $105^\circ$  respectively.

The fitted function and FEM data point are illustrated in Figure 5-9. It is assumed that crack size is 0.15m; maximum stiffness value is calculated to be 1500 KN/m based on tire deformation at  $0^\circ$  and minimum stiffness is 82% of the maximum stiffness at  $90^\circ$  rotation angle.

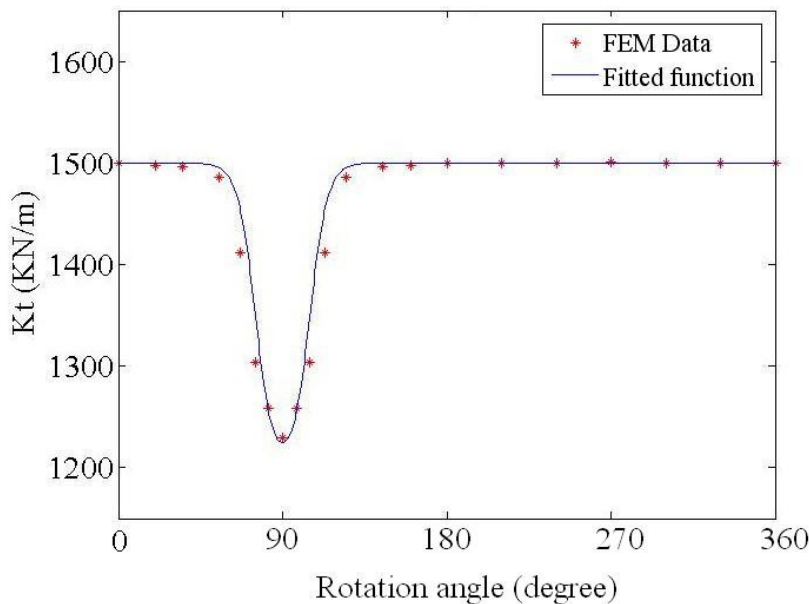


Figure 5-9: Estimated tire stiffness function with respect to rotation angle

## 5.6. Solving the governing equations

In this project a MATLAB code has been developed to solve the governing equations of motion using ODE45 considering typical haul truck and road parameters listed in Table 5-1. Stiffness of tire is defined as above mentioned sigmoid function versus rotation angle. The speed of the truck is a constant value; therefore the angle of rotation can be defined as a function of time. Consequently, the stiffness can be represented as function of time.

## 5.7. Tire dynamic model results

The analysis is based on two different road conditions and whether the tire is undamaged or has a fault. Figure 5-10, depicts the vertical displacement and vertical velocity of the simulated tire in the time domain when the road is assumed to be vertical step disturbance. In parts (a) and (c), the tire is assumed to have no fault and the plots can be compared to parts (b) and (d) respectively, where the road profile are the same but tire suffers from a fault at a certain angle.

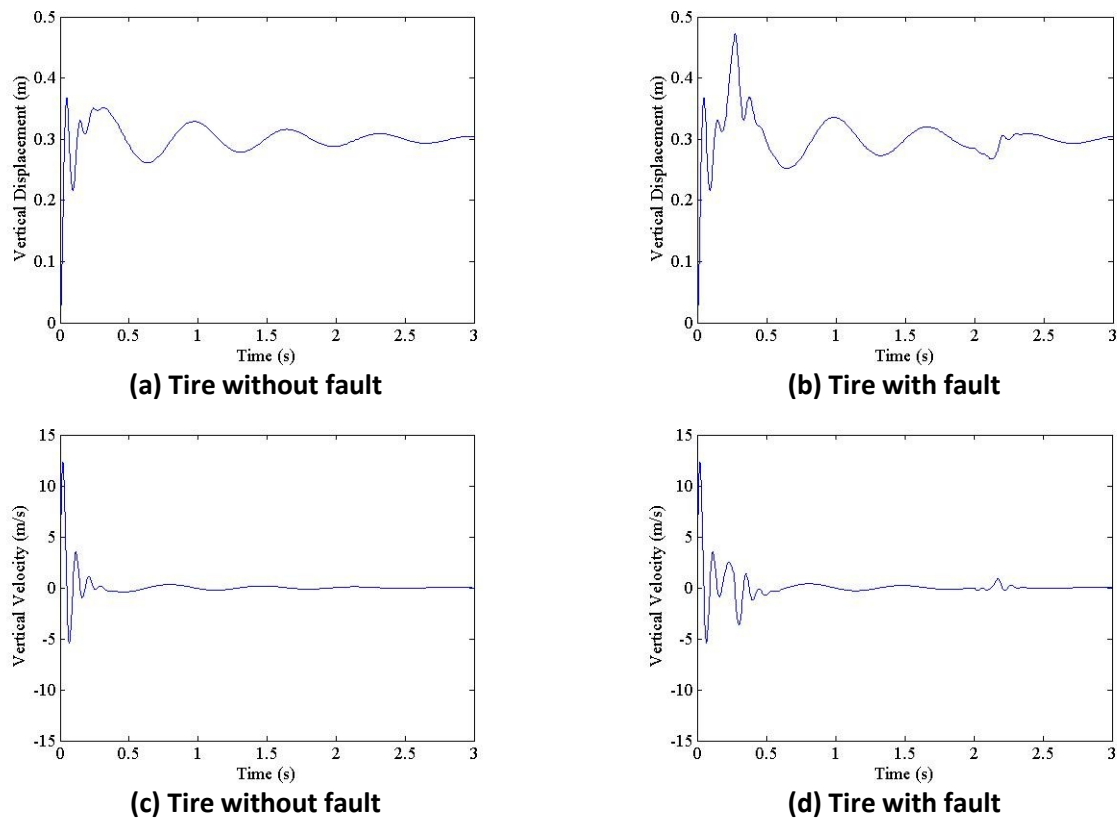
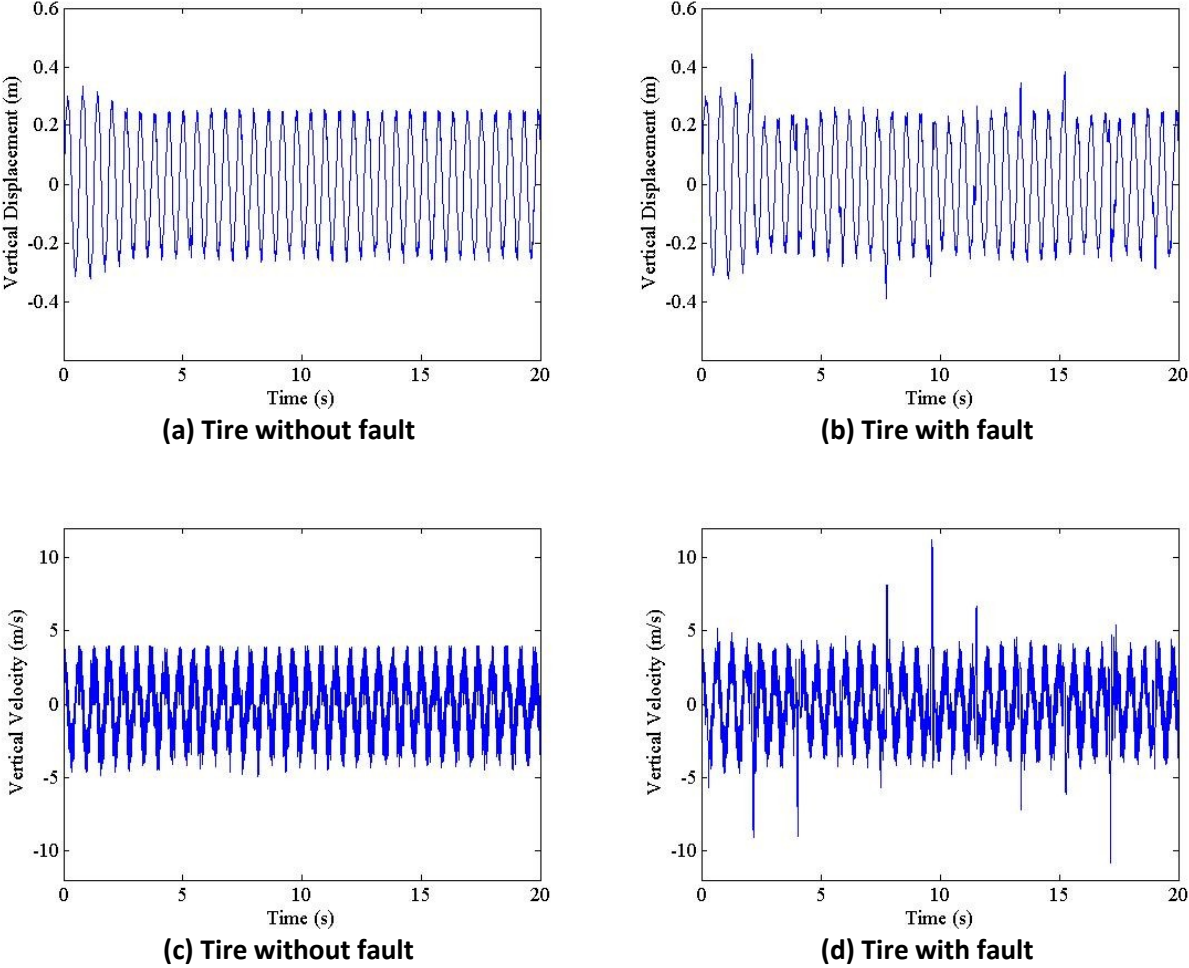


Figure 5-10: Plots of vertical displacement and velocity of tire excited by step disturbance

In Figure 5-11, the profile of road has been changed to account for road roughness as parts (a) and (c) show the response of tire without a fault as a function of time; and parts (c) and (d) is the displacement and velocity of tire in the presence of fault.



**Figure 5-11: Plots of vertical displacement and velocity of tire exited by road roughness**

As can be seen in the above figures, the difference between tire behavior in different road conditions helps us determining whether tire has fault or not. Analyzing the different tire responses to road disturbance and roughness reveals that rough road simulation is a convenient condition to simulate the faults in tire. As can be seen tire displacement trajectories show distinguishable differences and this difference in response to road condition is consequently reflected in velocity results as well.

## **5.8. Concluding remarks on tire dynamic modeling**

This chapter described a model to simulate the dynamics of haul truck tires when a fault is present to determine the effects of physical parameter changes that relate to faults. To simulate the dynamics, a lumped mass 'quarter-vehicle' model has been used to determine the response of the system to a road profile when a failure changes the original properties of the tire. A two dimensional finite element model is provided to estimate the stiffness of tire when crack rotates along tire rotation. The result is a model of tire vertical displacement that can be used to detect a fault, which should be tested under field conditions.

The dynamic simulation presented in this chapter has shown that the differences between tire motions can be an indicator to determine the presence of fault in the tire, even with changes in different road conditions. The response of the system can help to detect a fault in a tire in comparison with intact tire.

The validity of the provided dynamic model should be tested. To better mimic the tire responses and hence achieve reliable results, real tire stiffness function should be considered, which can be obtained from validating the finite-element model with experimental results. Therefore different constitutive relationships should be investigated, with the intent of applying parametric system identification methods for feature extraction related to dynamic parameters and stiffness functions, and assessing the sensitivity of parameters on observable system outputs. Also a high-order model may be necessary to describe how a fault progresses, and how a fault may be observed.

Since displacement and velocity are not measured directly, they can be inferred from different methods such as strut pressure measurement, optical method to observe the vertical deflection of tire and other measurement techniques such as contact sensors.

## Chapter 6. Rubber Damage Study

---

Strain measurement on a tire surface is important as it allows the analysis of the behavior of a tire to detect faults. Cracking or splitting of the tire material introduce a discontinuity in the displacement and strain field, or develop a strain concentration. The hypothesis is that the deformation field can be related to a fault in a tire. The presence of faults in a tire changes the strain field; therefore, it can be used for fault detection purposes using taken images. Digital image correlation (DIC) is a full field, computer-based, non-destructive, non-contact method to measure surface deformation.

In this chapter, to obtain the effect of faults on rubber strain field, different steps are necessary to be considered. At the first step, the DIC method is applied to find the deformation of the rubber under controlled loading condition and known faults. At the next part, finite-element model is developed for specimens of rubber with the same condition. The result is compared to the finite element model to define stress-strain relationship of crack rubber. Also a brief description of rubber heat generation and its effect on the stiffness is covered. The result of this chapter is a validated FE model of rubber used to estimate tire stiffness of tire in presence of a crack (presented in Section 5.5.).

### 6.1. Rubber strain measurement using Digital Image Correlation method

#### 6.1.1. *Digital image correlation principle*

DIC is an optical technique to measure the deformation of an object using images of the surface provided by a camera which collects data during deformation. The main idea of the method is based on tracking the motion of points in a small region, which is called subset, when the object is undergoing mechanical or thermal stress [Moser and Lightner, 2007]. As it is illustrated in Figure 6-1, by matching the two images at unloaded and loaded conditions the displacement corresponding to each point is calculated. Displacement of the points and maximum correlation function in the subset is determined to obtain the deformation vector of each segment to provide corresponding strain field of the whole region-of-interest.

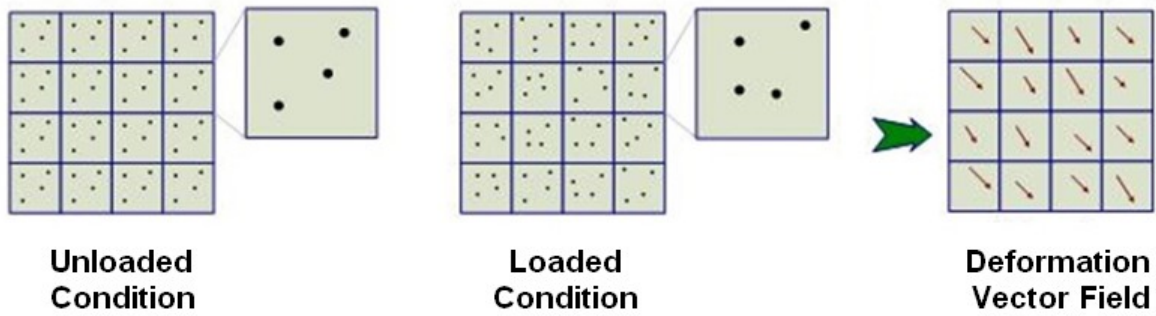


Figure 6-1 :Illustration of digital image correlation principle

Cross correlation is based on the relationship between deformed and un-deformed images by splitting them into interrogation windows and finding their movements. A correlation function compares the interrogation window to its neighbors in subsequent frames and is defined by a function [McCormick and Lord, 2010] as:

$$C = 1 - \frac{\sum f \cdot g}{\sqrt{\sum f^2 \cdot \sum g^2}} \quad \text{Equation 6-1}$$

Where:

$f$  = light intensity value (grayscale level)

$g$  = corresponding intensity value of the same point after deformation

$C$  = correlation function

DIC uses a correlation algorithm to obtain the displacements by identifying areas of matching grey scale values between the speckle pattern in each subset of the deformed and undeformed images. The corresponding point to the maximum correlation function, which is called the correlation peak, determines the subset displacement vector [Crammond et al., 2013]. Strain field is determined by dividing the displacements vectors to the original size of the object:

$$\epsilon = \frac{\Delta L}{L} \quad \text{Equation 6-2}$$

Where:

$\epsilon$  = strain value

$L$  = original size of subset

$\Delta L$  = displacement vector of subset

### 6.1.2. Digital image correlation apparatus

Using a single camera gives only the in-plane strains and consequently two dimensional deformation measurements. To obtain the third component of strain field, another camera would be needed to allow determination of the out-of-plane strain component. Pictures of an object from two different directions are recorded and compared the corresponding subsets in images; therefore, the information about the shape and three-dimensional deformation of the object can be obtained [Huang, 2002].

The experimental setup of three dimensional DIC method, shown in Figure 6-2, contains two Charge-Coupled Device (CCD) cameras, a lighting source and computer for system control and data acquisition. The procedure is to using images from both cameras to develop the correlation process. Digital cameras take pictures of the surface of sample and images are downloaded from camera to a frame grabbing circuit card and are stored for subsequent processing.

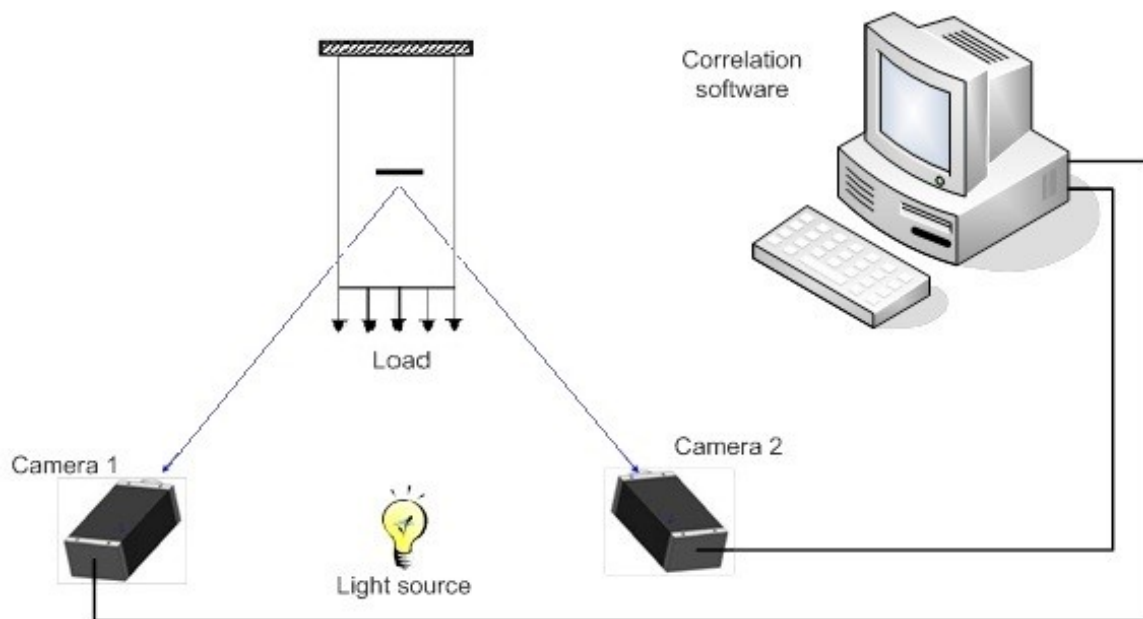


Figure 6-2 : Schematic of 3-D DIC experimental setup to measure rubber deformation

### 6.1.3. DIC experiment setup

The experimental setup of DIC method for rubber sample strain measurement is implemented at the University of Alberta in a laboratory scale illustrated in Figure 6-3. It involves an MTS hydraulic testing machine controlled by a digital function generator and a control panel to apply the desired loading. Two high resolution CCD cameras are mounted on a base to introduce flexibility in positioning them. The optical axis of both cameras was set perpendicularly to the frame of the testing machine and remained fixed to minimize the movement of cameras during the test. Cameras are controlled by a custom MATLAB code to produce the trigger signal for the cameras and collect the images of the test sample surface (rubber). The random pattern has been provided by air brush on the rubber sample as speckles which should be tracked. The white light is used to provide the optimum illumination.

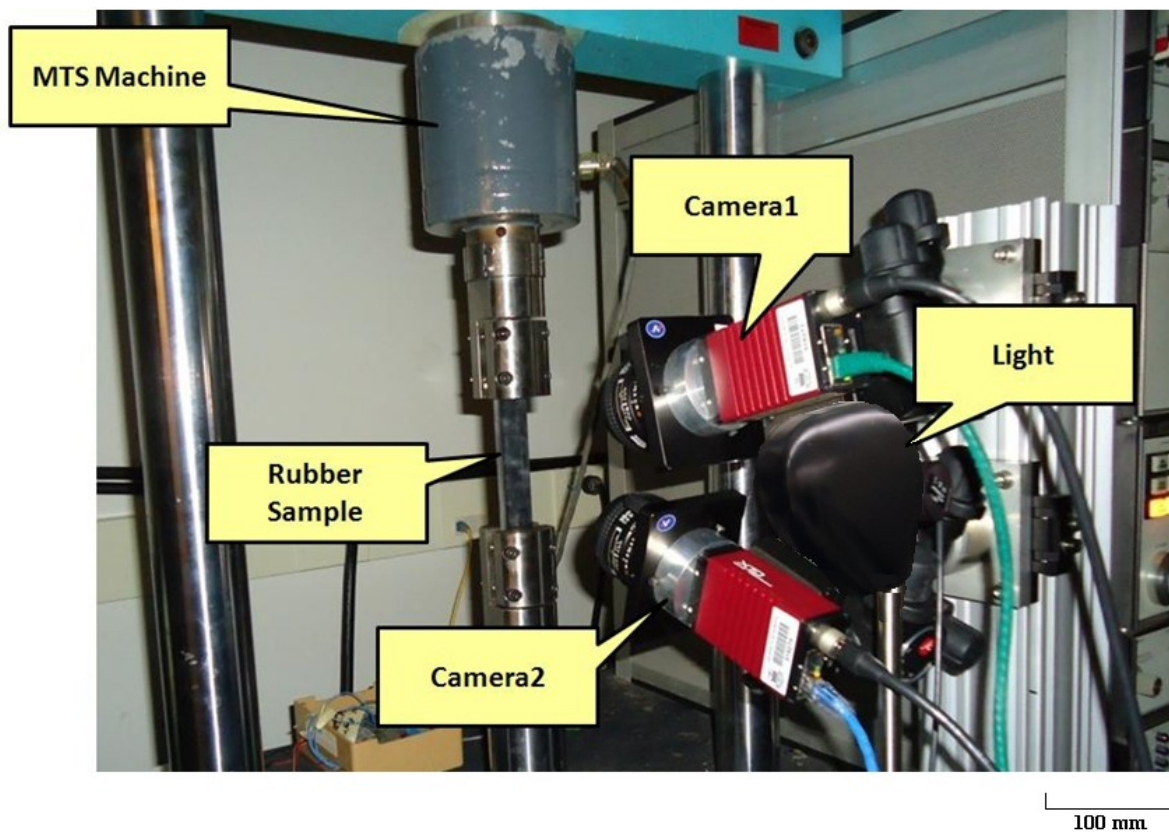


Figure 6-3 : Photo of 3-D DIC experimental setup

- Camera and lens

In optical experiments, selection of an appropriate detector leads to reliable and accurate results which can satisfy technical purposes with a reasonable price. For this project it is necessary to use enough resolution in the image to detect rubber sample small deformation.

The selected detector is AVT GX3300 which is a high resolution CCD camera with the specifications listed in Table 6-1. This type of camera has KAI-08051 sensor which has 8.0 mega pixels and 4/3 in dimension. Continuous mode rate is about 17 fps frame rate and also the data depth of 14-bit can deliver  $3296 \times 2472$  pixel images.

**Table 6-1: Specifications of AVT GX3300 camera and its components**

Model Name	AVT GX3300	
Camera Format	CCD	
Weight	365 g	
Size	136.3 x 53.3 x 33 mm	
Image Resolution	3296 x 2472	
Sensor Spec	Type	KAI-08051
	Resolution	8 megapixels
	Sensor dimension	18.1 × 13.6 mm
	Resolution	3296 x 2472 pixel
	Aspect ratio	4:3
Data Depth and Rate	Data depth	12-bit
	Continuous mode rate	17 (frames/sec)

For AVT GX3300 camera, an appropriate lens should be selected to take the picture of rubber sample. The AVT cameras were equipped with a 50mm Nikon Nikkor lens, with an aperture range from F2 to F16. Scheimpflug adapters were installed between the lens and camera to align the focal plane of each camera with rubber surface by adjusting the lens angle.

- Illumination

Lasers are predominant due to their ability to produce high-power light beams to capture small particle in fluid. In this project, there is no need to provide high intensity illumination since, the experiment condition is static and particles are not small. Therefore, white light source that uniformly illuminate over the rubber sample area can be selected. The amount of light is an important factor for designing the setup to take picture. A 60 Watt light source is used to illuminate the rubber surface.

- Software

Selection of software is based on its performance, accuracy, ease of use, calibration features and capability of exporting data. The software that is used in this project for cross correlation is DaVis 8.0 (LaVision GmbH) which usually is applied for fluid analysis purposes; however, it can be used to perform cross-correlation for strain measurement experiments. In addition, camera calibration algorithm is provided by DaVis using the target images to calculate calibration parameters discussed in section camera calibration. Matlab is the software for post-processing of the results of deformation vectors. Final step is displaying the data in the form of figures, contours or plots.

- Rubber samples preparation

Rubber is the main component of a tire providing the flexibility that is required in their structure. The percentage of natural rubber includes in haul truck tire is 80% of the total amount of rubber which is used in its construction [Kogel, 2009]. In order to achieve the most similar properties to tire material, abrasion resistant natural rubber (NR) samples have been chosen for this project. It has 3,800 psi tensile strength and can handle -28 °C to +82 °C temperature. The rubber surface is smooth finish and black color which is ideal to make required high contrast surface with white speckles in order to obtain an accurate correlation on the rubber images. There is not an absolute specimen size requirement except the limitations of testing machine grips width and maximum distance of machine mounts. The samples are cut by water jet machine to 100 mm length and 25 mm width while their thickness is 12.5 mm.

- Seeding rubber sample surface

The surface of the rubber sample is seeded with speckles that should be small enough for capturing smallest features of the domain and large enough to scatter light efficiently. These speckles, distributed with a random pattern, are selected to be perfect circle with the same diameter and also ideally with enough concentration to create low noise images.

There are different methods to provide the pattern on the surface of rubber sample, such as spraying paint, adhesive powder spray or using regular pattern to mark the surface. Studies show the effect of different speckle patterns on accuracy of the displacement measurement. Table 6-2 shows the required average speckle diameter based on three subset sizes.

**Table 6-2: Mean speckle size for the three subset sizes**

Subset size (pixels)	Mean speckle diameter (pixels)
13 × 13	3
23 × 23	10
33 × 33	>10

In small deformation measurements, it is recommended to apply colors that maximize the contrast between the speckles and background object. One of the challenges for seeding of rubber samples was providing a fine random pattern with uniform, small and predicted size of speckles. In addition, the pattern characteristics should be repeatable for all painting processes. In this project, the surface of the rubber sample is black; therefore, white speckles would be the best selection to maximize the contrast of the features. The technique of using air-brush is applied to provide random pattern on rubber surface to obtain a very fine mesh.

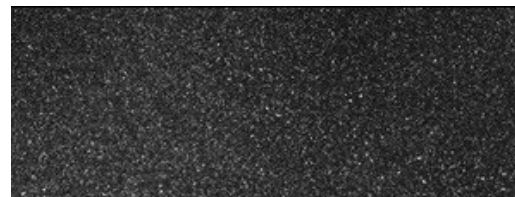


**Figure 6-4 : Using air brush technique to seed the rubber sample surface**

In the first trials, randomized pattern was spray-painted the white color paint on the rubber surface using an air brush, shown in Figure 6-4. The white dots on the surface are not uniform and also the size of them cannot be controlled as paint turn to drops in different areas. In addition there are areas with different density of speckles. To solve this problem a mixture of known size particles and transparent paint was sprayed by air brush on the surface of rubber samples. It was an effective method to provide a dense and uniform pattern.



**(a) Seeding method 1**



**(b) Seeding method 2**

**Figure 6-5: The random speckle pattern using air brush**

The particles were chosen to be Spherical 110P8 with the size of  $10\mu\text{m}$  which stick to the rubber sample. The transparent paint was the best adhesive which can be used to provide a layer that is invisible and also does not have variable visible characteristic during the experiments procedure. The key points of this method are the density of the mixture which should be high and air pressure supply of air brush should be low ( $\sim 40$  psi) to obtain the best result of seeding.

- Camera mounting

Cameras are installed on a bar, with a specific distance from each other and from the rubber sample surface. The configuration of the two cameras (distance between the two cameras and angle between their optical axis) affects the triangulation accuracy [Orteu, 2009]. Once the calibration has been carried out, it is vital that the cameras are not moved relative to each other and camera principal axes remain perpendicular to the rubber sample trajectory.

- Camera calibration

Calibration of cameras has essential effect on the performance of the experiment. The main goals of camera calibration are determination of magnification factor, location of the lens center, minimization of the lens distortion, mapping the images of two cameras, finding the relative position and orientation between the two cameras.

A calibration target with known geometry plate is used for camera calibration, as it is shown in Figure 6-6. There are different standard 2D and 3D calibration plates provided by LaVision to set a reference point and use the information to find the scale factor between the image and the object. In this project a standard calibration target (Type #11) has been employed.

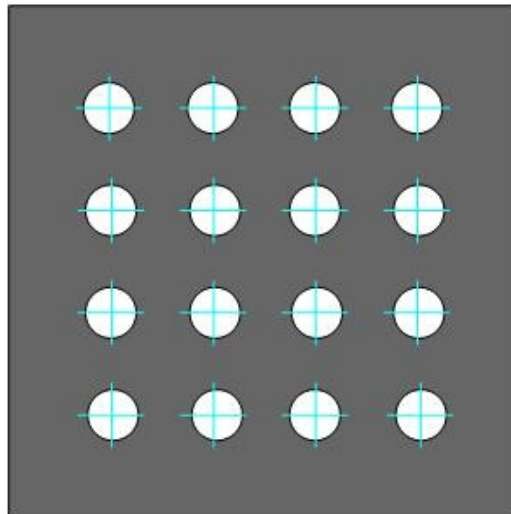


**Figure 6-6 : Schematic of a typical 2D calibration plate**

The calibration procedure is developed by taking a series of pictures from calibration target with both cameras at the same time. During the calibration process dots on the plate are detected automatically and evaluation algorithm calculates the intrinsic (focal length, principle point, distortion parameters) as well as the extrinsic parameters (translation vector and rotation matrix) for each camera [Orteu, 2009]. Furthermore, the uncertainties of the calibration parameters, resulting from the deviations of the detected markers from the model positions are calculated. These calibration data are required to compute the 3-D coordinates of a point corresponding to matched pixels on the two images. As it is illustrated in Figure 6-7, after calibration procedure, the angle between cameras is calculated to be  $22^\circ$  and their distance from each other is 120mm and 300mm from the rubber sample.

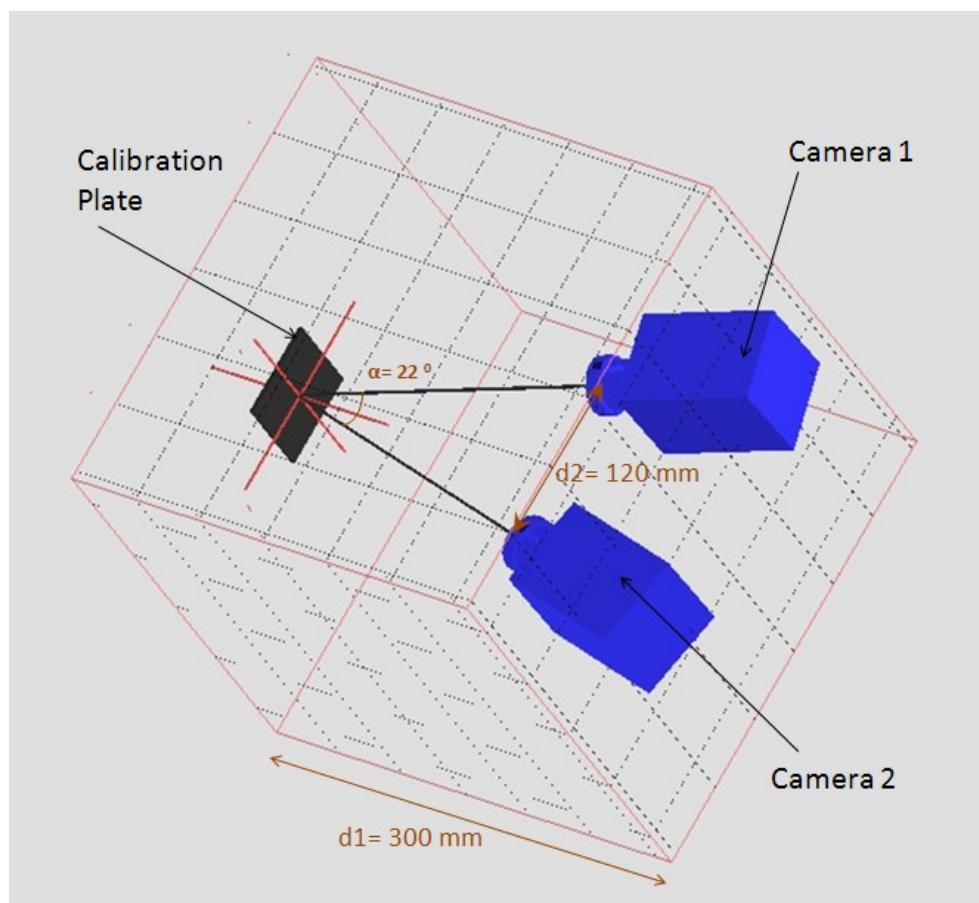


Figure 6-7 : Camera configuration as the result of calibration procedure

#### 6.1.4. Rubber deformation data collection

The next step of the experiment after installation and calibration of the setup, is taking images of the rubber sample surface. Mechanical load is applied using MTS machine and rubber sample deformation images are recorded simultaneously controlled by computer program. It is recommended to inspect the recorded pictures if there are blur or contrast problem that are detectable before image processing. Figure 6-8 shows the image of rubber sample in tension.

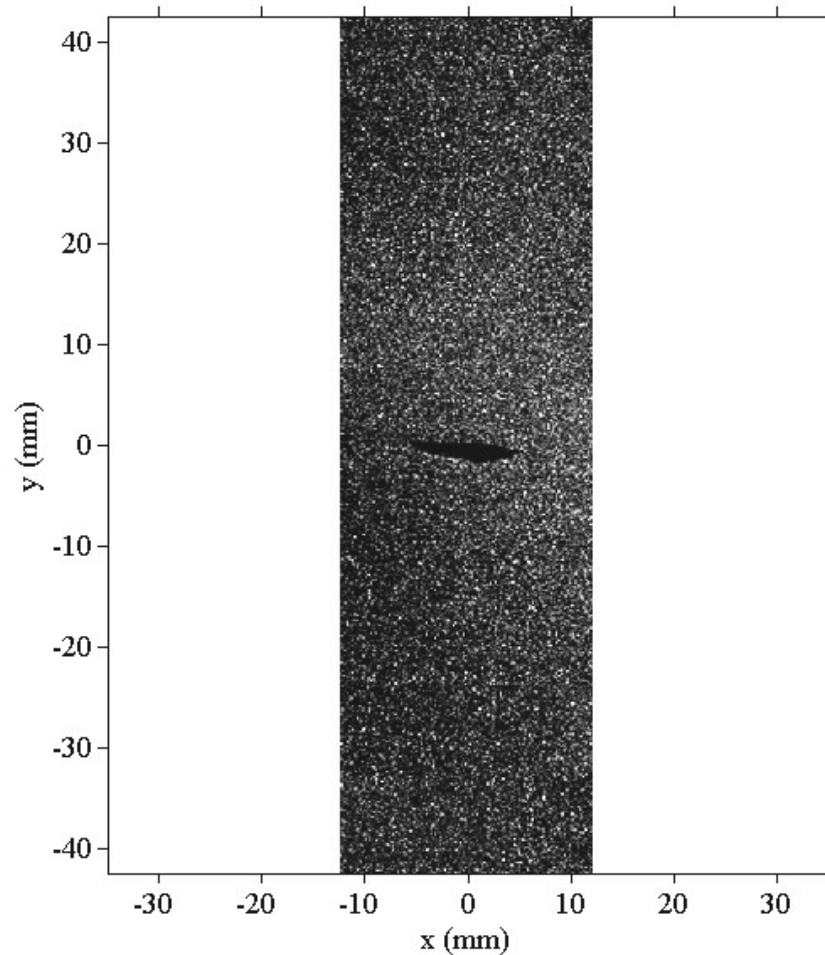
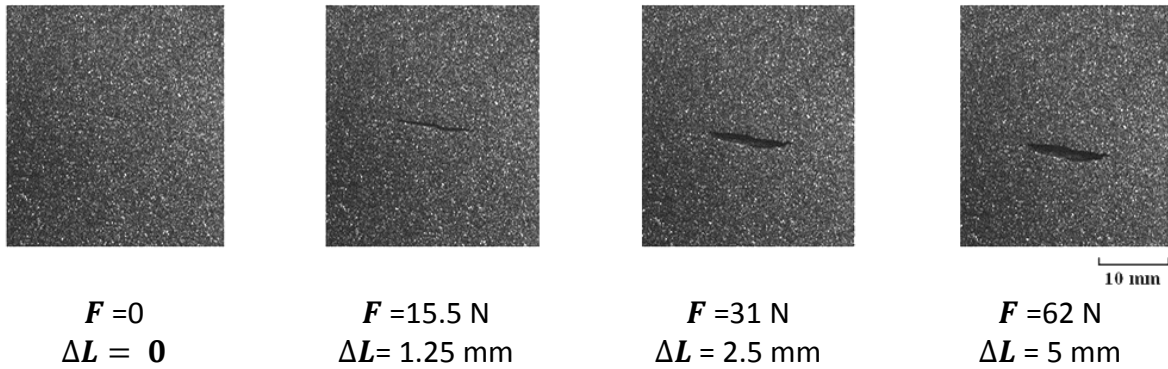


Figure 6-8 : Raw image of rubber sample in tension load 62 N

A crack opening sequence is illustrated in Figure 6-9 when rubber sample seeded with white particles is fixed at the top and stretch from lower part. The values of  $F$  and  $\Delta L$  represent loading and total deformation of rubber sample at each step. These images are collected in order to process in the next step.



**Figure 6-9 : Crack opening sequence in rubber sample**

### **6.1.5. Processing of recorded images**

Cross-correlation of interrogation region of the two images determines the displacement of particles in the region. Knowing the dimensions of images, the strain field can be obtained. To process the images, DaVis is used to load the data and setup processing scheme. The software can read images and process the image pairs to obtain the displacement. After analyzing the data the result of strain field was acceptable considering incorrect vectors and smoothness of the field. This procedure is categorized in three steps pre-processing, data cross-correlation and post processing.

After collecting a series of images from rubber sample the pre-processing of images is completed using DaVis software. The raw images files are imported to the software and multi-frame images are created. In this step, cameras specifications should be added as processing attributes and also other mapping like rotation can be implied to images if necessary.

Data cross-correlation is the next step to process images and to obtain the strain field using DaVis surface and vectors module. First of all a mask is defined to introduce a region for calculation in order to reduce processing time by selecting desired area. Reference seeding points and displacement calculation setting are set to start the cross-correlation procedure to obtain the outcome which is deformation vector field of selected area.

After getting the displacement field pattern, there would be incorrect vectors which do not follow the expected field which can be eliminated from the results by use of different filters. There are different filters to remove or improve unwanted vectors such as standard deviation filter, local median filter or manually reject vector. In this study, a MATLAB code has been used to be able to read the VC7 output file from cross-correlation step and obtaining the derivative of vector field with respect to different directions. Final step includes displaying the displacement and strain results in the form of image file.

### 6.1.6. DIC experimental results

The strain field measurement test was conducted by displacement controlled testing using a standard specimen dimensions as recommended in ASTM D 412-87. Dumbbell shape samples are commonly used to insure that failure happens in the middle of sample; but in this test natural rubber samples are cubic because of the size of specimens which are long enough to cancel the effect of grips stress concentration. Three different samples are chosen for tensile test (Figure 6-10) based on MTS machine dimensional limitations. Each rubber specimen contains a 10 mm cut placed at the center with a direction perpendicular to the tensile stress. This location is chosen in order to observe the effect of crack inside the specimen; far enough from both ends of grips.

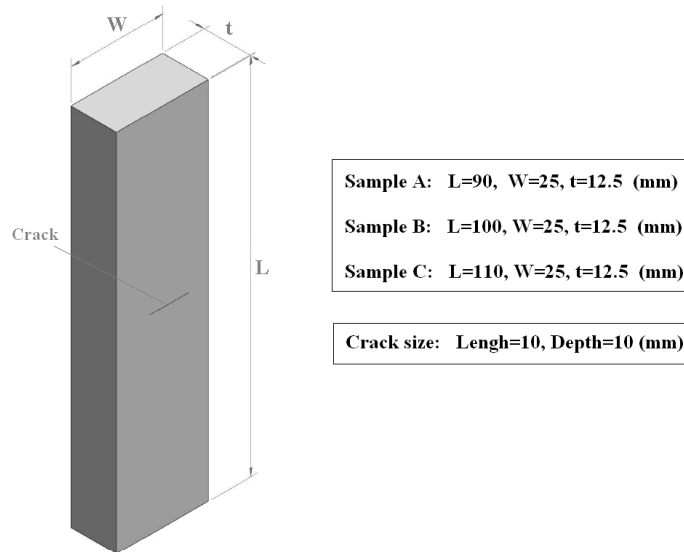
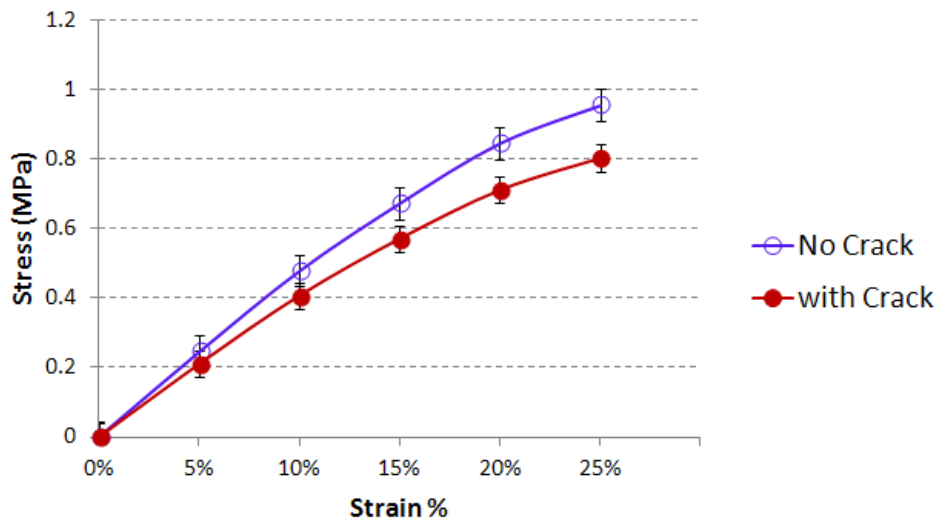
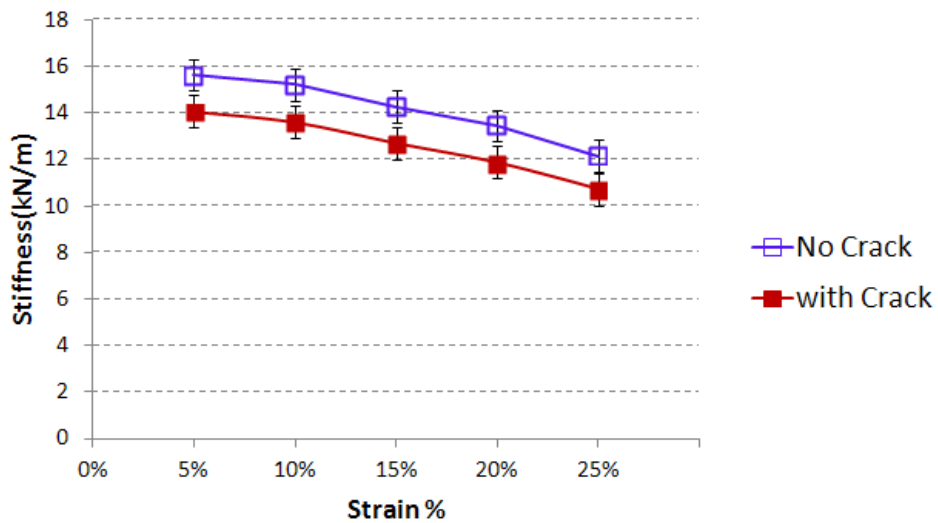


Figure 6-10: Rubber samples geometry in tension test

All testing was conducted at room temperature by applying the strain values as loading condition. The results of tensile test from control panel of tensile test machine and the average values for stress and stiffness are recorded as it is illustrated in Figure 6-11. These graphs present the effect of existence of a known crack in natural rubber coupons for varying strain value up to 25%.



(a) Recorded load cell values vs strain



(b) Calculated stiffness values vs strain

Figure 6-11: Stress and stiffness values in tensile test of rubber samples (crack size= 10mm)

DIC method has been employed to collect the deformation map of samples in tensile tests. The first seeding process using white paint was failed because the density and size of speckles were not controllable. In the first trials, the crack was not visible in the surface of samples after processing the collected data by DaVis software (Seeding method 1).

To improve the seeding step, micro particles and transparent paint were applied on the surface of rubber samples (Seeding method 2). The results of displacement map show the existence of the same crack clearly. The outcome of this improvement attempt is presented in Figure 6-12. It is evidence that the speckle pattern is a vital parameter for DIC method to obtain the accurate deformation field.

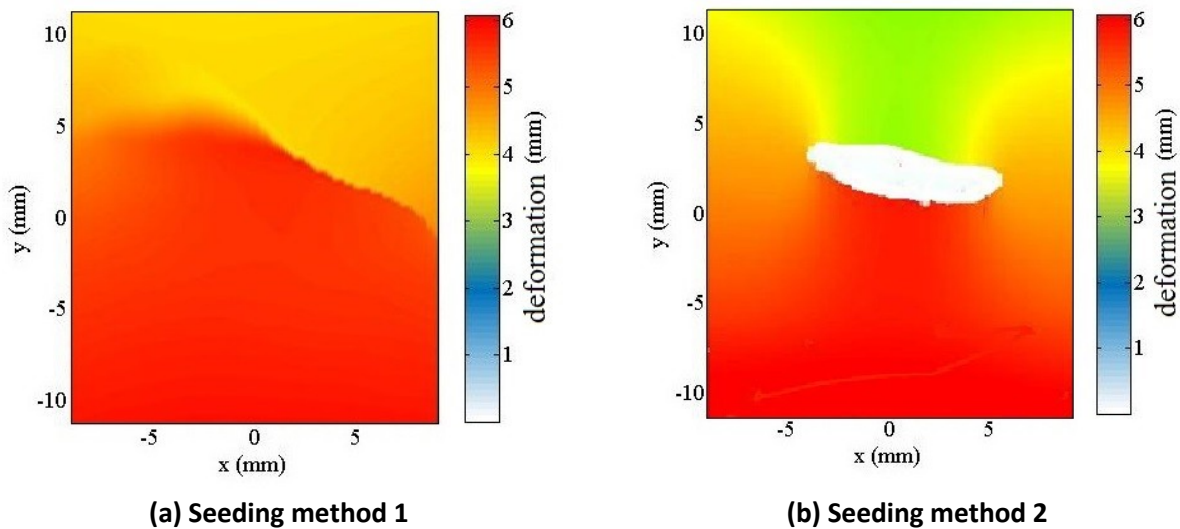


**Figure 6-12: Improvement of deformation measurement using different seeding methods**

The strain map can be calculated from deformation field:

$$\text{Engineering plane strain matrix} = \begin{bmatrix} \epsilon_{xx} & \epsilon_{xy} \\ \epsilon_{yx} & \epsilon_{yy} \end{bmatrix} \quad \text{Equation 6-3}$$

Where:

$$\epsilon_{xx} = \frac{\partial u_x}{\partial x} \quad ; \quad \epsilon_{xy} = \frac{1}{2} \left( \frac{\partial u_x}{\partial y} + \frac{\partial u_y}{\partial x} \right) \quad ; \quad \epsilon_{yy} = \frac{\partial u_y}{\partial y}$$

$u_x$  and  $u_y$  are displacement vector in  $x$  and  $y$  directions , respectively.

To present the strain results visually, a MATLAB code is developed to display the results in the form of contours that can describe the strain field of samples. It is essential to scale the results to be able to compare the strain values in different direction. The program is developed to read the output vector field from DaVis and calculate the strain field by taking the derivative of deformation field. The output of the code is a set of plots of the deformation contours with corresponding vectors and the plane strain values.

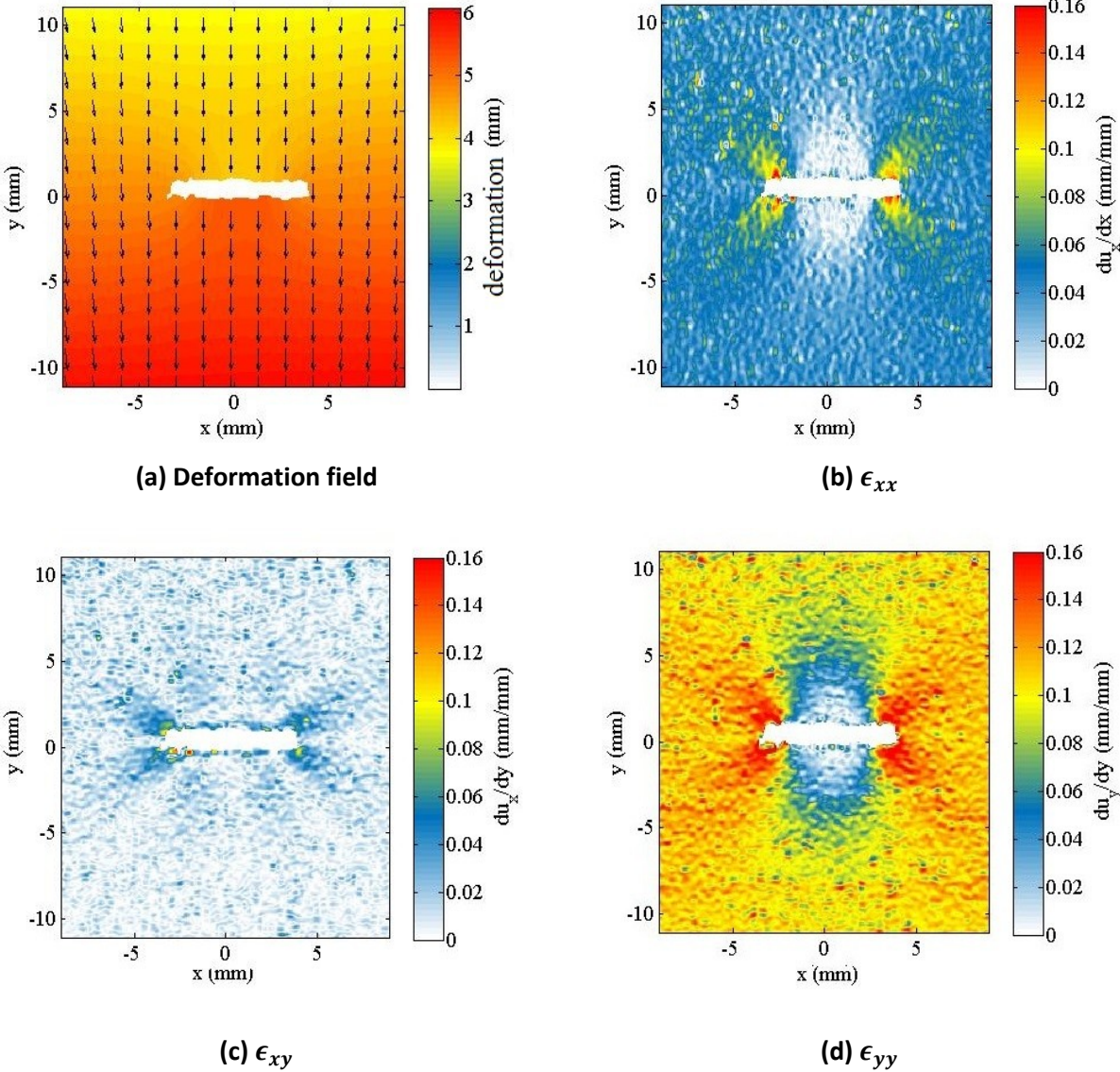


**Figure 6-13: Deformation and strain field of crack rubber sample in tension (Loading= 127.5 N, total strain= 10%)**

Figure 6-13 (a) is deformation field around crack tip with the deformation vector direction and magnitude represented by the black arrows. Figure 6-13 (b-d) illustrate the strain tensor components showing the absolute values of strain field in different directions. It can be determined from this set of images that deformation and strain fields provides a clear view of rubber cut as opposed to tensile displacement. It is important to note that in this study, the effect of loading in  $z$  direction is neglected since it was very small values to be considered as out-of-plane deformation. In the shear strain ( $\epsilon_{xy}$ ), the effect of the cut on the strain field is negligible, however, vertical strain ( $\epsilon_{yy}$ ) has the maximum value. In this case, the vertical strain due to the loading is greater than the horizontal strains, therefore; scaling of the results is essential when strain results are presented visually. Crack tip stress concentration can be observed in all strain components; in particular the maximum strain value happens at crack tips symmetrically.

## **6.2. Finite element model of rubber with crack**

The finite element analysis of rubber with known crack can be categorized into two steps: crack opening and crack propagation. This section focuses on finding the strain field of crack opening in the natural rubber specimen under pure tension force. Using finite element software, Mooney- Rivlin nonlinear hyper-elastic material is employed as common model used for rubber in finite element modeling. This study shows that the strain field of rubber specimen can be predicted by this model at desired strain ranges.

### ***6.2.1. Rubber specimen finite element model***

- Model Generation

A two dimensional finite element model of rubber sample has been developed using ABAQUS software while geometry and boundary conditions are chosen to follow experimental conditions. The first step is to create the two dimensional rectangular geometry with 100 mm length and 25 mm width where crack is a wire feature with the size of 10 mm. Figure 6-14(a) illustrates the rubber sample with an interior crack perpendicular to vertical load direction and Figure 6-14(b) shows the mesh of the model.

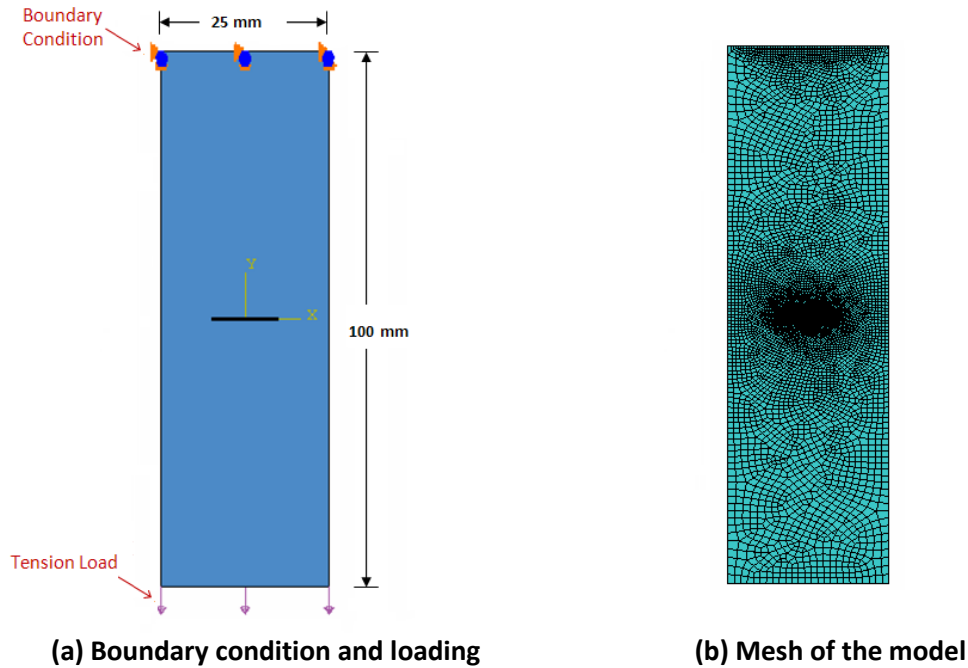


**Figure 6-14: Finite element model of rubber with crack**

The boundary conditions are based on experimental design, where the top edge is selected to be fixed edge and the bottom edge is selected as tensile loading. The tensile load is a displacement vector to create 10% strain at bottom edge. The element type is quad-dominated plane-stress element and mesh sizes are refined around the crack and fixed end of the sample.

- Material Modeling

Finite element analyses of rubber components need a constitutive model to represent the stress-strain relationship of the material. In this study, material is assumed to be natural rubber and Mooney-Rivlin hyperelastic material model was chosen for rubber material. Mooney-Rivlin model is capable of predicting stress-strain behavior by strain energy as:

$$W = C_{10}(I_1 - 3) + C_{01}(I_2 - 3) + D_1(I_3 - 3) \quad \text{Equation 6-4}$$

where  $I_1$ ,  $I_2$  and  $I_3$  are the first, second and the third invariant of the component of the left Cauchy–Green deformation tensor. The parameters  $C_{10}$ ,  $C_{01}$  and  $D_1$  are material constants that can be obtained by standard tests. In this study the values of material constants are chosen from literature to be 118.9, -71.8 and 0.04 (MPa) respectively [Lin and Hwang, 2004].

- Mesh generation around crack tip

The mesh around the crack tip should be finer because a fine mesh near the singular points resolves the rapidly varying stress field and gives accurate information around crack tip. For this reason, a bias mesh is generated in this region using features including datum points and partitions to achieve enough fine mesh around crack tip.

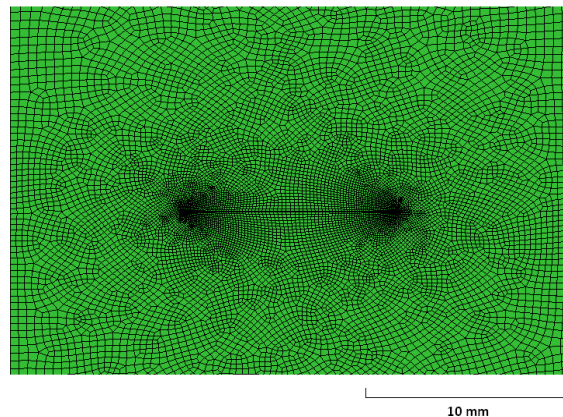


**Figure 6-15: Mesh generation around crack for FE model of rubber**

- Mesh convergence study

As it is described in section (5.5.1) to model the rubber sample, maximum von-Mises stress is chosen as the parameter of interest. Results of convergence study are summarized in Table 6-3.

**Table 6-3: Convergence study for rubber FE model**

Number of elements	max von-Mises stress (KN/m <sup>2</sup> )	CPU time (sec)
555	6,445	8
1,474	7,547	20
2,566	7,148	27
3,269	7,148	33
4,509	7,273	43
5,791	7,379	57
6,654	7,289	77
7,653	7,289	82
9,646	7,288	103
11,911	7,289	136

Figure 5-5 shows the maximum von-Mises stress is remained a fixed value by increasing the elements numbers after the number of elements is 6,654. The convergence criterion is based on the residual of each step to be less than %1. Therefore the number of elements which has been chosen to mesh the model is defined by the convergence study.

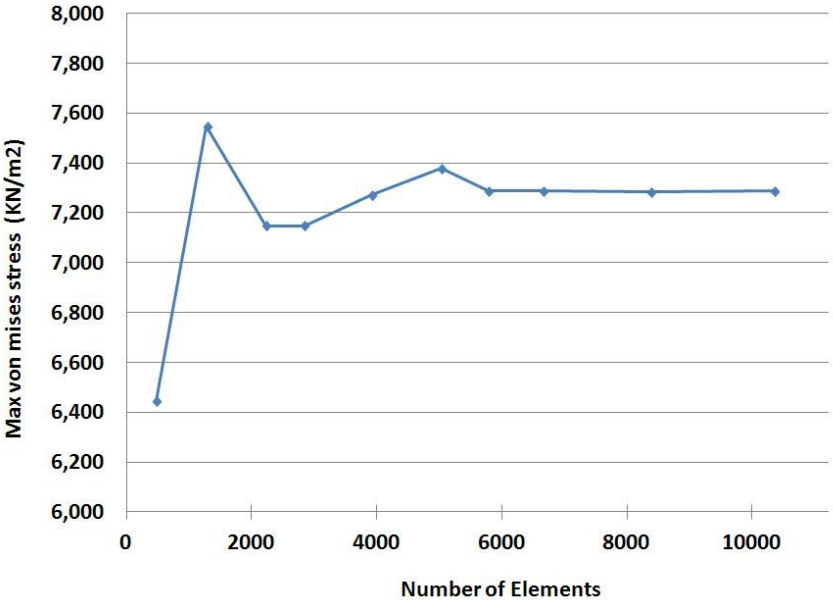


Figure 6-16: Convergence of maximum von-Mises stresses of rubber FE model

**6.2.2. FE model results of rubber with crack**

- Crack opening

The next step of modeling is applying the static tension load to the bottom edge of rubber sample which is displacement vector. The sequences of crack opening are shown in Figure 6-17 when rubber sample stretches 5 mm from lower edge and crack moves from start position to final state due to displacement force.

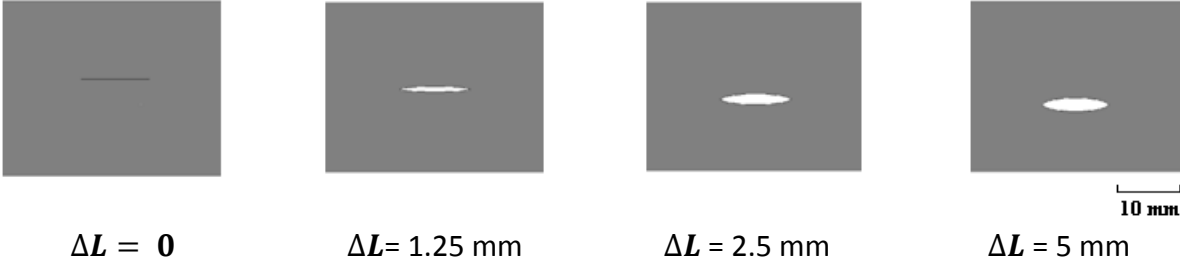
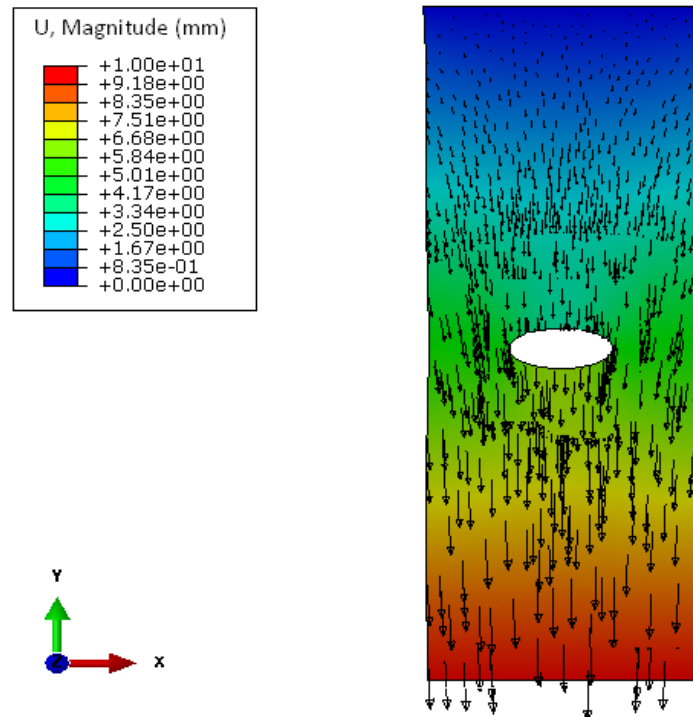


Figure 6-17 : Crack opening sequence in rubber FE model

- Deformation field

Figure 6-18 shows the deformation field of rubber sample under tensile loading to be 10 mm at the bottom edge. The deformation field is obtained for a crack with 10 mm length made perpendicular to the direction of the external force. Vector field direction and magnitude, that has been scaled for clarity, is shown by the black arrows.



**Figure 6-18: Deformation vector field of rubber in tension using FE model**

- Strain field

Strain field values are derivatives of deformation field in different directions as it is described in Equation 6-3. All strain fields in different directions are scaled and color bars limitations are adjusted to minimum and maximum values of strain. It is important to note that, the region above the crack is in compression having negative values while the lower part is in tension with positive values. A MATLAB code is developed to display the absolute values of deformation field and strain field of rubber model. Figure 6-19 (a) shows the deformation magnitude around the crack and Figure 6-19 (b-d) present the strain fields.

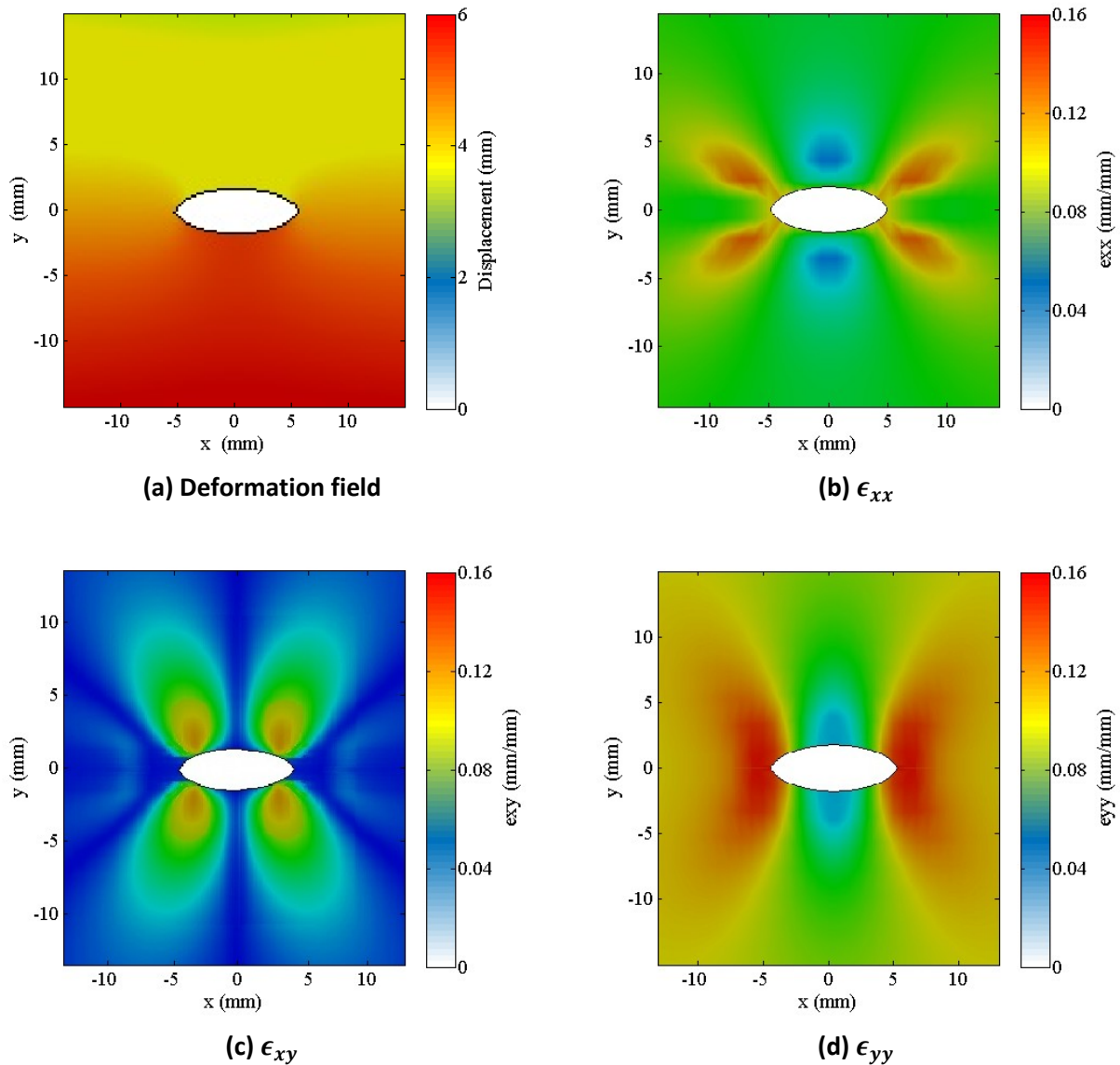


**Figure 6-19: Deformation and strain field of rubber FE model around the crack (BC: Fixed at top; Loading: 10% strain at lower edge)**

As it is shown in Figure 6-19 (a), crack opening is clearly visible in deformation field of rubber under tension loading condition. Figure 6-19 (b-d) present the absolute values of  $\epsilon_{xx}$ ,  $\epsilon_{xy}$  and  $\epsilon_{yy}$  which are strain tensor components in different directions. In the case of vertical strain ( $\epsilon_{yy}$ ) the effect of the cut on the strain field is dominant with the maximum value of strain fields. All of strain fields are symmetric with respect to crack position and also crack tip stress concentration can be observed in all strain components.

### **6.3. Heat generation of rubber with crack**

Tires generate heat during their operation because of hysteresis properties of the rubber under cyclic loading. Build up heat in rubber can affect the material properties and its life span. To avoid the temperature related failures many studies have been carried out to evaluate the rubber temperature [Li et al., 2012]. The rubber material loses strength and its stiffness is changed when the temperature increases; by softening the natural rubber structure or melting at higher temperature ranges [Gardner, 2006].

Rubber heat generation is a complex problem to be solved theoretically, therefore; temperature distribution of rubber usually is studied using experiments or finite element method [Li et al., 2011]. A simplified formulation can be employed to determine the heat generation and heat dissipation phenomenon in rubber. Thermomechanical models are also used to find the solution of rubber heat transfer problem in order to obtain the temperature distribution. This modeling is more challenging when the rubber has a crack, even in the purely elastic case. The rubber with crack can be modeled by using material characterization changes as well as the proper FE meshing and solution strategies.

If a structural analysis can be coupled to thermal analysis; the output is a model that relates the temperature and constitutive relationship variations. Therefore, this model determines the relationship between thermal gradients and changes of stiffness of rubber.

#### **6.3.1. Basic Theory of rubber heat generation**

It has been shown that rubber, as the main component of tire, contributes in more than 90% of tire energy loss due to its hysteretic property [Wong, 2001]. Therefore, in this approach it is assumed that the energy loss is completely caused by hysteresis effect of rubber and the heat generated by friction of tire and road surface is neglected. A simplified formula has been presented using the concept of hysteresis property of rubber material when it is under dynamic loading condition. The hysteresis constant ( $H$ ) is defined to be loss energy divided by total kinematic energy of rubber which is given as:

$$H = \frac{E''}{\sqrt{(E')^2 + (E'')^2}} \quad \text{Equation 6-5}$$

where; storage modulus ( $E'$ ) and loss modulus ( $E''$ ) can be obtained by Dynamic Mechanical Analysis (DMA) test for each material.

The heat generation rate ( $Q$ ) is energy loss per cycle of a volume unit per unit time, can be calculated by:

$$Q = H * W * f \quad \text{Equation 6-6}$$

where  $W$  and  $f$  are total strain energy and frequency of dynamic load, respectively.

There is a method to calculate the strain energy ( $W$ ) with harmonic sinusoidal form where hysteresis effect is defined by phase lag  $\delta$  between stress and strain as given:

$$\varepsilon = \varepsilon_0 \sin(\omega t); \quad \sigma = \sigma_0 \sin(\omega t + \delta) \quad \text{Equation 6-7}$$

where  $\varepsilon$  is strain and  $\sigma$  is stress;  $\varepsilon_0$  and  $\sigma_0$  represent the strain and the stress amplitude.

The loss strain energy per cyclic period is:

$$W = \int_0^{1/f} (\sigma \cdot \dot{\varepsilon}) dt = \pi \varepsilon_0^2 E'' \quad \text{Equation 6-8}$$

$W$ ,  $\varepsilon_0$  and  $E''$  are strain energy, strain amplitude and loss modulus [Song et al., 1998].

Now, the heat generation rate ( $Q$ ) can be calculated using strain energy ( $W$ ) and from there tire temperature can be obtained for heat conduction.

$$\frac{\partial T}{\partial t} = \frac{\lambda}{C \rho} \nabla^2 T + \frac{Q}{C \rho} \quad \text{Equation 6-9}$$

Where  $T$ ,  $t$ ,  $\lambda$ ,  $C$  and  $\rho$  are temperature, time, rubber thermal conductivity, rubber specific heat and rubber material density respectively.

This formulation is the basic theory of rubber temperature prediction assuming that the energy generation is because of the hysteresis effect of rubber and radiative heat exchange is neglected [Li et al., 2010].

### 6.3.2. Basics of thermomechanical modeling

The thermomechanical model of rubber has been employed for estimation of loss energy and the temperature profile. In recent years, researchers started to simulate the rubber heat generation physically and mathematically by nonlinear finite element analysis using computational capabilities. Several researchers suggested different simplified techniques to deal with the coupled thermomechanical problem for hyperelastic materials [Narasimha Rao et al., 2006]. The complicated thermomechanical model can be organized in three stages which are deformation, dissipation and thermal modules (Figure 6-20).

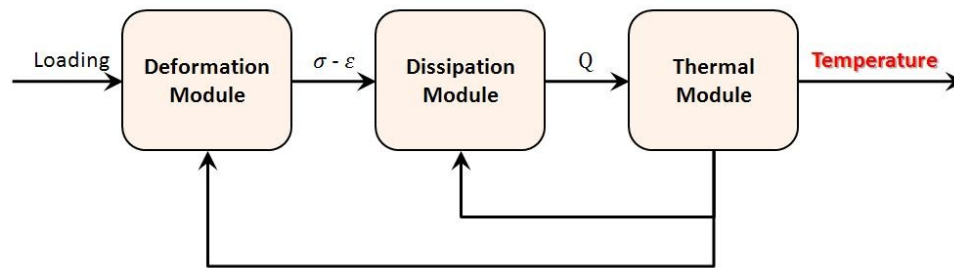


Figure 6-20: Fully coupled thermomechanical model

To decrease the complexity of the thermomechanical model different simplifying methods have been used:

- Uncoupled (using deformation and dissipation modules to compute temperature),
- Partially coupled (Temperature has effect on dissipation modules),
- Fully coupled (temperature has effect on both deformation and dissipation modules).

The simplification method depends on the type of material, desired accuracy, and the available computational resources [Futamura et al., 2004]. Besides all one-way method researches, there are some attempts to find the results in a partially and fully coupled form where the temperature dependency of material property is included by iteration of the computed temperature.

To perform a fully coupled analysis, the analysis starts with deformation (structural) model, where material properties are defined as a function of temperature. Initial temperatures and loading conditions are defined to calculate the elements strains.

The strains are used as an input to the energy dissipation module. In the energy dissipation module, the loss modulus is also defined as a function of temperature. Energy dissipation values and heat flux associated with elements are computed at this module.

In order to obtain the temperature distribution, the thermal model uses the heat fluxes from the energy dissipation module and thermal boundary conditions.

The end of this step and finding the temperature profile is considered as “uncoupled” one way analysis. The “partially coupled” method is completed when the calculated temperatures are applied in the energy dissipation module to update the loss modulus and thermal analysis provides new temperatures. The temperatures from the energy dissipation loop are recycled to deformation analysis to update the material properties for the new temperatures. The whole process proceeds again which is called “fully coupled” iterative calculation method.

### ***6.3.3. Thermomechanical model summary***

Structural analysis of rubber is affected by heat generation when temperature rises and loss of strength changes the material property due to devolcanization. Thermomechanical analysis of rubber provides an understanding of the effect of heat generation on rubber material property. This model is a measurement of the strain energy effect on heat generation and consequently time change of stiffness could be obtained.

In addition, other information can be measured by thermal cameras that could be implemented in a laboratory scale to examine heat generation in the rubber under different dynamic loads. The output of the experiments is the temperature distribution of rubber surface in time domain which is recorded by thermal camera. The temperature profile of rubber sample with crack can be used for validation of the finite element thermomechanical model.

#### 6.4. Concluding remarks on rubber damage study

This chapter is an investigation conducted to observe the effect of rubber damage on the displacement of its surface, using experimental and numerical methods. Natural rubber as the main component of haul truck tires is chosen as tested sample while static tensile loading is applied to obtain stress-strain relationship of rubber with crack.

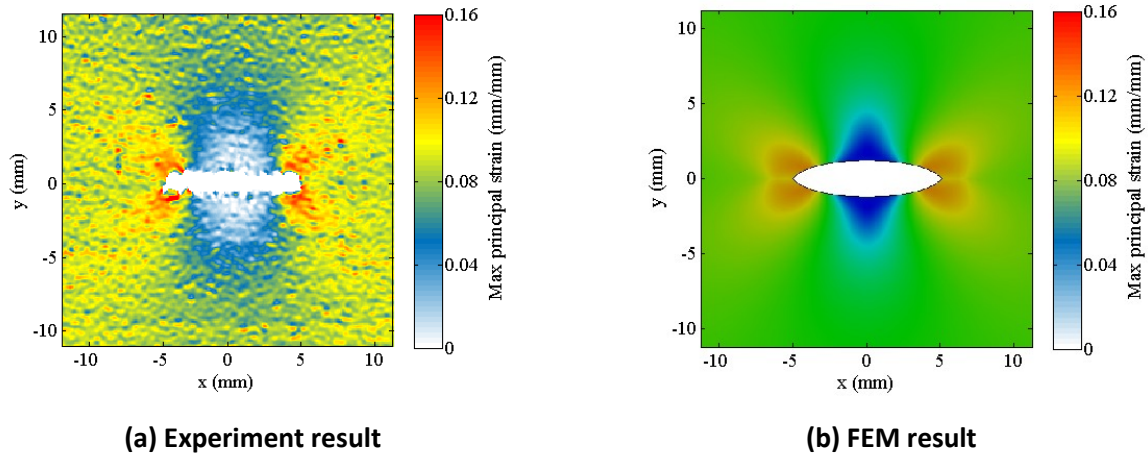
An experimental study was conducted to characterized natural rubber crack opening response to quasi-static load using DIC measurement technique. The experiments show that the speckle pattern and subset size are important factors to find the deformation field and visibility of crack on the surface of rubber. In this study, an efficient method for seeding the rubber surface is presented. The deformation of rubber specimen with known cut was calculated from recorded images of the sample under tensile loading. Calculated deformation vectors and strain tensor components over a region of interest are presented in Section 6.1.6.

In order to find the strain field of rubber, finite element analysis (FEA) was carried out using hyperelastic material properties of natural rubber using Mooney-Revinlin model. The FEA procedure included a convergence and mesh design study to obtain optimized model. The finite element model determined the deformation and components of strain field of the region around the crack in rubber specimen.

In this study, it is found that, visually, strain field is a clearer indication of rubber damage than displacement. To describe the strain field around the crack independent of  $x$  and  $y$  direction, the parameter of maximum principal strain is introduced. The associated maximum principal strain is given by:

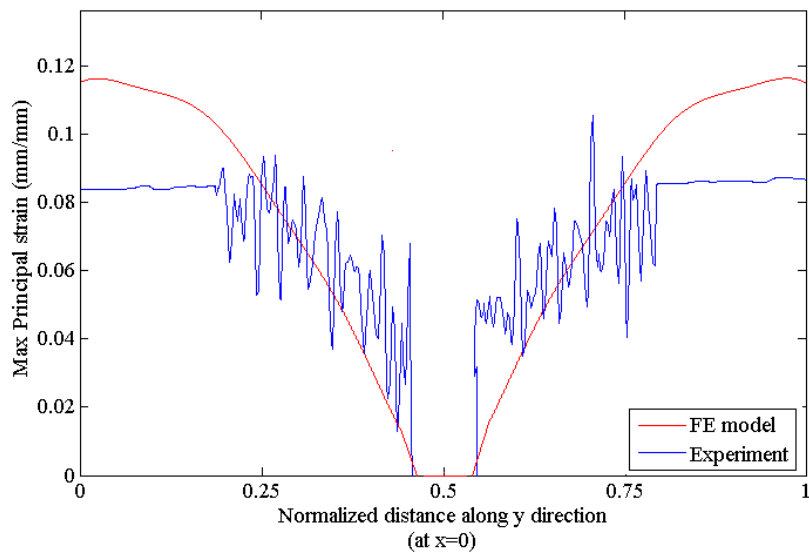
$$\epsilon_{max.principal} = \frac{\epsilon_{xx} + \epsilon_{yy}}{2} + \sqrt{\left(\frac{\epsilon_{xx} - \epsilon_{yy}}{2}\right)^2 + \epsilon_{xy}^2} \quad \text{Equation 6-10}$$

The maximum principal strain from experiments and FE model are plotted in Figure 6-21 showing the symmetric strain field around the crack. Maximum strain points are located at crack tips and middle regions of crack have minimum values of strain values.



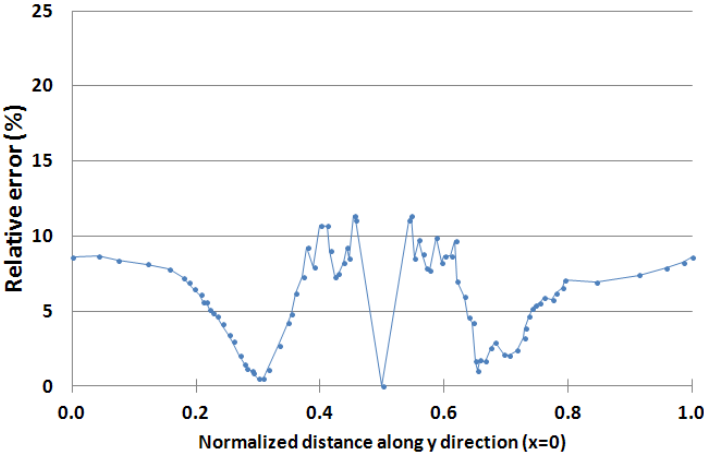
**Figure 6-21: Maximum principal strain field around crack**

Figure 6-22, illustrates the maximum principal strain values along  $y$  direction at  $x = 0$ . A MATLAB code was developed to plot this graph showing the variation of strain for both experiment measurements and finite element model. The plot can be used to define crack opening value which has zero maximum principal strain.



**Figure 6-22: Maximum principal strain along y direction**

Maximum principal strain predicted by finite element model can be compared to the value obtained using DIC in experiments. The relative error of FEM and DIC methods is plotted for Maximum principal strain along y direction. As it is shown in Figure 6-23, the relative error value is under 12% for the calculated parameter.



**Figure 6-23: Relative error of FEM and DIC methods (maximum principal strain)**

The experimental results show good agreement with numerical simulation; validating the properties employed to model rubber material. This result suggests an acceptable model for rubber stress-strain relationship which can be used to find the overall vertical stiffness of the finite-element tire model presented in Section 5.5.

It is shown in section 5.5.2 that tire stiffness function versus tire rotation angle can be presented by a sigmoid function using FE model of tire. The stiffness changes due to crack opening can be calculated from rubber experiments. In order to find the stiffness function of tire, a set of experiments can be defined to simulate the rotation of tire. The experiment design to measure stiffness of rubber with changes of crack angle is suggested in Figure 6-24.

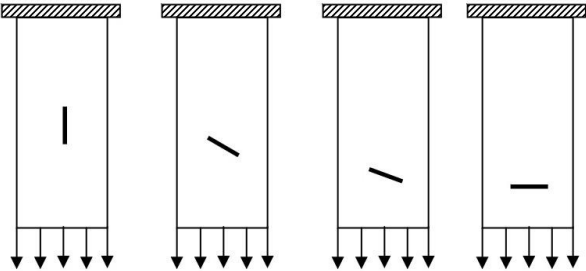


**Figure 6-24: Experiment design to observe the effect of crack angle**

## Chapter 7. Conclusions and Future Work

---

### 7.1. Conclusions

In this research, mining haul truck tires failure was the focus of study to contribute to understanding the behavior of damaged tires, and also the future development of a tire condition monitoring and fault detection system.

Initially, haul truck tire failure modes and the effect of different parameters such as haul road condition and seasonal effect on their lifetime is investigated based on oilsands service tire database. Following these studies, life time of haul truck tires is predicted by reliability modeling showing that the 90% of tire lifetime distribution is between 2000 to 8000 operating hours.

In this project, due to the complex nature of tire problem, a reduced order dynamic model is developed to describe the effect of damage on overall system behavior. The key challenge of developing this dynamic model is the unknown changes of the original properties of the tire when a fault exists. Therefore, a finite element model is developed to estimate the tire stiffness variations when a crack rotates along tire rotation. The tire model material is assumed natural rubber since it is the main component of mining haul truck tires.

The suitability of the material properties is verified by comparing the finite element model of rubber material with experimental results. To accomplish this, a laboratory-scale system is developed to obtain deformation and strain of damaged rubber specimen using optical DIC technique. The finite element analysis of rubber specimen was carried out to find the deformation and strain field of rubber specimen. The experimental and numerical simulation results suggest an acceptable material constitutive relationship for crack opening in rubber.

The verified rubber material property is used to find the variations of overall tire stiffness due to tire damage. The obtained stiffness function was incorporated in the dynamic model resulting in the displacement response of the system that can be used to detect faults in a haul truck tire.

In conclusion, the main observations of this study can be summarized as below:

- The presented dynamic simulation has shown that the tire vertical displacement can be an indicator to determine the presence of fault in the tire.
- Based on simple tire finite element, the minimum tire stiffness value occurs when crack position is near to contact patch.
- The minimum tire stiffness value decreases by the crack size.
- Digital image correlation is a full-field, non-contact measurement technique that can be applied to measure rubber surface deformation.
- This research suggested an acceptable constitutive relationship for crack opening of rubber; using the experimental and numerical simulation.
- In rubber tensile condition, the maximum value of strain is in the direction of loading direction based on experimental and finite element results.
- Maximum strain and stress values happen at crack tip in both experimental and finite element results.
- The experiments show that the speckle pattern and size are important factors to find the deformation field and visibility of crack on the surface of rubber.
- In this study, an efficient method for seeding the rubber surface is presented using particles with controlled size and transparent paint. Using this method, crack opening could be clearly distinguished in the deformation and strain field.
- It was found that strain field provides a visually clearer indication of rubber damage than deformation field.

## **7.2. Future work**

There are applications for the development of model based systems for tire condition monitoring, in both research and industry. This section presents future possibilities for improvement of developed tire dynamic model, as well as its industrial applications.

### ***7.2.1. Recommendation for future studies***

- The order of dynamic model and the corresponding parameters have a determining effect on the fault diagnosis system accuracy. Therefore, using of higher order model and field level measured parameters of real mining truck condition is recommended.
- The type of fault, operating conditions, as well as tire internal pressure and temperature are suggested to be considered in modeling since they affect the tire stiffness.
- One of the main factors in tire dynamic modeling is road profile which is assumed in this research. Therefore, a more realistic road pattern should be evaluated by using an actual observable variable such as strut pressure, or wheel axle and frame vertical accelerations, as an indirect measure of road quality.
- Three dimensional finite element modeling of tire containing its structural components will provide better mimic of tire behavior.
- Different crack size, location and direction are recommended to be tested experimentally and numerically.
- Using steel cord rubber or real tire specimen coupons for experiment will provide more reliable results of tire response to loading condition.
- One area of interest is crack propagation in rubber, where DIC results could be compared to FE models to evaluate damage mechanisms in rubber.
- Tire damping coefficient can represent the heat generation characteristics of tire. It is recommended to find the relationship between damping coefficient and heat generation.
- A thermal camera is suggested to be implemented in a laboratory setup to examine heat generation in rubber to observe the effects of tire damage on heat generation.

### **7.2.2. Industrial application**

The research reported herein should be considered as an initial step toward the design and development of model-based automated tire inspection and fault detection system to be used at operational field level.

Modeling of a tire considering discrete spring and damper elements can be one of the most effective candidates for industrial application, since the tire structure is defined by sufficient detail avoiding large computations. In addition, the presented method can be used to supervise the tire condition which requires measurements of the road profile and tire vertical displacement. Displacement and velocity can be measured by different methods such as strut pressure measurement, optical method to observe the vertical deflection of tire and other measurement techniques such as accelerometers (with integration constants to yield vertical displacement and velocity).

Methods described in this work can be used to simulate the dynamic response of a tire if a fault exists. It has been shown that it is possible to detect damage in a tire from dynamic modeling. In summary, the model developed in this work can be used to gain a better understanding of changes in tire behavior due to damage, and potentially extend tire life.

## References

---

- Al-Garni, A. Z. and Jamal, A., 2011, "Artificial neural network application of modeling failure rate for Boeing 737 tires," *Quality and Reliability Engineering International*, 27(2), pp.209–219.
- Allouis, C., Amoresano, A., and Giordano, D., 2012, "Measurement of the Thermal Diffusivity of a Tire Compound by Mean of Infrared Optical Technique," *International Review of Mechanical Engineering*, 6(6) pp. 1104-1108.
- Bennett, R. D. V., Ceato, H., Lake, G. J., Rollason, R. M., and Pittman, G. A., 1975, "Mechanisms of Heat Build-Up Failure in Tyres," *International Rubber Conference*, Kuala Lumpur, pp. 1-20.
- Blackwell, G.F., 1989, "Machine vision in the tire industry," *IEEE Conference, Conference of Electrical Engineering Problems in the Rubber and Plastics Industries*, pp. 67–79.
- Bolster, M.J.A., and Joseph, T.G., 2005, "Tire-Rim Interactions for Ultra Class Trucks in The Mining Industry," *The 19th International Mining Congress and Fair of Turkey IMCET2005*, pp. 161 – 168.
- Brothen, C., Lee, T., 2008, "An ounce of prevention," *Canadian Institute of Mining Magazine*, 3(1).
- Camera (GX3300) website, <http://www.alliedvisiontec.com/emea/products/cameras/gigabit-ethernet/prosilica-gx/gx3300.html>, 2013.
- Carter, R., 2011, "OTR Tire Supply Comes Under Pressure," *Coal age* 116, pp. 34-37
- Castillo, J., De La Blanca, A., Cabrera, J., and Simon, A., 2006, "An optical tire contact pressure test bench," *Vehicle System Dynamics*, 44(3), pp. 207-221.
- Chen, Q., Weaver, J. M., and Xu, G., 2014, "Research on Real-time Identification for Tire Failure," *American Journal of Mechanical Engineering*, 2(3), 54-57.
- Chevalier, L., Calloch, S., Hild, F. and Marco, Y., 2001, "Digital image correlation used to analyses the multiaxial behavior of rubber-like materials," *European Journal of Mechanics A/Solids*, 20, pp.169–187.
- Chu, T.C., Ranson, W.F., Sutton, M.A., and Peters, W.H., 1985, "Applications of the digital-image-correlation techniques to experimental mechanics," *Experimental Mechanics*, 25, pp.232-244.
- Clark, S.K. 1981, "Mechanics of pneumatic tires (2nd Edition)", U.S. Dept. of Transportation, National Highway Traffic Safety Administration.
- Cloud, G., 1998, "Optical Methods of Engineering Analysis," Cambridge University Press.
- Conant, F.S., 1971, "Tire Temperatures," *Rubber Chemistry and Technology*, 44(2), pp. 397-439.
- Crammond, G, Boyd, S, and Dulieu-Barton, J., 2013, "Speckle pattern quality assessment for digital image correlation," *Optics and Lasers in Engineering*, 51, pp. 1368-1378.

- Cui, S., Song, X., and Li, Z., 2011, "The study of vehicle tire's temperature rising mechanism," Proceedings 2011 International Conference on Transportation, Mechanical, and Electrical Engineering, TMEE 2011, pp. 755-758.
- Dey, A., Bhattacharya, J. and Banejee, S., 1994, "Prediction of field reliability for dumper tires, " International Journal of Surface Mining, Reclamation and Environment, pp. 23-25.
- Dhillon, B.S., 2008, "Mining Equipment Reliability," Mining Equipment Reliability, Maintainability, and Safety, pp. 57-70.
- Donati, S. ,2004, "Electro-optical Instrumentation Sensing and Measureing with Lasers," Prentice Hall PTR.
- Ebbott, T.G., 1996, "An Application of Finite Element-Based Fracture Mechanics Analysis to Cord-Rubber Structures," Tire Science and Technology, 24(3), pp. 220-235.
- Elsinga, G.E., Scarano, F., Wieneke, B., and Van Oudheusden, B.W., 2006, "Tomographic particle image velocimetry," Experiments in Fluids, 41, pp. 933-947.
- Erne, O., 2009, "Determination of 3D Deformations of Tire Surfaces Under Extreme Driving Conditions," GOM mbH.
- Feng, X., Yan, X., Wei, Y. and Du, X., 2004, "Nonlinear Finite Element Modeling of Delamination Crack Growth Process between Belts of a Radial Tire," Journal of Reinforced Plastics and Composites, 23(4), pp.373-388.
- Gardner, J. D., and Queiser, B. J., 2006, "The Pneumatic Tire," Department of Transportation, National Highway Traffic Safety Administration, Akron, OH, Chap.15.
- Ghoreishy, M., 2008, "A State of the Art Review of the Finite Element Modeling of Rolling Tyres," Iranian Polymer Journal (English Edition), 17(8), pp. 571-597.
- Green, P.E., 2009, "Analysis of Data from the Thermal Imaging Inspection System Project," The University of Michigan Transportation Research Institute.
- Gros, X. E., 1997, "Detection of delamination in tires using eddy currents," Journal of Automotive Engineering, 211(D1).
- Hajizadeh, M., Lipsett, M. G., 2013, "Anomaly detection in mining haul truck suspension struts, " International Journal of Condition Monitoring
- Han, Y.H., Becker, E.B., Fahrenthold, E.P. and Kim, D.M., 2004,"Fatigue life prediction for cord-rubber composite tires using a global-local finite element method," Tire Science and Technology, 32, pp. 23-40.
- Huang Y., 2002, "Development of digital image correlation method for displacement and shape measurement," Peking University.

- Ivanov, V., 2010, "Analysis of Tire Contact Parameters Using Visual Processing," Hindawi Publishing Corporation Advances in Tribology, pp.11
- Kaang, S., Jin, Y.W., Huh, Y.-i., Lee, W.-J., Im, W.B., 2006, "A test method to measure fatigue crack growth rate of rubbery materials," Polymer Testing, 25 (3), pp. 347-352.
- Kainradl, P., and Kaufmann, G., 1976, "Heat Generation in Pneumatic Tires," Rubber Chemistry and Technology, 49(3), pp. 823-861.
- Kaliske, M., Naser, B. and Meiners, C., 2007, "Inelastic fracture mechanics for tire durability simulations," Tire Science and Technology, 35, pp. 239-250.
- Kerchman, V., and Shaw, C., 2003, "Experimental Study and Finite Element Simulation of Heat Build-Up in Rubber Compounds with Application to Fracture," Rubber Chemistry and Technology, 76(2), pp.386-404.
- Khan-Jetter Z.L. and Chu T.C., 1990, "Three-dimensional Displacement Measurements Using Digital Image Correlation and Photogrammic Analysis," Experimental Mechanics, 30(1), pp.10-16.
- Kogel, J., 2009, "Industrial Minerals & Rocks: Commodities, Markets, and Uses," SME.
- Kotchon, A., 2013, "Damage detection in tires from strain values calculated using digital Image correlation," MSc dissertation, Department of Mechanical Engineering, University of Alberta, Canada.
- Krivtsov, V.V., Tananko, D.E. and Davis, T.P., 2002, "Regression approach to tire reliability analysis," Reliability Engineering and System Safety, pp. 267–273.
- Li, Y., Liu, W. Y., and Frimpong, S., 2012, "Effect of Ambient Temperature on Stress, Deformation and Temperature of Dump Truck Tire," Engineering Failure Analysis, 23, pp. 55-62.
- Lin, P., Chawla, M., and Ulrich, P., 1994, "Optical technique for measuring tire deformation and strains Preliminary results," SAE Aerospace Atlantic Conference and Exposition
- Lin, Y., and Hwang, S., 2004, "Temperature Prediction of Rolling Tires by Computer Simulation," Mathematics and Computers in Simulation, 67(3), pp. 235-249.
- Lipsett, M., and Vaghar-Anzabi, R., 2013, "Seasonal Effects on Haul Truck Tire Life," International journal of Strategic Asset Management, 13 pp.
- Lipsett, M., Vaghar- Anzabi, R., Kotchon, A., and Nobes, D., 2011, "Condition monitoring for mining haul truck tires," Proceedings of the Eighth International Conference on Condition Monitoring and Machinery Failure Prevention Technologies (CM 2011 and MFPT 2011), Cardiff, UK, 12 pp.
- Malamasa, E.N., Petrakisa, E.G.M, Zervakisa, M., Petitb,L., and Legat, J., 2003,"A survey on industrial vision systems, applications and tools," Image and Vision Computing 21, pp. 171–188.
- Mars, W. V., and Fatemi, A., 2004, "Factors that Affect the Fatigue Life of Rubber: A Literature Survey," Rubber Chemistry and Technology, 77(3), pp. 391-412.

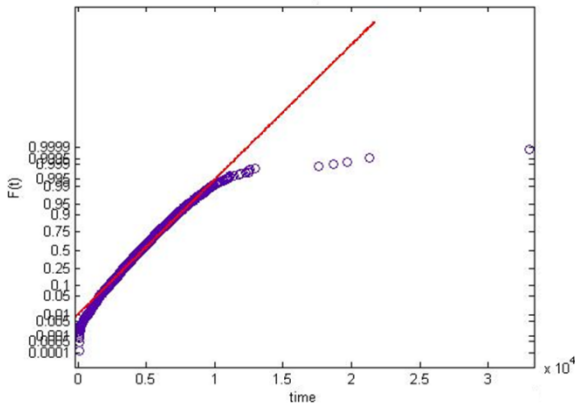
- Mars, W.V, Fatemi, A., 2002, "A literature survey on fatigue analysis approaches for rubber," *International Journal of Fatigue*, 24(9), pp. 949-961.
- Matthews, P.A. and Nowatzki, E.A., 1989, "The effect of pneumatic tire characteristics on the performance of off-highway trucks," *International Journal of Mining, Reclamation and Environment*, 3(2), pp. 99 – 105.
- McCormick N. and Lord J., 2010, "Digital image correlation," *Mater Today*, 13(12): 52–54.
- McGarry, P., 2007, "Haul Truck Tires and Open-pit mining," Department of Mining Engineering, Queen's University, Canada.
- Mery, D., 2002, "Automated Flaw Detection in Aluminum Castings Based on the Tracking of Potential Defects in a Radioscopic Image Sequence," *IEEE Transactions on Robotics and Automation*, 18 (6).
- Michelin data book, 2011, "Michelin truck tire data book, Mttddb," 13th edition.
- Miede, A. J. P ,2004, "Tyre model for truck ride simulations," CPGS dissertation, Department of Engineering, University of Cambridge, UK.
- Miller, D., Schandelmeier, R., and Zegel, F., 2000, "Predicting Truck Tire Problems with the Thermal Image Inspection Station (TIIS) in the Lab and in the Field," *SAE Technical Paper*.
- Modarres, M., Kaminskiy, M. and Krivtsov, V., 2009, "Reliability Engineering and Risk Analysis: A Practical Guide," CRC Press.
- Moser R. and Lightner, J.G., 2007, "Using three-dimensional digital imaging correlation techniques to validate tire finite-element model," *Experimental Techniques*, 31(4), pp. 29-36.
- Moser, R. , James Sube, H.b , Turner, J.L. , Zakelj, P., 2010, "3D digital imaging correlation: Applications to tire testing," *Tire Science and Technology*, 38 (2), pp. 100-118.
- Moser, R., and Lightner, J. G., 2007, "Using three-dimensional digital imaging correlation techniques to validate tire finite-element model," *Experimental Techniques*, 31(4), 29-36.
- Netscher, N. W., Aminossadati, S. M., and Hooman, K., 2008, "A Review of Patents in Tyre Cooling," *Recent Patents on Engineering*, 2(2), pp. 87-94.
- Oh, B.S., Kim, Y.N., Kim, N.J., Moon, H.Y., and Park, H.Y., 1995, "Internal Temperature Distribution in a Rolling Tire," *Tire Science and Technology*, 23(1), pp. 11-25.
- Ok, A., Ozupek, S. and Becker, EB., 2007, "Crack simulation in pneumatic tires using the finite element method," *Proceedings of the Institution of Mechanical Engineers, Part D: Journal of Automobile Engineering*, 221(2), pp. 157-166.
- Orrell, J.R., 2008, "Tire failure detection," *US Patent Publ.* 2008/0018441.

- Orteu, J., 2009, "3-D computer vision in experimental mechanics. Optics and Lasers in Engineering," 47(3-4), 282-291.
- OTR tires handbook, 2010, "Yokohama off-the-road tires handbook"
- Otraco, 1993, "Developments in Tyres for Quarrying," OTRACO (International) Pty Ltd.
- Prevorsek, D. C., Beringer, C. W., and Palley, I., 1985, "Application of fracture mechanics in tire endurance analysis," Kautschuk Und Gummi, Kunststoffe, 38(5), pp. 363-371.
- Ramji, K., Goel, V. K., and Saran, V. H., 2002, "Stiffness properties of small-sized pneumatic tyres," Proceedings of the Institution of Mechanical Engineers, Part D: Journal of Automobile Engineering, 216(2), 107-114.
- Réthoré, J., Hild, F. and Roux, S., 2008, "Extended digital image correlation with crack shape optimization," International Journal of Numerical Methods in Engineering, 73, pp. 248-272.
- Ruel, S., English, C., Anctil, M. and Church, P., 2005, "3D Lasso: real-time pose estimation from 3d data for autonomous satellite servicing," ISAIRAS 2005 Conference, Germany.
- Schaefer, R.J., 2002, "Mechanical properties of rubber," Harris' Shock and Vibration Handbook (5th edn), McGraw-Hill: New York.
- Sheikh, A. K., Al-Garni, A. Z. and Affan Badar, M., 1996, "Reliability analysis of airplane tires," International Journal of Quality and Reliability Management, pp. 28-38.
- Sokolov, S. L., 2009, "Analysis of the Heat State of Pneumatic Tires by the Finite Element Method," Journal of Machinery Manufacture and Reliability, 38(3), pp. 310-314.
- Steen, R., and Nijmeijer, H., 2007, "Tire/road friction modeling, Eindhoven University of Technology," Department of Mechanical Engineering, Dynamics and Control group.
- Strain of Optical, 2005, Draft SPOTS Standard Part III (6).
- StrainMaster, 2007, Product Manual, LaVision GmbH 107-130.
- Syncrude staff, Personal communication with Syncrude Canada Ltd staff, 6 Oct. 2011.
- Tannant, D., and Regensburg, B., 2001, "Guidelines for Mine Haul Road Design," University of Alberta, School of Mining and Petroleum Engineering.
- Thompson, R., Visser, A., Miller, R. and Lowe, T., 2003, "Development of Real-Time Mine Road Maintenance Management System Using Haul Truck and Road Vibration Signature Analysis," Journal of the Transportation Research Board, 1819A, pp. 305-312.
- Tiffany D. ,2009, "Health Monitoring for Condition-Based Maintenance of a HMMWV using an Instrumented Diagnostic Cleat," SAE International.

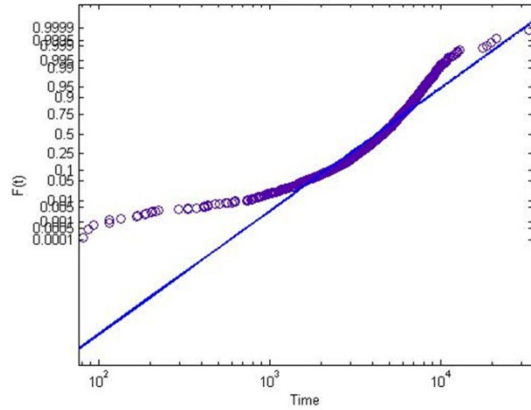
- Tobias, P., 2012, Engineering Statistics Handbook, Reliability Data Analysis, chapter 8, section 8.4.1.2
- Vaghar Anzabi, R., and Lipsett, M.G., 2011, "Reliability analysis and condition monitoring methods for off-road haul truck tires," Proc 24th COMADEM Stavanger Norway, 10 pp.
- Vaghar- Anzabi, R., Nobes, D.S. and Lipsett, M.G.,2012, "Haul truck tire dynamics due to tire condition," Journal of Physics: Conference Series , 364(1).
- Wei, Y, Tian, Z, and Du, X., 1999, "A Finite Element Model for the Rolling Loss Prediction and Fracture Analysis of Radial Tires," Tire Science and Technology, 27(4), pp. 250-276.
- Weispfenning, T., 1997, "Fault Detection and Diagnosis of Components of the Vehicle Vertical Dynamics," Meccanica 32: 459–472.
- Wilson, A., 2010, "X-Ray Vision," Vision Systems Design, pp. 19-21.
- Wiseman, Y., 2010, "Take a picture of your tire," Vehicular Electronics and Safety (ICVES), 2010 IEEE International Conference.
- Wu J., 2011, "Survival analysis of real-world tire aging data," Proceedings of the 22nd International Technical Conference on the Enhanced Safety of Vehicles (ESV).
- Yeow, S. H., El-Sherbiny, M., and Newcomb, T. P., 1978, "Thermal Analysis of a Tyre during Rolling Or Sliding," Wear, 48(1), pp. 157-171.
- Yin, H. S., Hu, Y. S., Zhang, H., 2006, "Truck Tire Thermal-Mechanical FEA and DMA with Application to Endurance Evaluation," Tire Science and Technology, 34(4), pp. 220-236.
- Zhong, X.A., 2006, "Computational Fracture Mechanics Analysis of Truck Tire Durability," Journal of Applied Mechanics, 3(5), pp. 799-806.
- Zhou, J., Hall, R., Huntingford, K., and Fowler, G., 2008, "Effect of off-the-road tyre rotation practices on tyre life: a case study," Mining Technology: IMM Transactions Section A, 117(3), pp. 101-110.
- Zhou, J., Hall, A., Fowler, G. and Huntingford, K., 2008, "Evaluation of the effect of off-the-road tire air pressure setting on tire performance," International Journal of Mining, Reclamation and Environment, 22(3), pp. 237-244.
- Zhu, Y., Chen, X., and Owen, G.S., 2011, "Terramechanics based terrain deformation for real-time off-road vehicle simulation," 6938 LNCS (PART 1), pp. 431-440.

# Appendices

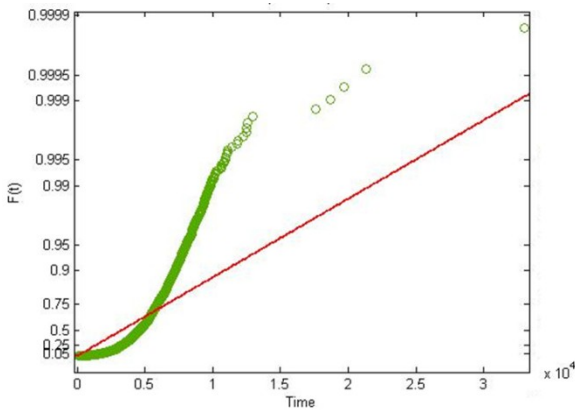
## Appendix 1– Different Cumulative Distributions



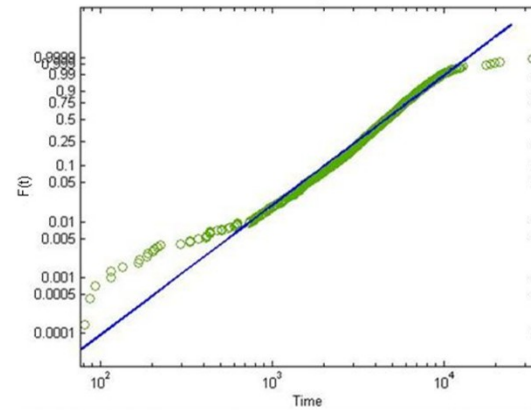
(a) Normal plot



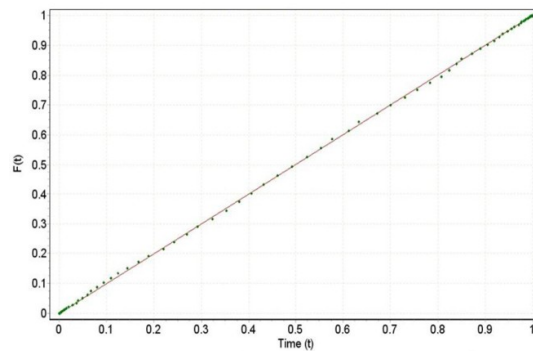
(b) Lognormal plot



(c) Exponential Plot



(d) 2parameter Weibull Plot



(e) 3parameter Weibull Plot

Figure A1-1: Fitting Different Cumulative Distributions to Data

## Appendix 2– Mean Time to Failure Calculation

In this section, Mean Time to Failure (*MTTF*) of haul truck tires is calculated as part of their reliability analysis. Mean time to failure describes the expected time to failure of a system and can be obtained from its reliability function:

$$MTTF = \int_0^{\infty} t f(t) dt = \int_0^{\infty} R(t) dt$$

The reliability function for the set of haul truck tire failures can be presented as 3-Parameter Weibull distribution defined by:

$$R(t) = \exp\left(-\left(\frac{t - \gamma}{\alpha}\right)^{\beta}\right)$$

From the above mentioned equations *MTTF* can be obtained:

$$MTTF = \gamma + \alpha \Gamma\left(\frac{1}{\beta} + 1\right)$$

where  $\Gamma$  is gamma function and is defined by:

$$\Gamma(n) = \int_0^{\infty} e^{-x} x^{n-1} dx$$

After using the parameters of reliability function to be  $\alpha = 5399.0033$ ;  $\beta = 2.5219$  and  $\gamma = 34.6234$  the value for Mean Time to Failure (*MTTF*) of haul truck tires is calculated:

$$MTTF = 4826.015 \text{ hours}$$

### Appendix 3– Lens selection calculations

In this section, parameters that are needed to select an appropriate lens are calculated.

The procedure of choosing a lens includes the following steps:

Determining field-of-view(*FOV*) and object conjugate ( $S_1$ )

Calculating magnification factor ( $m$ ) and focal length ( $f = S_2$ )

Choosing the lens

Calculating spatial resolution, depth-of-field (*DOF*) and  $f\#$

Repeating above calculations to final lens selection

It is shown in following figure, the object conjugate ( $S_1$ ) in comparison with image conjugate ( $S_2$ ) is very large; therefore, using the thin-lens model, the focal length ( $f$ ) equals to  $S_2$ .

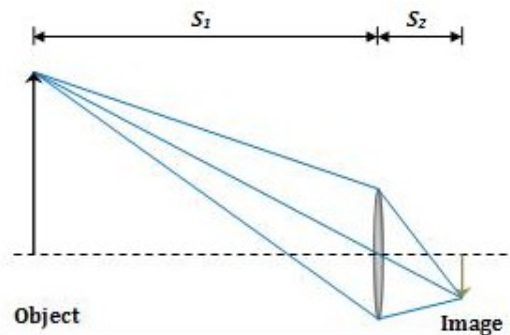


**Figure A3-1: Schematic of geometry of picture with respect to the object**

As the first step, field-of-view (*FOV*) for taking a picture of the rubber is assumed:

$$FOV = 200 \text{ mm} \times 150 \text{ mm}$$

Sensor dimension is known and can be taken as width and height of the camera:

$$W_{camera} \times H_{camera} = 18.1 \text{ mm} \times 13.6 \text{ mm}$$

From the above mentioned equations camera magnification ( $m$ ) can be calculated:

$$m = \frac{W_{camera}}{W_{FOV}} = \frac{18.1 \text{ mm}}{200 \text{ mm}} = 0.091$$

Where  $W_{camera}$  is the width of sensor and  $W_{FOV}$  is the width of *FOV*.

From geometry it can be seen that  $m = \frac{S_2}{S_1}$ , and also  $S_2 = f$  where  $f$  is focal length; therefore the value of  $f$  can be calculated if  $S_1$  is assumed to be 300mm.

$$f = S_1 \times m = 300 \text{ mm} \times 0.091 = 27.2 \text{ mm}$$

The lens with characteristic close to the result of calculations can be selected from the lenses that can be installed on AVT GX3300 camera. Selected lens  $f\#$  is 2 – 16 and also from specifications its focal length ( $f$ ) is 50mm is used to modify the previous calculations.

$$m = \frac{S_2}{S_1} = \frac{f}{S_1} = \frac{50 \text{ mm}}{300 \text{ mm}} = 0.17$$

$$FOV = \frac{W_{camera}}{m} = \frac{18.1 \text{ mm}}{0.17} = 110 \text{ mm}$$

The next parameter to compute is spatial resolution indicating the number of pixels in unit of length, its dimension is pixel per inch ( $ppi$ ), by considering different amount of pixels and  $FOV$ , spatial resolution in different directions can be obtained as

$$W_{FOV} = 110 \text{ mm}, H_{FOV} = W_{FOV} \times \frac{H_{camera}}{W_{camera}} = 82.7 \text{ mm}$$

$$N_x = \text{Number of pixels in } x \text{ direction} = 3296 \text{ pixels}$$

$$N_y = \text{Number of pixels in } y \text{ direction} = 2472 \text{ pixels}$$

$$\text{Spatial resolution})_x = \frac{N_x}{W_{FOV}} = \frac{3296}{110} = 29.9 \text{ ppmm} = 760 \text{ ppi}$$

$$\text{Spatial resolution})_y = \frac{N_y}{H_{FOV}} = \frac{2472}{82.7} = 29.9 \text{ ppmm} = 760 \text{ ppi}$$

Depth-of-field ( $DOF$ ) can be calculated from:

$$DOF (\mu\text{m}) = 2 \times \left( \frac{W_{pixel} (\mu\text{m})}{m} \right)^2$$

Where  $W_{pixel}$  is the width of pixel that is:

$$W_{pixel} = \frac{W_{camera}}{N_x} = \frac{18.1 \text{ mm}}{3296} = 5.49 \mu\text{m}$$

$$DOF (\mu\text{m}) = 2 \times \left( \frac{5.49(\mu\text{m})}{0.17} \right)^2 = 21 \text{ mm}$$